BIOCOMPATIBLE GAS BUBBLE FORMATION IN LASER INDUCED TITANIUM MELTS FOR IMPLANT PROTOTYPING

von der

NATURWISSENSCHAFTLICHEN FAKULTÄT

DER

GOTTFRIED WILHELM LEIBNIZ UNIVERSITÄT HANNOVER

zur Erlangung des Grades eines

DOKTORS DER NATURWISSENSCHAFTEN

Dr. rer. nat.

genehmigte Dissertation

von

M. Sc. MD. AFTAB ALI SHAIKH

geboren am 01.01.1974 in Jessore, Bangladesh

2008

Referent: Prof. Dr. Josef-Christian Buhl

Korreferent: PD Dr. habil Thorsten M. Gesing

Prof. Dr. Peter Behrens

Tag der Promotion: 17.11.2008

DEDICATED TO

THE SOUL OF MY MOTHER

ACKNOWLEDGEMENTS

I owe my present research work to a number of contributors' assistance and suggestion. Without their patience and intelligence, I undoubtedly can not present this thesis.

My first and foremost sincere gratitude must go to my respected supervisor, PD Dr. habil Thorsten Michael Gesing, who has been providing me the most decisive and effective support and encouragement. His valuable instructions and constructive suggestions have constantly inspired me to proceed on this study, so that I am able to complete the PhD thesis smoothly. He always brings people comfortable feeling during talking and discussion. His outstanding and innovative ideas in different aspects of research make me an enthusiast to smoothly carry on the current PhD work. I really learned a lot from him not only on the attitude of academic research but also on the art of making good relationship with people. In fact, from him I learned on how to independently organize the research work. My deeply sincere gratitude is also because of his tireless effort in editing, designing and suggestions that have brought my thesis to its present format. I am really grateful to him.

My sincere gratitude is also delivered to my first examiner, Professor Dr. Josef-Christian Buhl. I really owe to him for his exceptional support and endless patient in learning basic crystallography. Basically, I have learned from him how to deal with SEM and EDX. Without his sincere support I would not be able to be experienced in the field of crystallography and structural chemistry. His outstanding knowledge in crystallography, iconic patient and wonderful behavior makes him a great man whom I ever seen in my life.

I am humbly indebted to Professor Dr. Claus H. Rüscher for his guidance and assistance in learning IR spectroscopy. His constructive suggestions help me to investigate my materials comfortably. His amicable behavioral pattern and enormous patient in scientific discussions overwhelm me. I am thankful to him for his great efforts.

My sincere gratitude is also presented to Dr.-Ing. Oliver Meier. I am not only grateful for his support to carry on my research work in the Laser Zentrum Hannover e.V. (LZH) but also for his continuous valuable suggestions in different aspects of my research.

My especial acknowledgement to the Ministry of Science and Culture, Land Niedersachsen, Germany for awarding me the "Georg-Christoph-Lichtenberg-Stipendium" as financial support.

Md. Aftab Ali Shaikh

TABLE OF CONTENTS

LIST OF ABBREVIATIONS

E_{foam} = Young's modulus of porous material

E_{solid} = Young's modulus of solid material

ρ_{foam} = Density of porous material

ρ_{solid} = Density of solid material

FA = Foaming agent

TNZT = Ti-35Nb-5Ta-7Zr alloy

GPR = Gas producing reaction

MTG = $MgTiO_3$/graphite

MGG = $MgCO_3$/graphite

LTG = Li_2TiO_3/graphite

LNG = $LiNbO_3$/graphite

MgT = $MgTiO_3$/graphite + Li_2TiO_3/graphite

MTM = $MgTiO_3$/graphite + Li_2TiO_3/graphite + $MgCO_3$

MTMC = $MgTiO_3$/graphite + Li_2TiO_3/graphite + $MgCO_3$/graphite

MLN = $MgTiO_3$/graphite + $LiNbO_3$/graphite

MLNM = $MgTiO_3$/graphite + $LiNbO_3$/graphite + $MgCO_3$

MTBM = $MgTiO_3$/graphite + Li_2TiO_3/graphite + $BaCO_3$ + $MgCO_3$

MTBMC = $MgTiO_3$/graphite + Li_2TiO_3/graphite + $BaCO_3$ + $MgCO_3$/graphite

APPS = Average powder particle size

ACS = Average crystal size

MC-ICPMS = Multiple collector inductively coupled plasma mass spectrometry

MCTM = Microcomputed tomography

MGDM = Mass and geometric dimension method

IBM = Immersion-buoyancy method

AG = Anatase/graphite

RG = Rutile/graphite

sphr = Spherical

D. = Deformed

ellip = Ellipsoidal

ABSTRACT

Besides high specific strength, low density and excellent corrosion resistance, biocompatibility is one of the outstanding properties of pure titanium. Due to this reason, titanium is widely used as implant material. However, the mismatch of Young's modulus between the bone and titanium implants is one of the major problems concerning metallic implants for medical applications. Although the Young's modulus of Ti (110 GPa) is relatively low compared to that of stainless steel (about 210 GPa), there is a huge difference in elasticity between the titanium implant and the tissue (30 GPa) in which it is inserted. Due to the mismatch in mechanical properties most of the load is borne by the titanium implant which leads to bone degradation in surrounding areas. In order to minimize the risk of implant loosening caused by these factors endoprosthesis with adapted macroscopic elasticity to human bone is needed. It has been found that the introduction of pores in the titanium materials increases the elasticity while reducing the Young's modulus of the implants. To achieve this aim, there is the idea to create a hollow endoprosthesis scaffold which is filled up with porous metal. The implant elasticity can thus be adapted to bone elasticity by controlling the amount of porosity of the material. It has been assumed that depending on the pore morphology a porosity of 40%-60% is required to adapt the elasticity of a closed cell titanium porous matrix to that of the human bone. Laser induced foaming process has been used to generate pores in the Ti porous matrix. In this study, a number of biocompatible foaming agents have been investigated which allow a laser induced foaming of titanium without leaving toxic degradation products in the porous matrix.

It has been found that foaming agents such as magnesium metatitanate/graphite, lithium titanate/graphite and lithium niobate/graphite generate Ti porous structure with high of porosity, nearly uniform pore shapes and sizes, and almost homogeneous pore distribution in the porous matrix. As a foaming agent, $MgTiO_3$/graphite creates comparably homogeneous pore with maximum porosity of 22% while a mixture of $MgTiO_3$/graphite and $MgCO_3$ create a porosity of 23% and cause inhomogeneous pore distribution in the porous sample. In samples generated with $MgCO_3$/graphite as foaming agent a maximum porosity of 43% is found while only $MgCO_3$ create porous samples with a maximum porosity of 24%. The pore distribution in samples generated with $MgCO_3$ is nearly homogeneous whereas pore distribution in samples generated with $MgCO_3$/graphite is inhomogeneous. Li_2TiO_3 with and without graphite, and $LiNbO_3$/graphite as foaming agents, generate porous samples with considerable amounts of porosity, and nearly homogeneous pore distribution in the samples. A mixture of $MgTiO_3$/graphite, Li_2TiO_3/graphite and $MgCO_3$ or $MgCO_3$/graphite and a mixture of

MgTiO$_3$/graphite, LiNbO$_3$/graphite and MgCO$_3$ as foaming agents generate Ti porous samples with significant amounts of porosity. Amongst them LiNbO$_3$/graphite based foaming mixture generate porous samples with well defined distribution of pores and higher porosity while Li$_2$TiO$_3$/graphite based foaming mixture create lesser amount of porosity in Ti porous samples. Nevertheless, the mixture of MgTiO$_3$/graphite, LiNbO$_3$/graphite and MgCO$_3$ as foaming agent generates Ti porous sample with highest porosity (57%) and well defined pore distribution in the sample. Therefore, MgTiO$_3$/graphite, Li$_2$TiO$_3$/graphite and LiNbO$_3$/graphite based materials could be potential candidates for the generation of Ti porous material with required elasticity for implant. To achieve the necessary elasticity of the material more precious investigations are necessary, which were not part of this work. Moreover, the analysis of the porous materials by EDX, electron microprobe, micro-XRF and laser ablation coupled with MC-ICPMS shows that as residual material of foaming agent only Ti was found.

KURZZUSAMMENFASSUNG

Neben der sehr hohen spezifischen Festigkeit, der niedrigen Dichte und der exzellenten Korrosionsbeständigkeit ist die Biokompatibilität eine der herausragenden Eigenschaften von reinem Titan, weswegen dieses Material weitverbreitete Anwendung als Implantatmaterial findet. Eines der größten Probleme, welche metallische Implantate für medizinische Anwendungen betreffen, ist jedoch die Fehlanpassung des Young-Modulus zwischen dem des natürlichen Knochens und des Titanimplantats, so das, obwohl der Wert von 110 Gpa des Young-Modulus für Ti. verglichen mit einem Wert von z.B. 210 Gpa für rostfreien Stahl relativ gering ist, es einen großen Unterschied in der Elastizität zwischen dem Titanimplantat und dem Gewebe (30 Gpa,) in welches es eingefügt wird, gibt. Aus dieser Abweichung der mechanischen Eigenschaften entstehen die meisten von Titanimplantaten verursachten Spannungen, welche zu u.a. zu Knochenabbau in den umgebenden Bereichen führen können. Um das daraus resultierende Risiko der Lockerung von Implantaten zu minimieren, werden der makroskopischen Elastizität des menschlichen Knochens angepasste Endoprothesen benötigt. Die Einführung von Poren in Titan erhöht in diesem Zusammenhang die Elastizität des Materials, während sich das Young-Modul des Implantats verringert. Eine Möglichkeit dieses Ziel zu erreichen ist die Herstellung einer hohlen Prothesenform, welche mit porösem Metall aufgefüllt wird. Die Elastizität des Implantats kann auf diese Weise, kontrolliert durch den Anteil der Poren im Material, an die Elastizität des Knochen angepasst werden. Dabei wird angenommen, dass abhängig von der Morphologie der Poren eine Porosität von 40%-60% benötigt wird, damit eine Anpassung der Elastizität einer geschlossenen Einheit aus poröser Titanmatrix an die Elastizität eines menschlichen Knochens erreicht werden kann.

Um diese Poren in einer Titan-Matrix zu generieren, wird ein laserinduzierte Aufschäumprozess benutzt. In dieser Arbeit wird eine Anzahl von biokompatiblen Treibmitteln untersucht, welche ein laserinduziertes Aufschäumen von Titan erlauben, ohne dabei toxische Degradationsprodukte in der porösen Matrix zu hinterlassen. Es konnte gefunden werden, dass Treibmittel wie Magnesiummetatitanat/Graphit, Lithiumtitanat/Graphit und Lithiumniobat/Graphit in Titan Strukturen mit einer hohen Porosität, Poren mit einer fast einheitlichen Form und Größe und eine relativ homogene Verteilung der Poren in der Matrix generieren. Als Treibmittel produziert $MgTiO_3$/Graphit eine homogene Verteilung der Poren mit einer maximalen Porosität von 22%, während eine Mischung von $MgTiO_3$/Graphit und $MgCO_3$ bei einer inhomogene Porenverteilung in der Probe zu einer Porosität von 23% führt. In mit $MgCO_3$/Graphit als Treibmittel hergestellten Proben wird eine maximale Porosität von 43%

gefunden, während bei der alleinigen Verwendung von $MgCO_3$ nur eine maximale Porosität von 24% vorliegt. Die Porenverteilung in Proben, die mit $MgCO_3$ aufgeschäumt werden, ist annähernd homogen, wohingegen in mit $MgCO_3$/Graphit hergestellten Proben die Porenverteilung inhomogen ist. Li_2TiO_3 mit und ohne Graphit und $LiNbO_3$/Graphit als Treibmittel generieren Proben mit beträchtlichen Mengen an Porosität und vergleichbarer homogener Porenverteilung in den Proben. Eine Mischung von $MgTiO_3$/Graphit, Li_2TiO_3/Graphit und $MgCO_3$ oder $MgCO_3$/Graphit und eine Mischung von $MgTiO_3$/Graphit, $LiNbO_3$/Graphit und $MgCO_3$ als Treibmittel bilden Proben mit einer signifikanten Porosität. Unter diesen verursacht die $LiNbO_3$/Graphit-Aufschäummischung poröse Proben mit gut definierter Verteilung der Poren und hoher Porosität, während die aus Li_2TiO_3/Graphit hergestellte Aufschäummischung weniger Porosität in den Proben zeigt. Die Mischung aus $MgTiO_3$/Graphit, $LiNbO_3$/Graphit und $MgCO_3$ als Treibmittel produziert die Proben mit der höchsten Porosität von 57% und gut definierter Porenverteilung in der Probe. Daher sind die auf der Basis von $MgTiO_3$/Graphit, Li_2TiO_3/Graphit und $LiNbO_3$/Graphit gewonnenen Materialien geeignete Kandidaten für die Herstellung von porösem Titan-Material mit der für Implantate benötigten Elastizität. Um exakt die notwendige Elastizität des Materials zu erreichen sind allerdings noch weitere Nachforschungen nötig, die nicht Teil dieser Arbeit waren. Zuletzt zeigt die Analyse des synthetisierten porösen Materials mit EDX, Mikrosonde, XRF und Laserablation/MC-ICPMS, dass Titan der einzige Rückstand nach der Laserbestrahlung der Treibmittel ist.

Keywords: Treibmittel, Porosität, Titanimplantat

1. INTRODUCTION

The study of solid metallic porous material has increasingly become attractive to researchers interested in both scientific and industrial applications. Porous materials show a wide range of attractive properties: because of their low density compared to the massive porous material offer great potentials in light-weight constructions. Due to its deformability, the pore structure of a porous material possesses a high absorbance of kinetic energy and low specific weight or high compression strengths [1, 2, 3]. Whilst the industrial mass production of porous polymer materials is already carried out successfully, only a small number of metal and porous metal alloys can be manufactured fully automated and reproducible. Especially the manufacturing of porous materials with complex, three dimensional structures show the limitation of today's foaming methods.

An example for such a complex device is the shaft of an artificial hip joint. The implantation of an endoprosthesis as an artificial replacement for a pathologic hip joint is one of the most numerous operations carried out per year in Europe. A number of factors are motivating improvements in artificial hip joint prostheses. Due to demographic changes, there are an increasing number of revision surgeries, necessitated by aseptic inflammation and loosening of the prosthesis. Moreover, the age range window over the last decade has been broadened to include older patients who have greater incidence of co-morbidities. Additionally, total hip replacements are now routinely performed all over the world on younger patients, whose implants would be exposed to higher mechanical stresses for longer periods. Up to now the available biomaterials for implants have some inherent limitation for long term fixation. A summary of the physical and mechanical properties of various biomaterials in comparison with natural bone is shown in Table 1. One of the main problems concerning these metallic implants in orthopaedic surgery is the mismatch of the Young's modulus between bone (10-30 GPa) and metallic material (110 GPa for Ti and 230 GPa for Co-Cr alloys). Owing to this mechanical property mismatch, bone is insufficiently loaded and becomes stress-shielded, leading to higher bone resorption. Stress-shielding refers to the condition whereby fully dense titanium, which is significantly stiffer than bone, shields surrounding tissue from stresses, resulting in interfacial resorption and implant loosening. Physiologically appearing forces are transmitted through the endoprosthesis due to the higher Young's modulus of the implant compared to that of human bone. There are only little forces loaded onto the articular femur, which is therefore unloaded

compared to the load radiation in a healthy human hip joint. As a result, the degeneration of the less loaded bone substance occurs as it is described in Wolff's law (The form being given, tissue adapts to best fulfil its mechanical function) of transformation of bone, associated with a loosening of the implant in this area [4]. It is identified that one of the major reasons for implant loosening following stress-shielding of bone is the mismatch of Young's moduli [5-7]. Moreover, the moduli mismatch leads to excessive relative movement between the implant and the surrounding hard tissues. Relative movements larger than a critical level hinder bone formation and ingrowth, thereby preventing the desired implant osseointegration [8]. As the composition of metallic implant materials is significantly different from that of the natural bone (natural bone is a composite material made up of collagen fiber matrix stiffened by hydroxyapatite $Ca_{10}(PO_4)_6(OH)_2$ crystals) the second problem with metallic implants lies in the interfacial bond between the tissue and the implant. Due to this stiffer replacement materials a weak interfacial bond is formed which reduces the implant lifetime.

In order to minimise the risk of implant loosening caused by these factors, demands are made on endoprostheses with adapted macroscopic elasticity to human bone. An alternative to overcome stress-shielding and weak interfacial bonding between the tissue and the implant is the use of porous materials. Such porous materials can reduce the stiffness mismatches and achieve stable long-term fixation of implant. The mechanical properties of porous materials can be tailored and optimized by controlling porosity, pore size and shape, and pore distribution in the material matrix to suit with natural bone. A number of approaches to the fabrication of porous implant surface have been reported, including Ti powder sintering, plasma spray coating and the void-metal composite method [9-17]. Nevertheless, due to stress concentrations at the porous interface porous surface implants suffer from a loss of physical properties [18-20]. Very recently a group of researchers has successfully fabricated Ti porous structures with substantial amount of porosity using powder metallurgy for implants [21]. However, a limitation of this process is that the pore size and shape are dependant to powder size and shape and also difficult to control. Moreover, sintered metal powders are often very brittle and prone to crack propagation especially under fatigue conditions [8]. Because of theses reasons, outstanding manufacturing methods for porous metals that can ensure uniform pore size and shape, and pore distribution in material system for biomedical applications are in present demand [22].

Table 1: Summary of the physical and mechanical properties of various implant materials in comparison to natural bone, (Taken from Refs. 23, 24, 25)

Material	Density /g/cm^3	Elastic modulus /GPa	Compressive strength /MPa	Toughness /MPa m$^{1/2}$	Comments
Natural bone	1.8-2.1	3-20	130-180	3-6	Higher strength and
Ti and Ti alloys	4.4-4.5	55-117	590-1117	55-115	elastic modulus
Co-Cr-Mo alloys	8.3-9.2	200-253	450-1896	100	compared with
Stainless steels	7.9-81	189-205	170-310	50-200	natural bone leading
Magnesium	3.1	41-45	65-100	15-40	to "stress-shielding"
HDPE	0.94-0.96	1-2	25	-	Relatively low
UHMWPE	0.41-0.49	1	28	20	strength and modulus
PTFE	2.1-2.3	0.4	11.7	-	limits the use of
PMMA	1.16	4.5	144	1.5	polymers for load-bearing applications
Zirconia	6.1	220	2000	9 (MNm$^{-3/2}$)	Inherent brittleness
Alumina	3.98	380-420	4000-5000	3-5	and low fracture
Bioglass	2.7	75	1000	-	toughness
Hydroxyapatite	3.1	73-117	600	0.7	
AWglassceramic	-	118	1080	1.9-2	

HDPE = High density polyethylene, UHMWPE = Ultrahigh molecular weight polyethylene
PTFE = Polytetrafluoroethylene, PMMA = Polymethylmethacrylate,

1.1. Closed-cell versus open-cell porosity

Concerning pore morphology, two types of porous metals or metallic foams are generally categorized; closed-cell and open-cell [2]. In closed-cell porous structure each cell is completely enclosed by a thin metallic wall or membrane, whilst in an open-cell porous material the individual cells are interconnected, permitting tissue to infiltrate the porous material and anchor it into position. Closed-cell porous metals are normally the results of a random foaming process. Depending on the parameter of the fabrication process the size shape and the location of pores within the material matrix varies. Although limited porosity and, often significant, variation in pore size and shape generates, by the careful selection of the foaming

parameters can improve pore homogeneity [26]. The open-cell porous materials are identical to the closed-cell ones except the membranes between cells have been removed which produces large channels of interconnected cells. The main advantages of this interconnected channel are its "flow-through" capability [27]. Actually, for bone ingrowth and extensive body fluid transport through the porous scaffold matrix open-cell porous metallic materials are necessary. This can trigger bone growth if substantial interconnectivity of porosity is available in the system [22]. There is another type of novel porous structure which has recently been developed [28, 29]. This newly generated porous structure is known as lotus-type (because they look like lotus roots) growth. Fig. 1 shows different variants of porous metal structures.

Table 2: Various fabrication methodologies for porous materials and their types according to the resulting distribution of pores, (Taken from Ref. 22)

Closed-cell		Open-cell		
Randomly pore distribution	Graded pore distribution	Non-homogeneous	Homogeneous	Functionally graded
Gas injection into the metal melt Decomposition of foaming agent	Plasma spraying	Sintered metal powders Sintered metal fibres Space holder method Replication Combustion synth. Plasma spraying	Orderly oriented wire mesh Vapour deposition Ferromagnetic fibre array Rapid prototyping	Rapid prototyping Electro discharge compaction

A number of approaches have been used to generate porous metallic material with closed-cell [12, 30, 31] and open-cell [20, 32, 33] porosity. Summary of various fabrication methods for porous metal and their types is given in Table 2 according to their pore distribution.
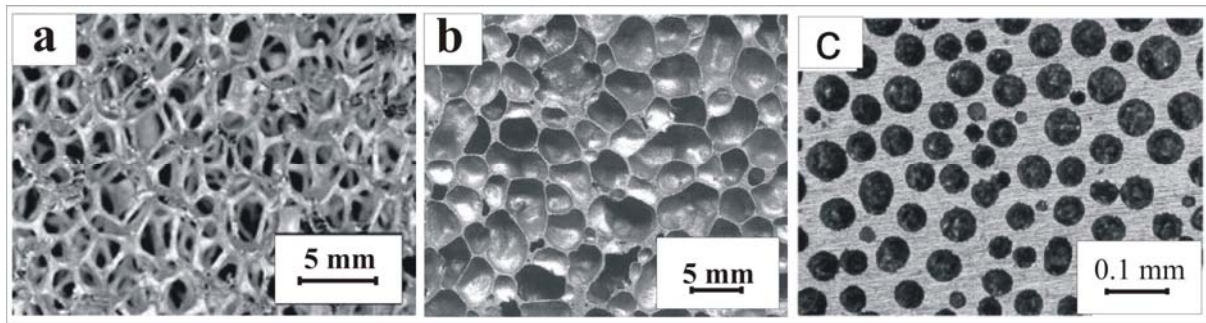
Fig. 1. A typical example of porous metal (a) Open-cell, (b) closed-cell and (c) lotus-type morphologies, (Taken from Refs. 2, 22, 29).

1.2. Requirements for ideal biomaterials

Two critical issues in material science of new implant biomaterials are mechanical properties and compatibility. The ideal materials for implant applications, especially for joint replacements, is expected to exhibit the following properties: a "biocompatible" chemical composition to avoid adverse tissue reactions, an excellent resistance to degradation in the human body environment, acceptable mechanical strength to sustain the cyclic loading endured by the joint, a low modulus to minimize bone resorption, low-density and a high-wear resistance to minimize debris generation [34]. The compatibility issue includes surface compatibility, mechanical compatibility and also osteocompatibility. All these three compatibilities are to be fulfilled by an ideal biomaterial. The biomaterials are also classified as bioactive (illicit a favourable response from tissue and bond well), bioinert (no tissue reaction) and biodegradable (enables the patient's cells to replace the graft by natural tissues). The general requirements for the appropriate biomaterial for implant are given in Fig. 2. Anyway three very important requirements of the biomaterials for implants are biocompatibility, mechanical compatibility and appropriate manufacturing methodology.
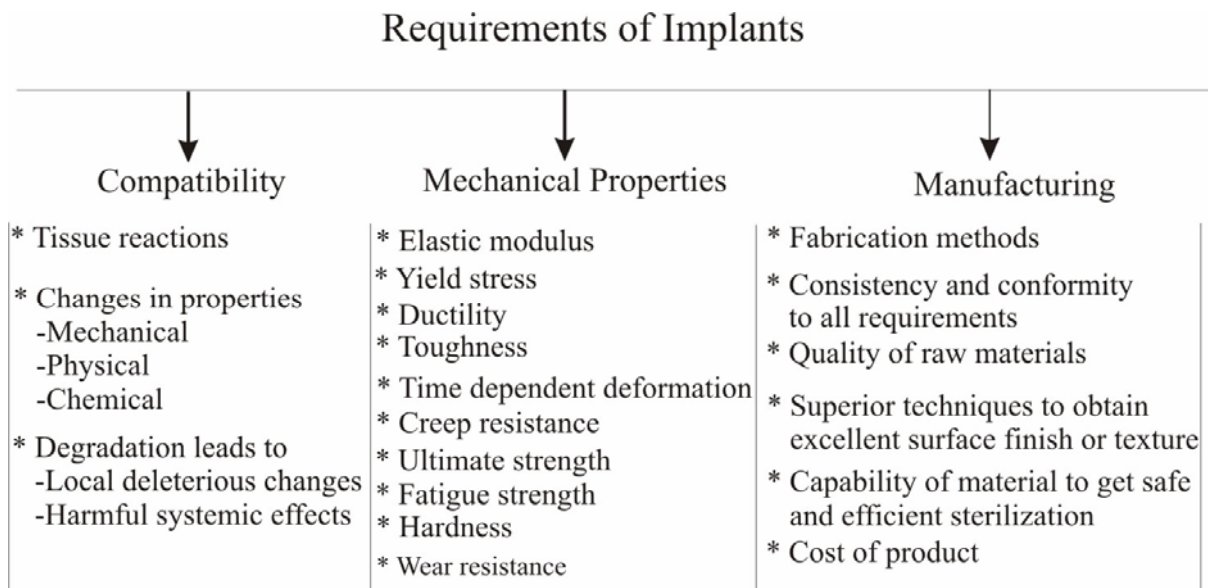
Fig. 2. Implant materials requirements in orthopaedic applications, (Taken from Ref. 35).

1.3. Biocompatibility and surface interactions

Biocompatibility is a general term describing the property of a material capable of being compatible with living tissue where it is inserted. According to Williams biocompatibility is the ability of a material to perform with an appropriate host response in a specific application [36]. In another definition the quality of biocompatible materials must not having toxic or injurious effects on biological systems. Anyway, biocompatible materials do not produce a toxic or immunological response when exposed to the body or body fluids. They are central for use in orthopaedic implants and prosthesis to avoid rejection by the body tissue and to support harmonious biological functioning. In general the selection of the materials used in the construction of prosthesis is basically focused on their ability to maintain mechanical, chemical and functional integrity and on various characteristics which allow this function to substitute any hard tissue appropriately. It must also exhibit safe and effective performance within the body fluid media. Actually to determine the biocompatibility of a biomaterial, it is important to understand the interface phenomena between the biomaterial and the biological system into which it is implanted. The biocompatibility of pure metals and representative biocompatible metallic materials can be shown in Fig. 3.
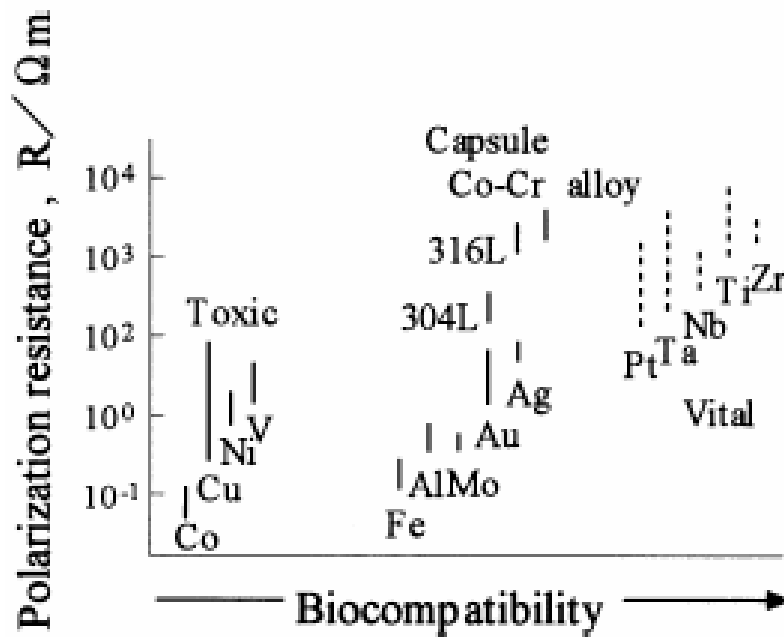
Fig. 3. Schematic representation of polarization resistance versus biocompatibility of pure metals and Co-Cr alloy, and stainless steels, SUS 316L and SUS 304L, (Taken from Ref. 23).

Due to the surgical trauma the insertion of an implant is unavoidably associated with an inflammatory response. This reaction is well dependent on the selected materials [37, 38], as well as the site of implantation and the amount of load on it. The events what are happened in bone-implant interface after insertion of implant are schematically shown in Fig. 4. Various physico-chemical reactions are occurred. Some of the important reactions which occur after the immediate insertion of the implant material into the body fluid media are described here. The release of super oxide and hydrogen peroxide from inflammatory cells into the extra cellular space is one of the important features of an inflammatory response [39]. Obviously an interaction between these species and the foreign implant body is expected. Hydrogen peroxide is formed from super oxide (O_2^-) through the following reaction catalysed by the enzyme superoxidase dismutes.

$$O_2^- + O_2^- + 2H^+ \rightarrow H_2O_2 + O_2 \tag{1}$$
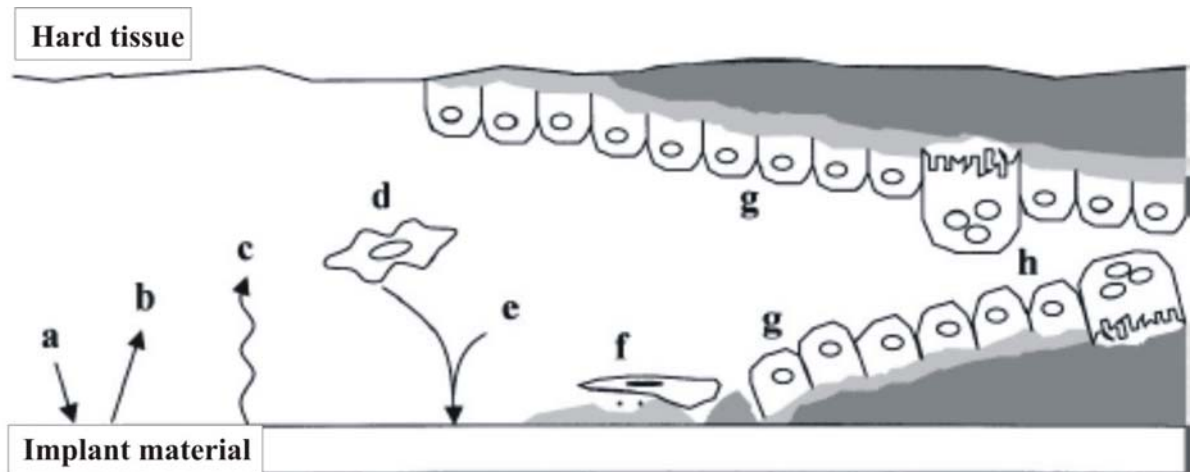
Fig. 4. Schematic representation of events between bone and implant interface: (a) adsorption of protein from body fluids, (b) desorption of protein, (c) change of surface and release of material, (d) inflammatory and connective tissue cells approach the implant, (e) possible targeted release of matrix proteins and selected adsorption of protein, (f) formation of lamina limitans and adhesion of osteogenic cells, (g) deposition of bone on both the exposed bone and implant surfaces, (h) remodeling of newly generated bone, (Taken from Ref. 40).

The previous research [39, 41, 42] shows that after insertion of metallic implant a hydroxyl radical ($OH^\bullet$) is formed during hydrogen peroxide (H_2O_2) decomposition through the Fenton reaction.

$$M^{n+} + H_2O_2 \rightarrow M^{(n+1)+} + OH^- + OH^\bullet \qquad (2)$$

The hydroxyl radical formed during the above reaction cause injury in the biological systems in various ways [41, 42]. This hydroxyl radical may be able to degrade glucose-aminoglycans, binding proteins and hyaluronic acid present in the extracellular fluids. Considering the various essential characteristics titanium is said to be the best compliant implant material *in vitro* and *in vivo* [39, 42, 43]. This is ascribed to the dense and close adherent oxide layer on the surface, which is presented to the body cells. The spontaneous development of this stable and insoluble, passive oxide layer with a thickness of a few nanometers [44] when exposed to atmosphere even in aqueous solution provides a high biocompatibility which is associated with a high corrosion resistance in aggressive biological environments [45]. This thin oxide layer, predominantly consisting of amorphous or low-crystalline and non-stoichiometric TiO_2,

[44, 46] with a minor amounts of Ti_2O_3 and TiO [44] perfectly regenerates within milliseconds [47] even if destroyed mechanically. Due to the formation of rich oxide layer over Ti implant it has very interesting properties such as low inherent toxicity [48], low solubility of TiO_2 in water, small reactivity of $Ti^{4+}_{(aq)}$ with biomolecules [42]. Concerning chemical reaction, Ti-complexes are formed on and outside the Ti surface because of the interaction between TiO_2 and H_2O_2 [42].

$$Ti^{4+}_{(aq)} + H_2O_2 \rightarrow TiO_2(OH)_{n-2}^{(4-n)+} + nH^+ \qquad (3)$$

Depending on the pH the generated Ti complex transform to dinuclear peroxide complexes [49, 50], $Ti_2O_5(OH)_x^{(2-x)+}$, with x=1-6. These complexes are polymerized as the concentration of H_2O_2 decreases with time [39]. The complex eventually precipitated after formation of peroxotitanium hydrate, $TiO_3(H_2O)_x$, where x is between 1 and 2. Concerning biocompatibility of Ti matrix this peroxotitanium hydrate gel is an excellent environment for proteins and living cell of biological system [39]. This gel-like thin oxide may provide the environment in which biological integration takes place [49]. Moreover, titanium is able to form a calcium phosphate-rich layer on its surface [51] to which bioactive properties are ascribed. The number and acuteness of complications resulting from the implantation of titanium prostheses is small compared to those showing up after insertion of an endoprosthesis of any other implant material.

1.4. Elastic Modulus of titanium materials

An elastic modulus or Young's modulus is the mathematical description of an object or substance's tendency to be deformed elastically when an external force is applied to it. An appropriate elastic modulus of biomaterial is present demand for integration and long term fixation of implant to the human bone. Long term experience indicates that inadequate load transfer from the implant to the adjacent remodelling bone may result in bone resorption and eventually loosening of the prosthesis [52, 53]. The various biomaterials and their elastic modulus can be shown in Fig. 5. Among various biomaterial titanium materials has comparably low values of Young's modulus. This may be another reason for the choice of titanium for this application. Therefore, its mechanical properties are already closer as to those of human bone. Foaming offers the possibility of further adaptation of the implants' properties to those of bone

according to the relation between Young's modulus and density developed by Gibson and Ashby [54].

$$\frac{E_{foam}}{E_{solid}} = c \left(\frac{\rho_{foam}}{\rho_{solid}} \right)^n \qquad (4)$$

The proportionality constant c and the exponent n reflect the porous material parameters, such as cell morphology and shape and arrangement of the cell walls. E_{foam} and E_{solid} describe the Young's modulus of porous titanium and pure titanium, respectively, and ρ_{foam} and ρ_{solid} are densities of porous titanium and pure titanium correspondingly. To adapt the elasticity of a closed cell porous titanium to the elasticity of bone, based on the Eq[n]. (4), it is assumed that porosities of 40 % to 60 %, depending on the pore morphology, require to be realized.
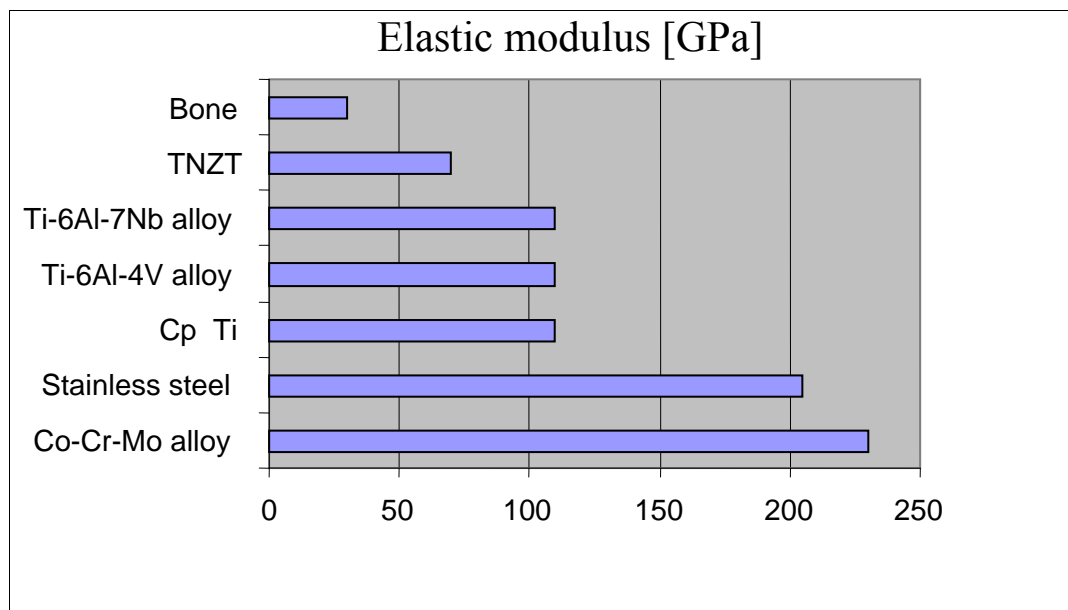
Fig. 5. Comparison of elastic moduli of various implant materials, [TNZT = Ti-35Nb-5Ta-7Zr alloy].

1.5. Background on metal foams and porous metals

1.5.1. Definitions

Although interest in porous materials is increasing, still some misunderstanding exists regarding the term "metallic foam" which is often used in a general way to describe materials which are not foam in actual sense. According to Gibson and Ashby [2] cellular materials are those materials in which space is filled by the packing of polyhedral cells surrounded by an interconnected network of solid struts (the cell edges) and plates (the cell faces). A *honeycomb* structure is obtained if the packing is performed two dimensionally. The packing of cells in three dimensions results in a *foam*. The cellular material is an open-cell material where the cells are interconnected, i.e. in the absence of the cell faces. If the cells are separated from each other by thin faces, a closed-cell material is obtained. Generally, a porous solid material can be characterized by its relative density ρ_{foam}/ρ_{solid}, where ρ_{foam} is the density of the porous material and ρ_{solid} is the density of solid materials constituting the cell edges and cell faces. The quantity given by (1- ρ_{foam}/ρ_{solid}) is a measure of the porosity level of the material (often given in %). Gibson and Ashby [2] stated that for a relative density greater than $\approx$ 0.3 (i.e. for porosity line below 70%), the structure of the material is better described as that of a solid containing isolated pore, rather than a cellular material. Consequently, for metals with relative densities higher than 0.3, the term "porous metals" could be of better use than "metal foam" [55]. The term "metal sponge" is sometime used to describe a material made of a continuous network of metal coexisting with a network of interconnected cavities [3]. All open-cell metal foams fit in the category of metal sponges.

Simancik [1] proposes a more restrictive definition for a metallic foam: it results from the nucleation and subsequent growth of gas bubbles in a liquid or semi-liquid metal. This definition fits well with the manufacturing methods studied in the present thesis. The material developed in the present work show porosity levels lower than 70%. The porous materials showing porosity greater than 70% will be referred to as metal foams, independently of their manufacturing process. Therefore, we are describing our materials as "porous metals".
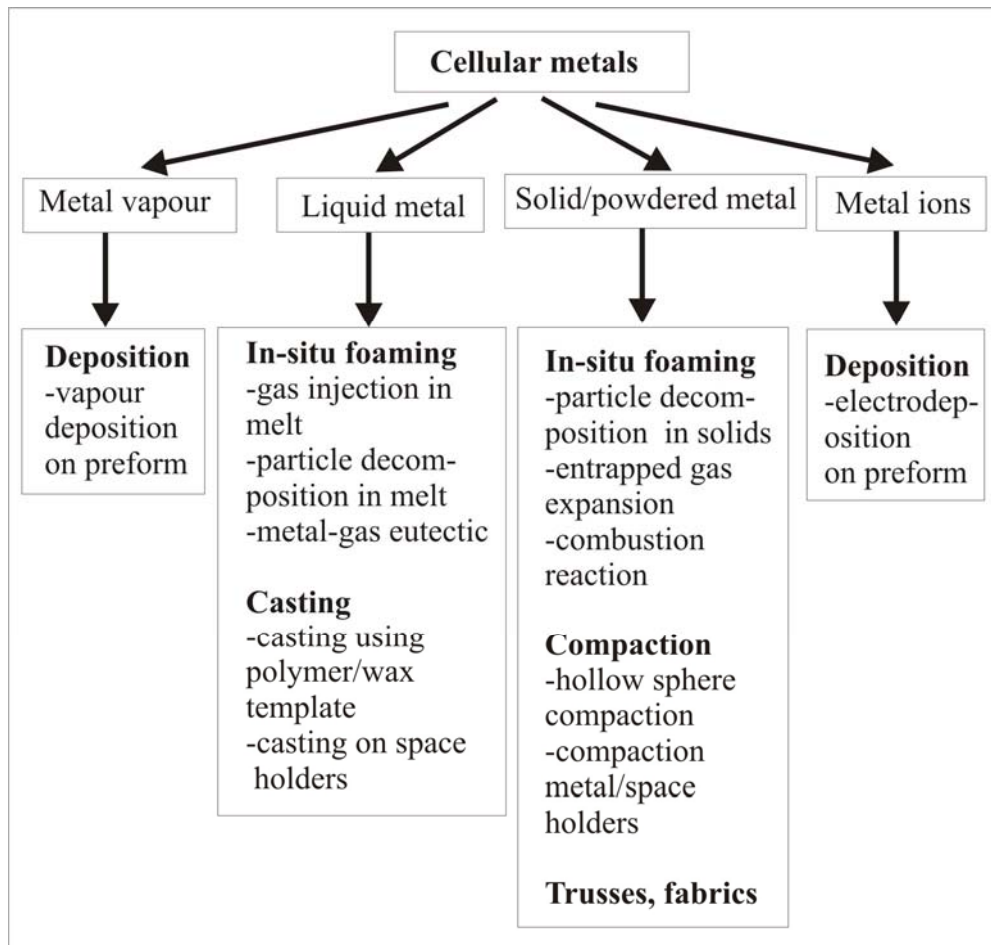
Fig. 6. Schematic representation of the types of main production methods for cellular metals.

1.5.2. Manufacturing methods

A number of approaches [1, 30, 31, 56, 57] to fabricate porous metals have been proposed and new techniques appear regularly. The most common way of classifying the manufacturing techniques is to sort them according to the physical state of the metal prior to the synthesis of the porous structure. Currently several ways are known for porous metal manufacturing: by injecting gas into the liquid metal, by causing an in-situ gas release in the liquid by admixing gas-releasing foaming agents to the molten metal and by causing the precipitation of gas which was previously dissolved in the liquid. Such classification can be shown in Fig. 6. Since new methods are regularly published this list is only an overview. In each of the four classes, a sub-classification based on the process by which the pores are obtained is made. The methods involving direct *in-situ* pore formation lead to unpredictable structures [30, 57]. The other techniques allow a better control of the pore structure and isotropy. In particular, they permit an

independent selection of the density and cell size. But materials with pre-designed structures are often more expensive than unpredictable ones due to additional cost in the production processes [30, 57]. More extensive information can be found in the reviews cited above [1, 30, 31, 56, 57].

1.6. Principle of the foaming process

The principle of the foaming process is manly based on the formation of pores in the melt by chemical reactions between base materials (for example Ti) and foaming or viscosity increasing agents under high temperature. It is produced by mixing powdered materials, foaming agent and reducing agent or viscosity increasing agents (where necessary) and heated under a high temperature. Generally, it is believed that at high temperature, the foaming agent decomposes into metallic materials by evolving carbon dioxide. The metallic matrix remains in the melt as a solidus material whereas the carbon dioxide gas tends to bubble out, causing the melt to expand and form pores. The porous structure can collapses or show inhomogeneous pore distribution because of mainly two phenomena. One is melt drainage and another is coalescence of pores [58-60]. The schematic representation of these phenomena can be shown in Fig. 7. Drainage can be descried as the transport of liquid through the generated porous metal due to gravity [60]. Density difference is created between liquid metal and gas pores. Therefore, the melt tends to sink to the bottom and the gas pores tend to float towards the surface of the melt. This leads to a non-uniform distribution of densities in the final material with a higher volume fraction of pores at the top of the porous samples [58]. Coalescence is the reunion of adjacent pores due to the rupture of the liquid film that separated them. This results in non-uniform distribution of pore size in the porous materials. Both of the described phenomena are closely related since drainage induces a thinning of the cell walls. That makes them more prone to breakage.

The stabilization of porous structure by introduction or precipitation of particles in the melt can be applied to address these aforementioned problems. These particles have two main purposes [61]. From a macroscopic point of view, the particles increase the overall viscosity of the melt, thus slowing down the drainage process. At a microscopic scale, they act as barriers between the pores to prevent coalescence. So-called *endogenous particles* [61] or a foreign particle that is denoted as *exogenous* can be able to stabilize the pore structures. The endogenous particles are precipitated during primary solidification of the metal, without adding of foreign elements

[61]. These particles are believed to hinder the thinning of the pore walls. The exogenous particles can be either foreign particles added in the initial stage of the process (for example SiC or Al_2O_3), or oxide particles precipitated when using an oxidizing foaming gas [62] or after addition of oxide forming elements (for example Ca in the Alporas process [3]). Those exogenous elements are found to agglomerate on the surface of the pores [62]. This effect is thought to "weigh down" the bubbles and reduce the buoyancy forces on them. In the present work, the endogenous particle stabilizing approach is chosen.
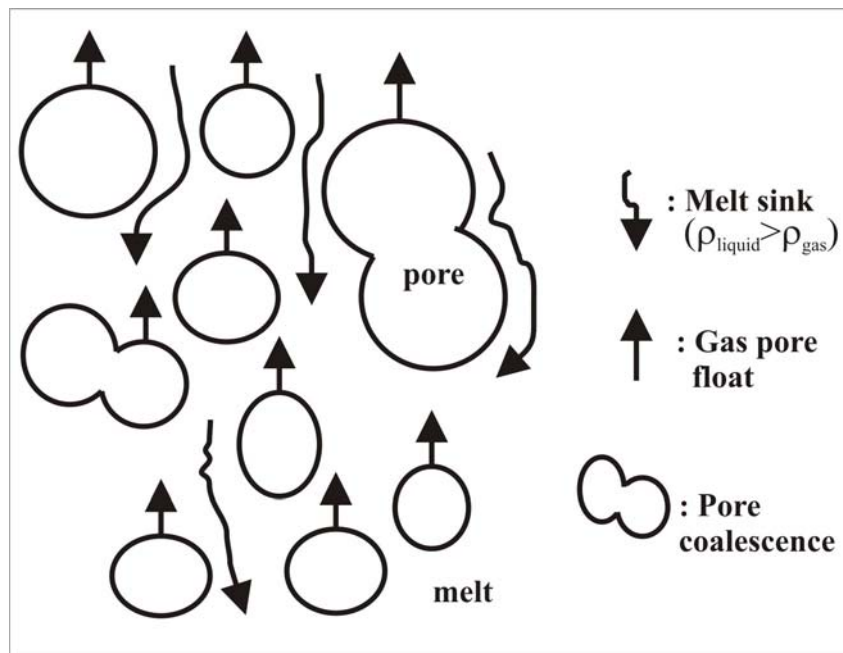
Fig. 7. Schematic representation of the drainage effect and pore coalescence during pore formation.

1.7. Phase transition of titanium with temperature

Like a number of other metals (e.g. Zr, Fe, Co, Sn) pure titanium can be stable in various crystal structures. It exhibits an allotropic phase transformation at 882 ± 2 °C strongly depending on the interstitial (e.g. C, N, O) and substitutional (e.g. Al, Zr, V) elements and therefore, depends on the purity of the metal. Pure titanium and most of its alloys, crystallizes at low temperatures in a modified ideally hexagonal close packed (hcp) structure, called α titanium. However, at high temperatures the body-centered cubic (bcc) structure, called β titanium is stable. The phase transformation temperature is called the transus temperature. The unit cells of hcp and bcc are schematically shown in Fig. 8. The lattice parameters a (0.295 nm)

and c (0.468 nm) are at room temperature. The resulting c/a ratio for pure α titanium is 1.587 while for an ideally close packed hexagonal lattice the ratio is 1.633. Also indicated in Fig. 8(a) are the three most densely packed types of lattice planes: the basal plane (0001), one of the three prismatic planes $\{10\bar{1}0\}$ and one of the six pyramidal planes $\{10\bar{1}1\}$. The unit cell of the bcc shows one variant of the six most densely packed {110} lattice planes and cell parameter a (0.332 nm) at 900 °C.

The most densely packed planes of the bcc (β) phase {110} transform to the basal planes (0001) of the hexagonal α phase upon cooling from the β phase field of titanium. The β to α phase transformation causes a slight atomic distortion due to the dissimilar distance between the basal planes in α and the corresponding distance between the {110} planes in β [63]. This result to a slight contraction of the c-axis compared to the a-axis in the hcp phase and reduces the c/a ratio than ideal value for hcp structure. Anyway, for pure titanium and titanium alloys the transformation of bcc β phase to the hcp α phase can either take place martensitically or by diffusion controlled nucleation and growth process basically depending on cooling rate and alloy composition. The crystallographic orientation relationship between α and β phases of titanium can also be shown by the following relationship:

$$(110)_\beta \parallel (0001)_\alpha$$
$$[1\bar{1}1]_\beta \parallel [11\bar{2}0]_\alpha$$

Since the Burgers vectors for Zirconium [64] can also describe the slip directions, this orientation relationship is called Burger relationship. The Burger relationship is strongly obeyed by Ti and Ti alloys for both the martensite transformation and the conventional nucleation and growth process [65]. The hexagonal martensite is designated as ά and is found in two morphologies. One is massive martensite or lath or packet martensite while the other one is acicular martensite [66]. In pure titanium, very dilute alloys, and in alloys with a high martensitic transformation temperature massive martensite occurs while acicular martensite takes place in alloys with higher solute content or lower martensitic transformation temperature.

When titanium alloys are cooled at sufficiently low rates from the β phase into (α + β) phase field, the incoherent α phase with respect to the β phase, first nucleates preferentially at β grain boundaries leading to a continuous α layer along β grain boundaries. The α plates nucleate

either at the interface of the continuous α layer or at the β grain boundary itself during continued cooling and grow into the β grain as parallel plates [67] or so called α colony. Again, α plate continues to grow into the β grain interior as long as meet other α colonies nucleated at other grain boundary area of the β grain. This process is called sympathetic nucleation and growth [65]. The α plates are also called α lamellae and the resulting microstructure is then designated as lamellar.
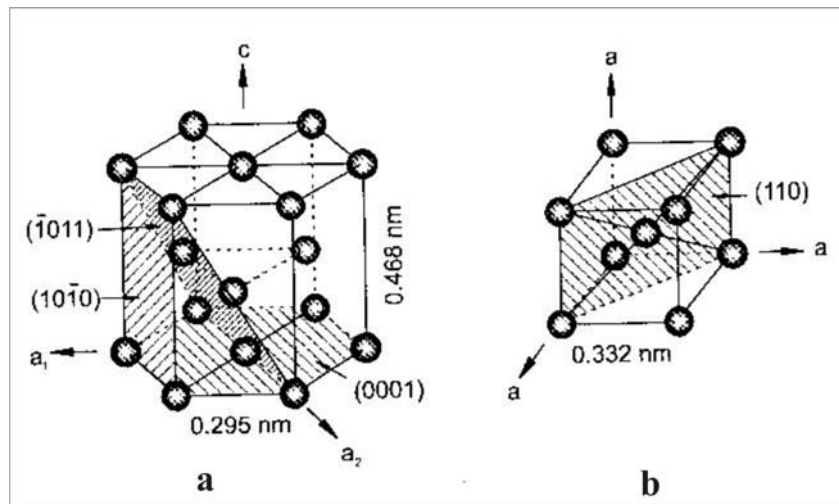
Fig. 8. (a) Unit cell of α phase and (b) Unit cell of β phase, (Taken from Ref. 63).

1.8. Objectives of present research

The need for adequate mechanical properties together with manufacturing flexibility for a wide range of metallic implant materials necessitates the use of novel design and approaches to fabricate functional implants. To overcome stress-shielding and weak interfacial bonding between the tissue and the implant, there was the idea to create a hollow endoprosthesis scaffold which is filled up with porous metal. Biocompatible foaming agents that can generate pores in the material matrix without leaving the toxic or allergic species are necessary for the filling up of the hollw space of the endoprosthesis. By this way the implant elasticity can be adapted to bone elasticity by controlling the amount of porosity of the material. Among the various metallic biomaterials (e.g. stainless steel, cobalt-base alloys and titanium-base alloys), Ti and its alloys have been recognized as desirable materials for bone implants because of their excellent corrosion resistance; superior biocompatibility, mechanical properties and high

strength-to-weight ratio [13, 68-73]. Due to its distinguished biocompatibility [74, 75], pure titanium is the implant material of choice in this study. To achieve the required porosity (40-60%) in the porous Ti metal, the present study will tremendously be involved with the investigation of suitable foaming agents which can generate pores.

2. MATERIALS AND METHODS

2.1. Choice of foaming agents

In oven based foaming processes, metal alloy powder and foaming agents are heated at heating rate of several hundred Kelvin per hour. Alloys are chosen based on the existence of a liquid-solid phase boundary in their binary phase diagram. A foaming agent is preferred which causes a gas producing reaction (GPR) in between liquidus and solidus line of the alloy composition. The evolved gas is entrapped in the liquid phase while the solid particles serve as nucleating agents. Due to the increased heating rates in a laser process compared to an oven process, it is awaited that foaming of pure metals is possible although a semi-solid phase does not exist. Therefore, it is suggested that a foaming agent causes a GPR just below the melting point of the pure metal, resulting in gas pore formation in the liquid metal matrix. The entrapping of gas is possible, because the GPR and melting of the metal matrix occur nearly simultaneously at typical heating rates in a laser process.

The melting point of titanium is 1941 K. The heating rate of a titanium laser cladding process is 3600 K/s. Since the melt viscosity is temperature dependent, foaming agents that cause GPR above the melt temperature of metal matrix are not promising. A superheated and low viscous melt not only tends to show drainage effects, but also causes the gas to rise quickly through the melt towards the surface and escape from it [76, 77]. On the other hand, if the decomposition temperature of the foaming agent is much lower than the melting temperature [78] of the matrix material, there is a risk of releasing the generated gas through the un-molten powder material. As a result, the sample may build up internal pressure and crack prematurely [77]. Ideally, decomposition temperature of the foaming agents should be close to the melting temperature of the base metal (in this case pure Ti). Numerous foaming agents have been investigated in order to correlate their amount, quality, and particle size with the porosity of resulting porous metals. Porous metals were synthesized with selected amounts of different foaming agents generally from 0.25 wt% up to 5.0 wt%. The foaming agents used in this study are:

(a) Anatase (TiO_2)/graphite, experimental grade
(b) Rutile (TiO_2)/graphite, experimental grade
(c) Calcium tungstate ($CaWO_4$)/graphite, Sigma-Aldrich Inc., Germany

(d) Magnesium metatitanate ($MgTiO_3$)/graphite, Sigma-Aldrich Inc., Germany

(e) Magnesium carbonate ($MgCO_3$), Sigma-Aldrich Inc., Germany

(f) $MgCO_3$/graphite

(g) $MgTiO_3$/graphite with $MgCO_3$

(h) Lithium titanate (Li_2TiO_3), Sigma-Aldrich, Inc., Germany

(i) Li_2TiO_3/graphite

(j) Lithium niobate ($LiNbO_3$)/graphite, Sigma-Aldrich, Inc., Germany

(k) Zirconium oxide (ZrO_2), Sigma-Aldrich, Inc., Germany

(l) ZrO_2/graphite

(m) $MgTiO_3$/graphite + Li_2TiO_3/graphite (MgT)

(n) $MgTiO_3$/graphite + Li_2TiO_3/graphite + $MgCO_3$ (MTM)

(o) $MgTiO_3$/graphite + Li_2TiO_3/graphite + $MgCO_3$/graphite (MTMC)

(p) $MgTiO_3$/graphite + $LiNbO_3$/graphite (MLN)

(q) $MgTiO_3$/graphite + $LiNbO_3$/graphite + $MgCO_3$ (MLNM)

(r) $MgTiO_3$/graphite + Li_2TiO_3/graphite + $BaCO_3$ + $MgCO_3$ (MTBM)

(s) $MgTiO_3$/graphite + Li_2TiO_3/graphite + $BaCO_3$ + $MgCO_3$/graphite (MTBMC)

Mechanically crushed titanium powder (99.9%, median particle size 45 μm, Medicoat, Switzerland) has been used as the base material for the laser induced foaming process. Pure graphite powder (Sigma-Aldrich Inc., Germany) was used as a reducing agent and was mixed with the foaming agent at an appropriate stoichiometric ratio to produce carbon dioxide at elevated temperatures. The initial content of the various elements present in the different precursor materials is provided in Table 3.

Table 3: Initial total content of 5 g powder with 0.25% foaming agents used for laser experiment

FA materials	FA:graphite (molar ratio)	Wt% of FA	Initial elemental contents of the Ti powder mixtures /g								
			Ti	C	Ca	Mg	Li	Nb	Zr	W	O
TiO$_2$/graphite	1:1	0.25	4.99125	0.00625	-	-	-	-	-	-	0.00250
CaWO$_4$/graphite	1:2	0.25	4.98750	0.00834	0.00058	-	-	-	-	0.00266	0.00092
MgTiO$_3$/graphite	2:3	0.25	4.98949	0.00750	-	0.00101	-	-	-	-	0.00199
MgCO$_3$		0.25	4.98750	-	-	0.00360	-	-	-	-	0.00712
MgCO$_3$/graphite	2:1	0.25	4.98750	0.00535	-	0.00240	-	-	-	-	0.00474
Li$_2$TiO$_3$		0.25	4.99295	-	-	-	0.00158	-	-	-	0.00547
Li$_2$TiO$_3$/graphite	2:3	0.25	4.98968	0.00750	-	-	0.00063	-	-	-	0.00219
LiNbO$_3$/graphite	2:3	0.25	4.98750	0.00750	-	-	0.00023	0.00314	-	-	0.00162
ZrO$_2$		0.25	4.98750	-	-	-	-	-	0.00925	-	0.00325
ZrO$_2$/graphite	1:1	0.25	4.98750	0.00625	-	-	-	-	0.00463	-	0.00162
MgT	-	0.25	4.98957	0.00750	-	0.00051	0.00032	-	-	-	0.00208
MTM	-	0.25	4.99682	0.00914	-	0.00099	0.00026	-	-	-	0.00289
MTMC	-	0.25	4.98926	0.00715	-	0.00080	0.00026	-	-	-	0.00251
MLN	-	0.25	4.98849	0.00750	-	0.00050	0.00012	0.00157	-	-	0.00181
MLNM	-	0.25	4.98834	0.00658	-	0.00099	0.00098	0.00132	-	-	0.00265
MTBM	-	0.25	4.98925	0.00650	-	0.00070	0.00026	-	-	-	0.00256
MTBMC	-	0.25	4.98926	0.00732	-	0.00061	0.00026	-	-	-	0.00237

Foaming agent = FA, Ba content in MTBM and MTBMC = 0.00069 g (for 0.25 wt% FA). Elaboration of MgT, etc. are mentioned before

2.2. Laser induced foaming process

The schematic representation of the overview of laser induced foaming process is shown in Fig. 9. It was initially though that porous metals could be produced by using the single step laser cladding process. The high number of process parameters regarding the powder feeding (feeding gas, feeding gas temperature, pressure, respective flow of the feeding gas, feeding rate, mix-ability), combined with different feeding behaviors of the foaming agents, does not allow one to draw conclusions about the potential of the foaming agent in titanium itself. Therefore, the process was transformed in to a two-step cladding process with a decreased number of parameters. Titanium powder was mixed automatically with certain amounts of the different foaming agents. The first process step is the pre-deposition of a definite powder mixture volume in the work zone. As the second process step, laser power is applied. The porous samples emerged from this process are therefore independent from feeding parameters but mainly influenced by laser parameters (laser power respectively intensity in the work zone, feed rate) and the properties of the foaming agent itself. The laser machine set-up used in this work is shown in Fig. 10. For simplicity a newly designed graphite sample holder was used. The sample holder contains six holes for powder mixture. Each hole has a dimension of 25x7x 4 mm^3.
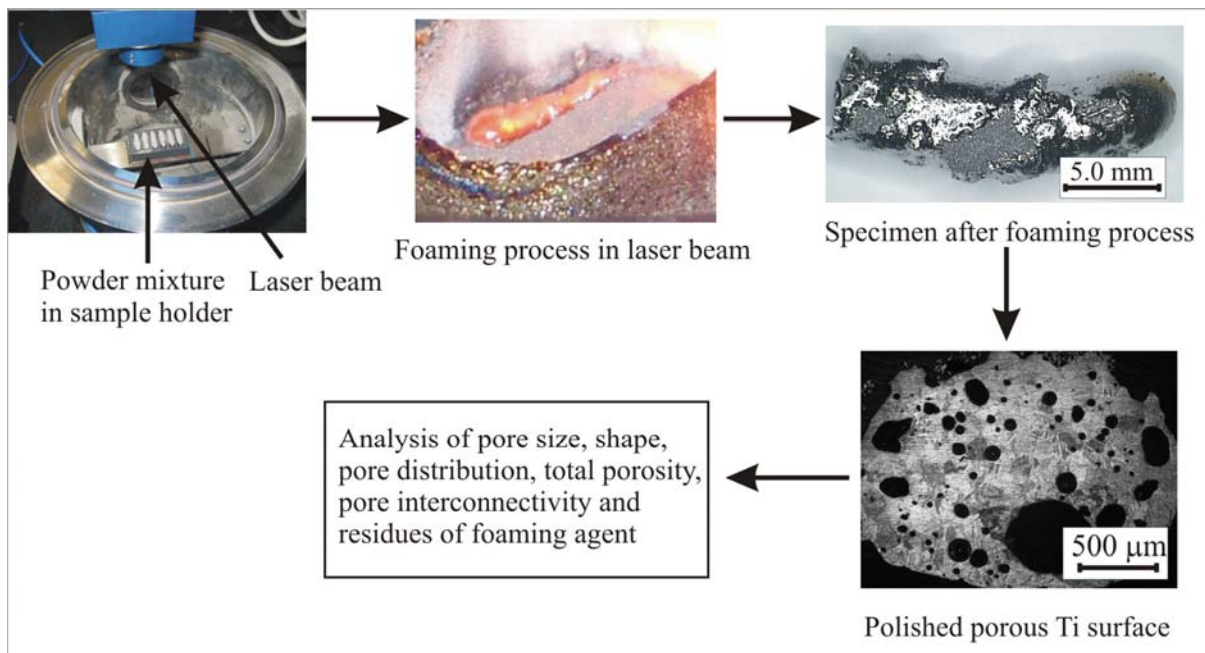
Fig. 9. Schematic representation of the overview of laser induced Ti foaming process.

For every laser experiment the laser power, feed rate, energy per length unit unput etc., were optimized. The typical laser parameters are as follow: laser power (200-350 W), feed rate (5 m/min) and energy per length unit input (1000-1750 Wm/min). In the conventional thermal melting process the average temperature gradient of the interface which varies as the bulk temperature is lower. This results a slow cooling rate. Therefore, it takes a long time for the porous metal to stabilize. However, in case of laser induced foaming process the average temperature gradient of the interface is much higher compared to conventional process. Consequently, a faster cooling rate is achieved which facilitates the porous structure stabilization. The influence of processing speed on cell morphology is shown elsewhere [79].
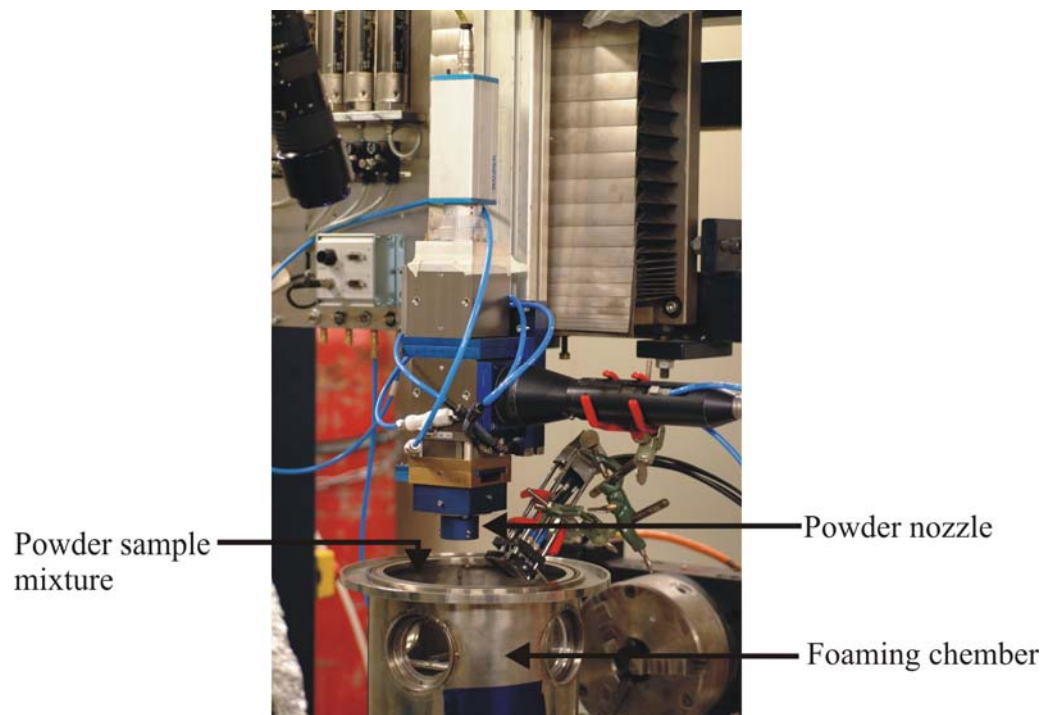
Fig. 10. Schematic representation of laser system used in this laser induced foaming process.

2.3. Characterization of precursor materials

As the quality of the porous metal depends of the purity, particle size and average crystal size of the precursor materials which have been characterized by various techniques. X-ray diffraction (XRD) pattern with a Bruker AXS D4 Endeavor X-ray instrument using Cu K$\alpha_{1,2}$-radiation coupled with Rietveld refinement (Diffrac Plus Topas 3.0, Bruker AXS GmbH, Karlsruhe) was employed to determine the average crystal size of different precursor materials. Table 4 shows

the particles sizes characterization of the provided materials. Scanning electron microscope (SEM) (Cam Scan S. 2, England) was used to evaluate the average powder particle size of the precursor materials which is also given in Table 4.

Table 4: Purity, degradation temperatures and size characterization of the precursors materials

Materials	APPS /μm	ACS /nm	Purity grade	Degradation temperature /K
Anatase (S230)	agglomerated	6.73 (14)	pure	2098
Anatase (PC500)		7.26 (13)		
Anatase (PC105)		26.13 (38)		
Anatase (PC100)		26.20 (37)		
Anatase (PC50)		40.57 (58)		
Anatase (PC10)		152.10 (40)		
Rutile (R15)	agglomerated	20.00 (30)	pure	2098
Rutile (R25)		27.51 (49)		
Rutile (R34)		36.15(53)		
$CaWO_4$	8.2	>1000	99.8%	1893
$MgTiO_3$	<7.0	480.0 (43)	pure	1883
$MgCO_3$	Inhomogeneous (0.8-8.0)	54.6 (7)	pure	623
Li_2TiO_3	1.5	41.6 (18)	99.9%	1837
$LiNbO_3$	2.0	184.9 (16)	99.9%	1513
ZrO_2	<1.0	84.4 (4)	99%	2900
Graphite	9.3	38.3 (4)	99.8%	3970

APPS = average powder particle size, ACS = average crystal size. In the first column anatase sample codes is written in parenthesis and in the third column standard deviation of the ACS measurement are provided in parenthesis.

2.4. Sample preparation for laser experiments

In an attempt to find a suitable foaming agent a two-step laser process was carried out. At first a certain amount of foaming agent was weighed out and mixed with graphite as reducing agent (where required) in an agate mortar until a homogeneous powder mixture was obtained. The

second stage was to mix the titanium powder with the foaming agent mixture (foaming agent and reducing agent mixture) automatically to reach a homogeneous distribution of the constituents and to guarantee reproducibility. A definite (2.0 g) amount of the powdered mixture was filled into a graphite sample holder which was placed in an argon-flooded shielding gas chamber. The powder mixture was treated with Nd:YAG- and accordingly diode laser radiation. Fig. 11 shows the schematic illustration of the various steps of sample preparation for the laser process. In preliminary tests, the influence of the wavelength of the radiation (Nd:YAG: 1064 nm, diode: 940 nm and 980 nm), and the beam diameter in the working plane have been investigated. It was found that the difference in wavelength of maximum 124 nm did not have an analyzable influence on the foaming result. The beam diameter was chosen to comply with the width of the sample holder (4 mm). The laser systems can generate stable output power in the range of 30-680 W.
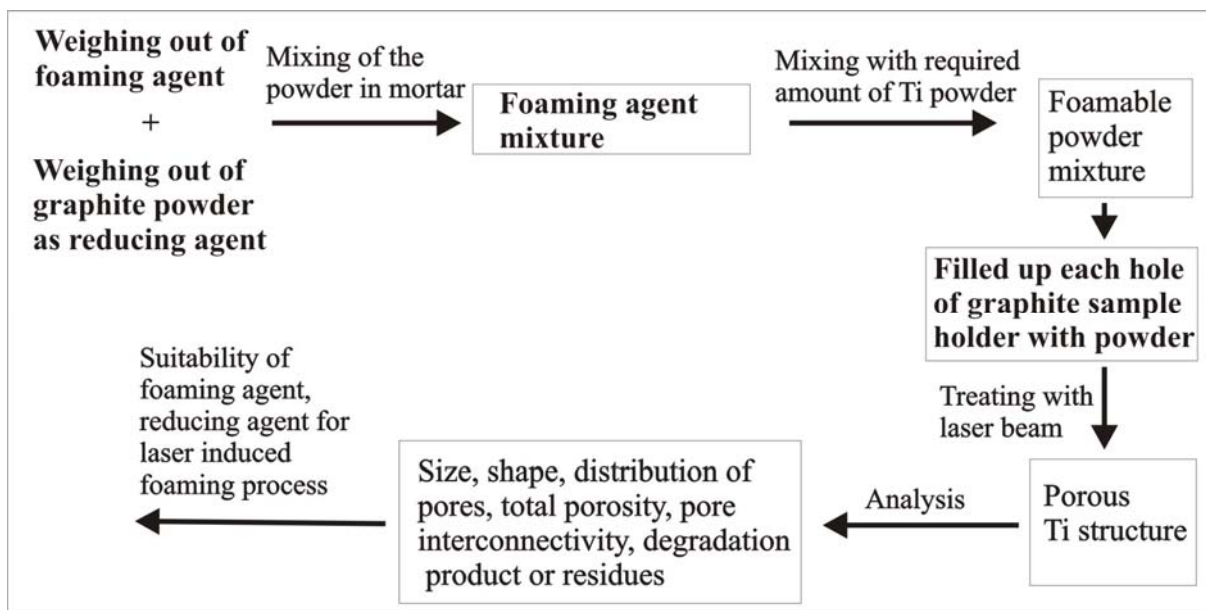
Fig. 11. Schematic illustration of the various steps of sample preparation for the laser process.

2.5. Characterization of porous structures

To compare the results of the laser induced foaming process, micrographs were taken from the generated specimens. Optical microscopic analysis (Leica 1M, version 4.0 microscope) and micro computed tomography (micro-CT) imaging and analysis (Scanco Medical micro-CT) were performed in order to determine the porosity, pore size, pore shape, pore interconnectivity

and the pore distribution within the samples. Surface analysis of the porous metal substrates was carried out by scanning electron microscopy (SEM) (Cam Scan S. 2, England). Micrographs of samples showing porosity were evaluated regarding the shape of pores, which are described as spherical, deformed spherical, ellipsoidal and deformed ellipsoidal (Fig.12). The size of the pores, smallest and biggest in diameter, as well as the medium pore diameter is measured.
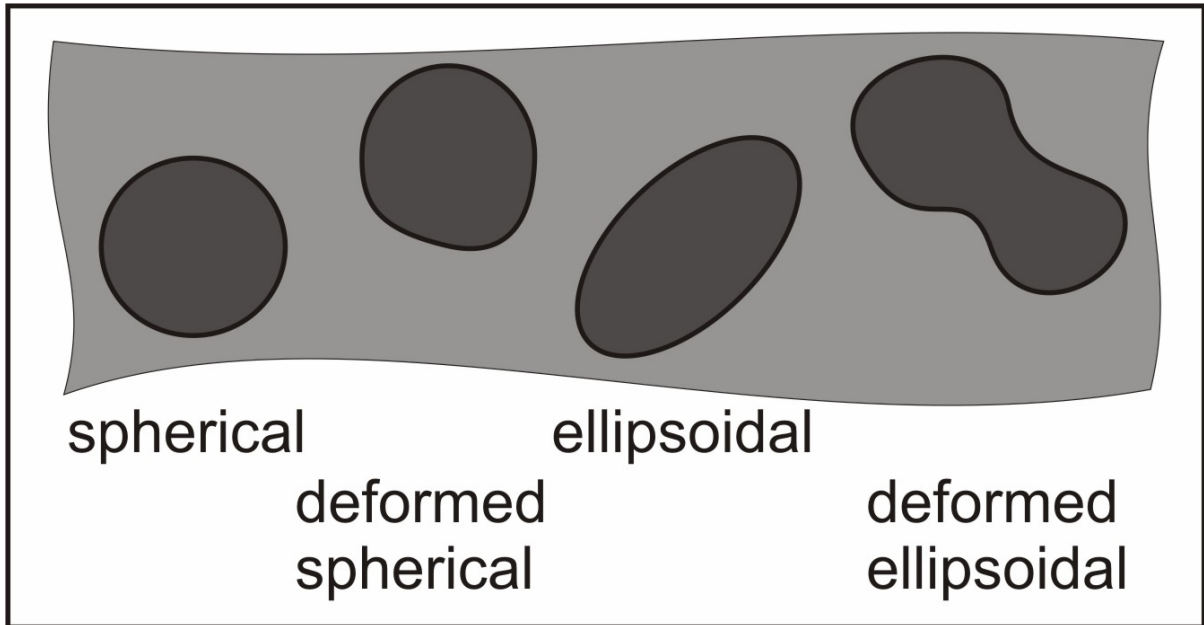
Fig. 12. Shapes of the generated pores in the Ti porous samples.

2.6. Compositional analysis of the porous Ti samples

2.6.1. MC-ICPMS measurement

An in-house built (Institute of Mineralogy, LUH) laser ablation system based on a 100 femtosecond Ti-sapphire regenerative amplifier system (Hurricane I, Spectra Physics, USA) operating at a fundamental wavelength of 785 nm in the infrared spectra was used. In this system subsequently harmonic generations produce the wavelengths 393 nm in the second, 262 nm in the third and 196 nm in the fourth stage. Among them 196 nm was used to determine magnesium, lithiumin, niobium and barium contents of the porous Ti matrix. A Neptune ThermoFinnigan multiple collector inductively coupled plasma mass spectrometry (MC-

ICPMS) was used to analyze the ablated mass of the porous Ti sample. This system is capable of providing high mass resolution in multiple collector modes.

2.6.2. X-ray fluorescence (micro-XRF) spectroscopy

To determine the residual materials in the porous Ti samples micro X-ray fluorescence spectroscopic measurement has been carried out. Eagle μ-probe II using a rhodium anode in the X-ray tube and a polycapillary lens with a spot size of around 50 μm (voltage 40 kV) micro-XRF was used for this measurement. The distance of measured points on the samples was approximately 100 μm.

2.6.3. Electron probe and energy dispersive X-ray analysis

Electron probe microanalysis (Cameca SX 100, France) with EDX (Oxford) detector was performed to evaluate the residues of the foaming agents in the porous Ti specimens. In all measurements, the voltage and current used were 15 kV and 15 nA respectively. Energy dispersive X-ray (EDX) analysis (Noran Voyager 3050, USA) was also performed to compare the chemical compositions of any residual foaming agent in the prepared Ti samples.

2.7. Microstructural observation

Microstructural observations of porous Ti structures have been carried out using optical microscopy (OM) and scanning electron microscopy (SEM). The samples for OM and SEM were prepared by mechanically polishing with OPS 0.25 μm to obtain a mirror surface finish. The polished samples were etched using Kroll's solution (96 ml H_2O, 2 ml HF, and 2 ml HNO_3). The XRD patterns for phase analysis were collected using a Bruker AXS D4 Endeavor diffractometer. Ni-filtered $CuK\alpha_{1,2}$-radiation was used for this measurements. Phases were identified by Rietveld refinements (Diffrac Plus Topas 3.0, Bruker AXS GmbH, Karlsruhe) analysis. The composition analysis by EDX was performed to evaluate α and β phase of Ti.

2.8. Porosity determination

Various methods were used to determine the porosity of the porous Ti samples. In addition to micro-CT measurement (MCTM), the porosity (in volume percent) of the porous materials was evaluated by both of mass and geometric dimension method (MGDM) and the immersion-buoyancy method (IBM) utilizing the Archimedean principle. Generally, the porosity of the Ti porous samples can be expressed by the following formula:

$$\text{Porosity, } P = (1 - \rho_{foam}/\rho_{solid}) \times 100 \tag{5}$$

where ρ_{foam} and ρ_{solid} are the density of the porous metal specimen and its corresponding theoretical density, respectively. In MGDM the apparent density (ρ_{foam} = weight of sample/ volume of sample) of the specimen was determined by measuring its mass and dimension as in Fig. 13 [80]. In this method a representative part of the specimen was sliced and the mass and dimension were measured. The later involves weighing the porous samples in two conditions such as in air and under immersion in water [81]. The density of different porous samples was measured by Sartorius YDK 01, YDK 01-0D, YDK 01 LP balance using the following formula:

$$\text{Density, } \rho = W_{(a)} \left[\rho_{(fl)} - 0.0012 \text{ g/cm}^3 \right] / 0.99983 \, G + 0.0012 \text{ g/cm}^3 \tag{6}$$

Where, ρ = density of porous sample, $W_{(a)}$ = weight of the porous metal in air, $\rho_{(fl)}$ = density of water, G = buoyancy of the immersed porous metal. Nevertheless, the obtained porosity in different method is comparable with one another.
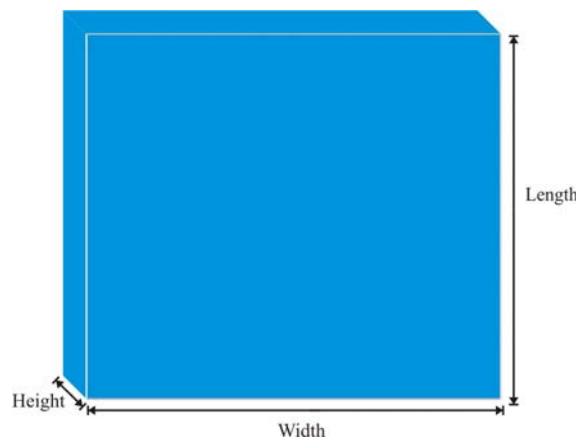
Fig. 13. Sample used for dimension and weight measurement in density calculation.

3. RESULTS

The generated porous Ti samples were investigated regarding the pore distribution, pore size and shape, porosity and pores interconnectivity. Micrographs were taken to investigate the dispersion of the pores. Besides surface morphology of polished Ti samples SEM micrographs show the interconnectivity of pores in the samples. Interconnectivity between pores was also detected in micro-CT imaging analysis. Additionally, EDX, electron microprobe, XRF analyses of mechanically divided porous specimens were carried out concerning the residues of the foaming agents. Moreover, laser ablation coupled with MC-ICPMS has been performed regarding the residues of the foaming agents after laser induced foaming process. The results of the porous Ti sample obtained by using several foaming agents are discussed bellow:

3.1. Results obtained with anatase or rutile/graphite as foaming agents

Porous titanium structure has been generated with 0.25 wt%-5.0 wt% of anatase/graphite as foaming agent. The optical micrographs of some generated samples are shown in Fig. 14 (upper line). Concerning the pore distribution, it is apparently observed that the pores are randomly distributed for every amount of foaming agent. For 0.25 wt% anatase samples with 26.20 nm average crystal size deformed spherical (big) pores with average pore diameter of about 510 μm, spherical (medium) pores with average pore diameter of about 280 μm, ellipsoidal (small) pores with average pore diameter of about 180 μm and also spherical (smallest) pores with average pore diameter of about 60 μm are found. In the same anatase sample with 5.0 wt% foaming agent, ellipsoidal (big) pores with average pore diameter of about 636 μm, spherical (medium) pores with average pore diameter of about 424 μm, spherical (small) pores with average pore diameter of about 148 μm and deformed spherical (smallest) pores with average pore diameter of about 60 μm are observed. In the samples created with 2.0 wt% of 152.10 nm average crystal size of anatase spherical (big) pores with average pore diameter of about 550 μm, deformed spherical (medium) pores with average pore diameter of about 255 μm, spherical (small) pores with average pore diameter of about 160 μm and ellipsoidal (smallest) pores with average pore diameter of about 60 μm are found. For the same anatase sample with 3.0 wt% of foaming agent spherical (big) pores with average pore diameter of about 318 μm, deformed spherical (medium) pores with average pore diameter of about 250 μm, spherical (small) pores with average pore diameter of about 150 μm and ellipsoidal (smallest) pores with average pore

diameter of about 60 µm are found. Table 5 shows the relationship between the average crystal size of anatase and rutile and generated pore diameters of the porous samples. From Table 5 it is found that on an average the higher (152.10 nm) and medium (40.57 nm) average crystal size of anatase samples: intermediate percentages of foaming agent create pores with increased pore diameter than the higher percentages. While for the relatively low (7.26 nm, 6.73) average crystal sizes anatase: higher amounts of foaming agent generate pores with increased pore diameter compared to lower foaming agent amounts (Table 5). Altogether, the generated samples show relatively decreasing diameter of pores with the decreasing average crystal sizes of anatase. Therefore, it is apparently speculative that the average crystal size of the anatase has an influence on the generation of the pores in the pure Ti foaming process. EDX and electron microprobe analyses showed that as a residual material of foaming agent Ti could be found in the specimens.
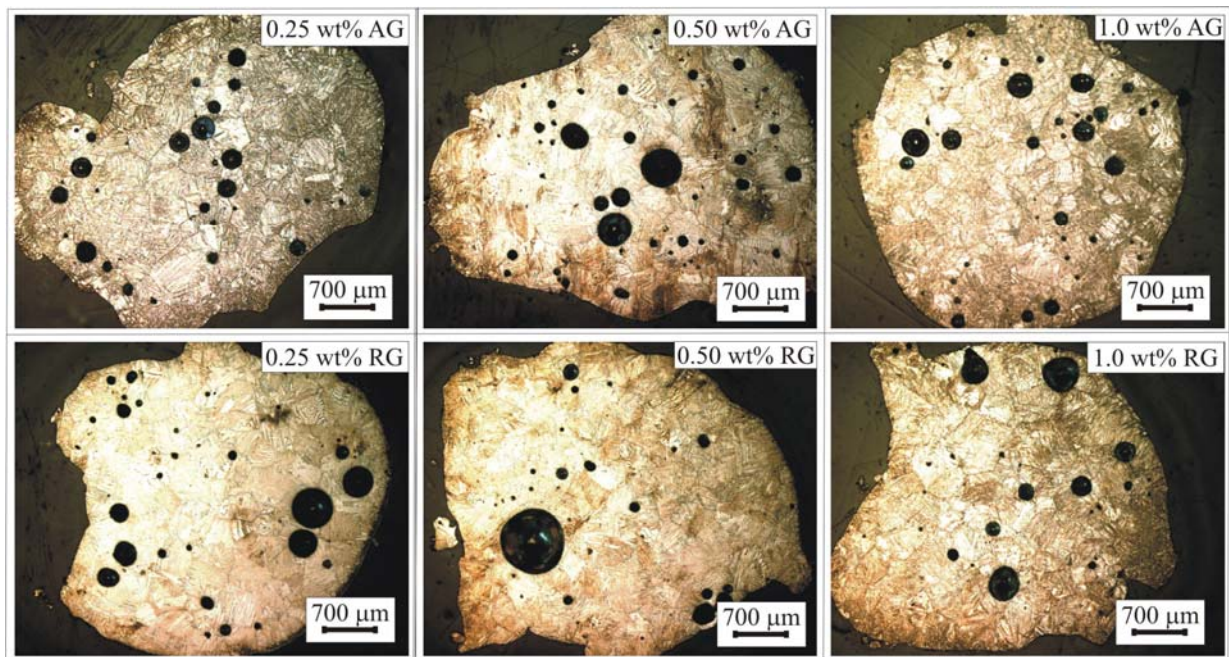
Fig. 14. Porous Ti samples generated with anatase/graphite (AG) and rutile/graphite (RG) as foaming agent in the laser induced foaming process.

Porous Ti samples could also be generated with rutile/graphite as foaming agent. Out of various samples optical micrographs of three generated samples are shown in Fig. 14 (bottom line). For rutile sample (2.0 wt% foaming agent) with average crystal size of 27.51 nm spherical (big) pores with average pore diameter of about 763 µm, deformed spherical (medium) pores with average pore diameter of about 318 µm, also deformed spherical (small) pores with average

pore diameter of about 169 μm and ellipsoidal (smallest) pores with average pore diameter of about 60 μm are found. Again, deformed spherical (big) pore with average pore diameter of about 466 μm, spherical (medium) pores with average pore diameter of about 275 μm, also spherical (small) pores with average pore diameter of about 169 μm and deformed spherical (smallest) pores with average pore diameter of about 60 μm are observed in the sample generated with 5.0 wt% of same rutile sample. In the sample generated with 2.0 wt% of 20.0 nm average crystal size of rutile ellipsoidal (big) pores with average pore diameter of about 510 μm, spherical (medium) pores with average pore diameter of about 270 μm, also spherical (small) pores with average pore diameter of about 140 μm and deformed spherical (smallest) pore with average pore diameter of about 60 μm are found. In the same rutile sample pore diameter of pores shows decreased trend in the sample generated with higher percentages (e.g. 5.0 wt%) of foaming agent. Samples created with different average crystal size of rutile show similar influence on the pore morphology as anatase does. Therefore, concerning the average crystal size of anatase and rutile an influence on pore formation can be concluded.

3.2. Results obtained with calcium tungstate/graphite as foaming agent

As a second series of foaming agents, a mixture of $CaWO_4$ and graphite (molar ratio of $CaWO_4$: graphite = 1:2) was carried out for the laser induced titanium foaming process. Porous titanium structure could be produced with 0.25 wt% to 5.0 wt% of foaming agent while for higher than 5.0 wt% unstable foaming process was observed. The generated porous Ti structures were transversely divided and optical micrographs were taken which are shown in Fig. 15. A sudden change in process emissions could be observed, as soon as even a small amount of foaming agent (0.25 wt%) was added to the titanium powder. Nevertheless, the optical micrographs show an appearance with a pore diameter lesser than 50 μm in the samples generated with 0.25 wt% and 0.50 wt% of foaming agent. Additionally, a few deformed spherical pores with average pore diameter of about 150 μm and spherical pores with average pore diameter of about 100 μm are observed for both amounts of foaming agent. Samples from test series with 1.0 wt% of foaming agent additionally show few deformed spherical pores with average pore diameter bigger than 160 μm. Again in sample generated with higher amounts of foaming agent (2.0 wt%, 3.0 wt%) pore with increased pore diameters are predominantly found. The surface morphology of the porous samples looks like a bonded fiber array like material which can be found in previous study [82].

Table 5: Pore size and shape of the generated Ti porous metal with anatase/graphite and rutile/graphite as foaming agents

Foaming agents	Amount of FA /wt%	ACS /nm	Size and shape of big pores		Size and shape of medium pores		Size and shape of small pores		Size and shape of smallest pores	
			Size /μm	shape	Size /μm	shape	Size /μm	shape	Size /μm	shape
Anatase/graphite	2.0	152.10	550	sphr	255	D. sphr	160	sphr	60	ellip
	3.0		318	sphr	250	D. sphr	150	sphr	60	ellip
Anatase/graphite	2.0	40.56	505	sphr	390	ellip	230	D. sphr	60	D. sphr
	3.0		360	D. sphr	233	D. sphr	148	sphr	60	sphr
Anatase/graphite	2.0	26.20	370	sphr	230	D. sphr	170	sphr	60	D. sphr
	5.0		636	ellip	424	sphr	148	sphr	60	D. sphr
Anatase/graphite	0.25	26.13	510	D. sphr	280	sphr	180	ellip	60	sphr
	5.0		450	sphr	275	sphr	169	D. sphr	60	D. sphr
Anatase/graphite	2.0	7.26	380	D. sphr	160	D. sphr	84	D. sphr	60	sphr
	4.0		420	D. sphr	180	D. sphr	106	sphr	60	sphr
Anatase/graphite	2.0	6.73	385	D. sphr	210	sphr	130	sphr	60	D. sphr
	4.0		400	sphr	230	sphr	120	sphr	60	D. sphr
Rutile/graphite	2.0	27.51	763	sphr	318	D. sphr	169	D. sphr	60	ellip
	3.0		848	D. sphr	212	sphr	148	ellip	60	sphr
	5.0		466	D. sphr	275	sphr	169	sphr	60	D. sphr
Rutile/graphite	2.0	20.00	510	ellip	270	sphr	140	sphr	60	D. sphr
	5.0		339	D. sphr	148	sphr	63	sphr	42	sphr

ACS = Average crystal size, sphr = Spherical, D. =Deformed, ellip = Ellipsoidal
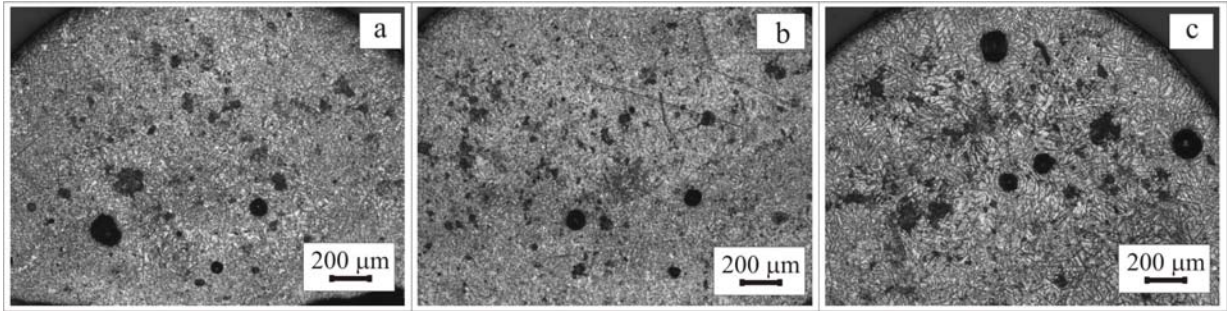
Fig. 15. Optical micrographs of porous Ti structures generated with: (a) 0.25 wt%, (b) 0.50 wt% and (c) 1.0 wt% of $CaWO_4$/graphite as foaming agent in laser induced foaming process.

The result of the micro-CT imaging and analysis as in Fig. 16 shows that big pores are partially interconnecting within the sample while the surrounding small pores have no interconnectivity to each other. The surface morphology of porous structures can be represented by the SEM micrographs (Fig. 17). Anyway, maximum total porosity calculated by MCTM is 10.4%. In electron microprobe and micro-XRF analyses only Ti can be found after laser process.
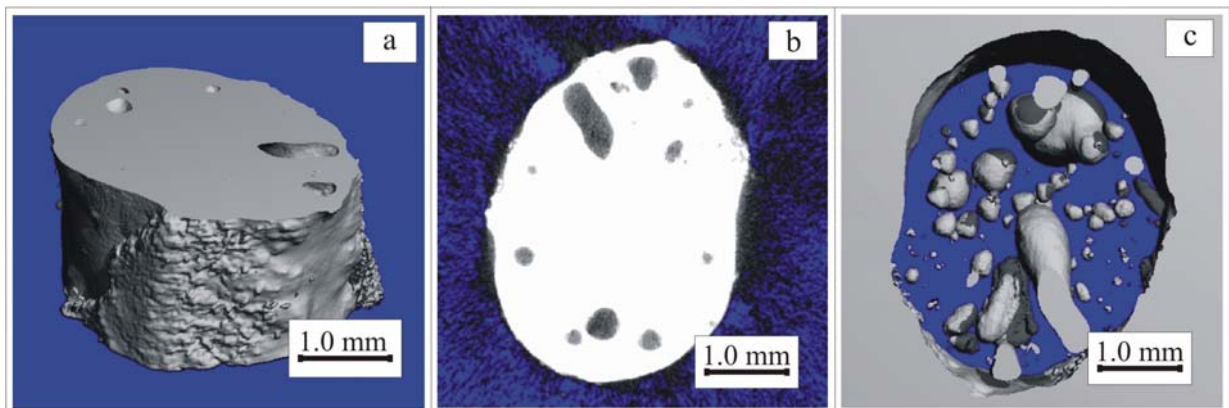
Fig. 16. micro-CT images of Ti porous sample generated with $CaWO_4$/graphite as foaming agent: (a) 3D image, (b) overview of the porous sample and (c) an inverted picture showing pores as solid structure.
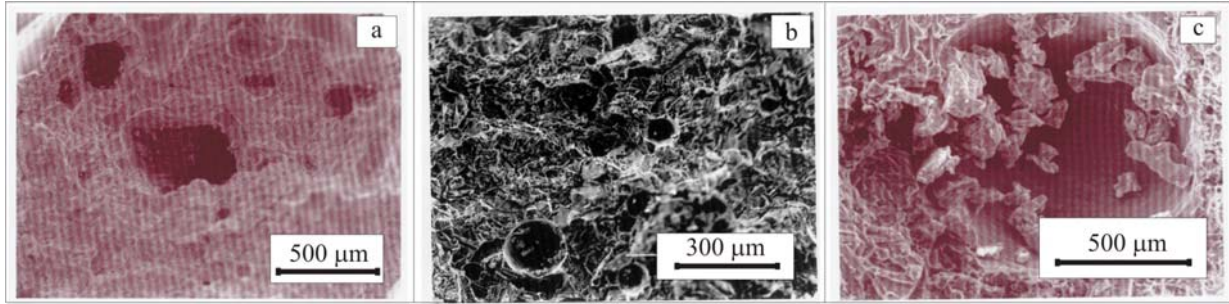
Fig. 17. SEM micrographs of porous Ti sample generated with CaWO$_4$/graphite as foaming agent: (a) big interconnective pores, (b) surface morphology of an unpolished sample and (c) unpolished porous sample surface showing big pore.

3.3. Results obtained with magnesium metatitanate/graphite as foaming agent

A mixture of MgTiO$_3$ and graphite (molar ratio of MgTiO$_3$: graphite = 2:3) was used as third test series of foaming agents for laser induced foaming process. In this case, 0.25 wt% to 5.0 wt% of foaming agent could be used to generate porous titanium structures. The optical micrographs of generated samples are shown in Fig. 18. Concerning the pore distribution, it is apparently observed that a mixture of big and small pores is randomly distributed across the whole area of a specimen. In a few samples pores tend to become increasing pore diameters toward the centre of the samples section. The pore morphology of generated samples is comparable to the previously [83] generated porous structures. For the lowest amount of foaming agent (0.25 wt%) deformed spherical (big) pores with average pore diameter of about 550 μm, spherical (medium) pores with average pore diameter of about 230 μm and also spherical (small) pores with average pore diameter of about 130 μm are found. In samples created with 1.0 wt% foaming agent, pores with an increased pore diameter of about 700 μm can be found as well. Altogether, with increasing amounts of foaming agent deformed ellipsoidal pores are found additionally in combination with increasing sizes of pore diameters up to 1150 μm. Pore sizes and distribution do not show major variations depending on the applied energy per length unit input. Anyway, the number of pores increase with increasing percentages of the foaming agent from 0.25 wt% up to 1.5 wt%, while above 1.5 wt% the pore size strongly increases in combination with a corresponding decrease of the number of pores, resulting in bigger pore diameters up to 1150 μm (Fig. 18 e).
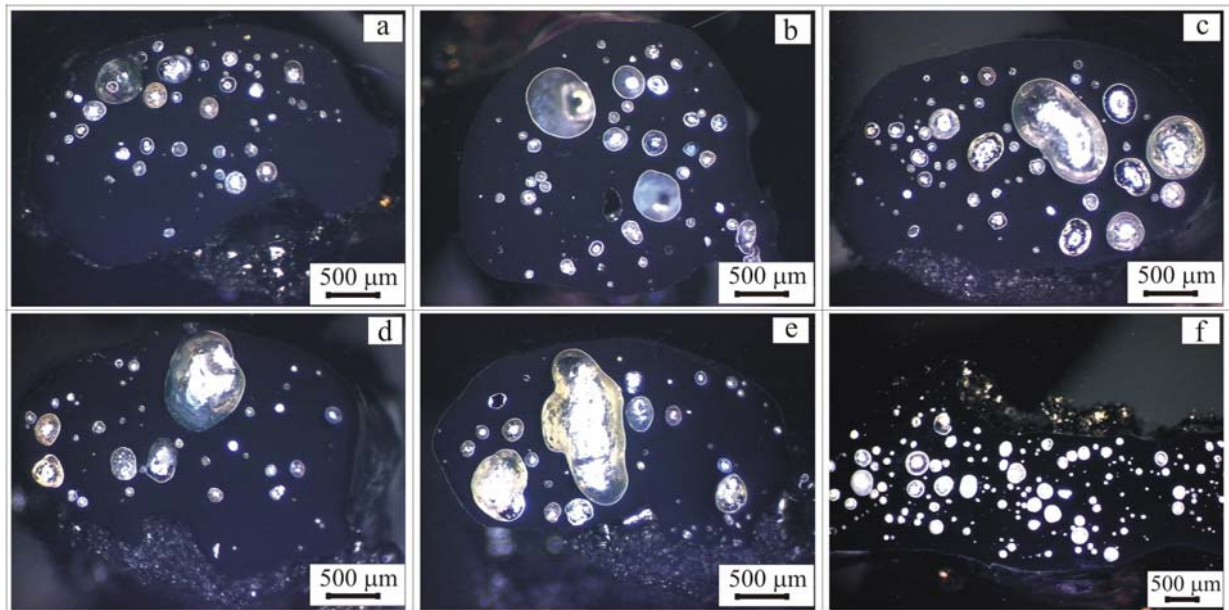
Fig. 18. Optical micrographs of the samples generated with various amounts of MgTiO$_3$/graphite mixture as foaming agent: (a) 0.25 wt%; (b) 1.0 wt%; (c) 1.5 wt%; (d) 3.0 wt% and (e) 4.0 wt% (transversely divided sample) and (f) 1.5 wt% (longitudinally divided sample).
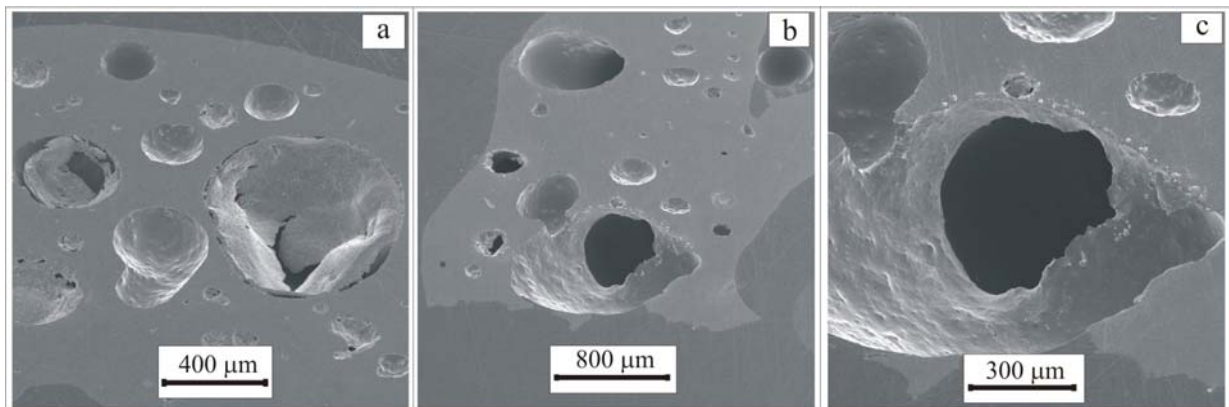
Fig. 19. SEM micrographs of porous Ti sample generated with MgTiO$_3$/graphite as foaming agent: (a) porous surface, (b) interconnective pore and (c) interconnectivity of pore with rough cell wall

With the increasing amount of foaming agent, the spherical small pores are partially transformed to deformed ellipsoidal or deformed spherical pores. The longitudinally divided sample in Fig. 18(f) shows that the pore spatial distribution is homogeneous, and shape and size

of pores do not show any significant variations. Microstructural observation using SEM and micro-CT analyses reveal that interconnectivity of pores in the titanium matrix. In SEM micrographs (Fig. 19) it is found that pore with increased pore diameter with rough cell wall are interconnective within the sample. While optical and SEM micrographs do not allow an assessment of the real three-dimensional pore structure, the accurate and non-destructive micro-CT measurements offer a 2D and 3D view of the porosity, pore connectivity and pore morphology of the specimens as given in Fig. 20. This result confirms that the pores are partly connected to each other. Additionally, it can be demonstrated that big pores are surrounded by coexisting small pores. In electron microprobe analysis, as residual material of foaming agent Ti could be found in the specimens after the foaming process. Additionally, micro-XRF analysis result also shows that only Ti is present in the specimen after foaming process. Moreover, laser ablation coupled with MC-ICPMS has been employed to determine the residual material of the foaming agent in porous Ti matrix. As Ti^{2+} is the major interference on ^{24}Mg, ^{25}Mg and ^{26}Mg therefore, in presence of a huge amounts of Ti^{2+} ions ^{24}Mg could not be deciphered from the 24 amu signal. As a result of this interference magnesium has not been determined. The porosity of porous Ti samples was determined by micro-CT imaging and analysis, and by MGDM and IBM of the representative samples. The estimated porosity of the different porous samples is shown in Table 6. The obtained results are comparable to each other.
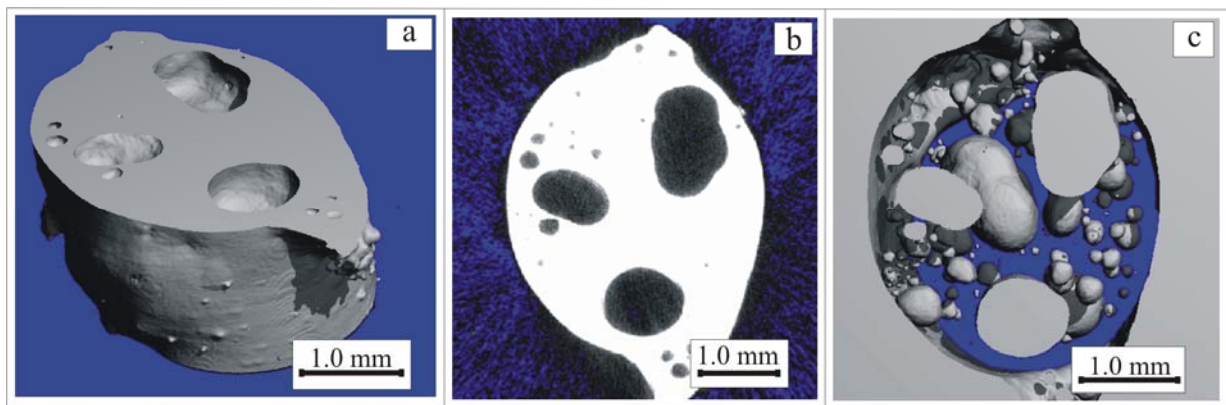
Fig. 20. micro-CT images of Ti sample representing (a) a 3D-view of a sample compared to a (b) 2D-picture and (c) an inverted 3D-picture showing pores as solid structure.

Table 6: The obtained porosity of porous Ti samples generated with various foaming agent

Foaming materials	Wt% of FA	Obtained total porosity /vol%		
		By MGDM	By MCTM	By IBM
$CaWO_4$/graphite	0.25	-	6.6	4.2
	0.50	-	9.7	6.1
	1.0	-	10.4	4.7
$MgTiO_3$/graphite	0.25	18.5 $\pm$ 1.9	18.1	11.2
	0.50	18.5 $\pm$ 1.8	20.5	15.9
	0.75	19.5 $\pm$ 1.5	20.6	20.8
	1.0	21.5 $\pm$ 1.5	21.2	19.5
	1.5	22.0 $\pm$ 1.5	22.1	20.1
$MgCO_3$	0.25	16.0 $\pm$ 1.2	-	-
	0.50	21.8 $\pm$ 1.8	-	-
	1.0	24.4 $\pm$ 1.5	-	-
$MgCO_3$/graphite	0.25	29.9 $\pm$ 1.4	-	-
	0.50	33.1 $\pm$ 1.9	-	-
	0.75	43.3 $\pm$ 1.1	-	-
$MgTiO_3$/graphite + $MgCO_3$	0.10 + 0.75	22.0 + 1.5	23.1	
	0.50 + 0.05	18.5 $\pm$ 1.8	17.5	14.5
	0.50 + 0.10	-	21.4	
	0.50 + 0.50	-	21.3	14.8
	0.75 + 0.05	-	20.5	13.9
	0.75 + 0.25	-	-	20.8
	0.25 + 0.75	-	-	20.1
	1.00 + 0.50	-	-	19.6
Li_2TiO_3	0.25	24.2 $\pm$ 1.0	-	-
	0.50	32.4 $\pm$ 1.4	-	-
	1.0	-	-	27.8
	1.5	-	-	28.4
Li_2TiO_3/graphite	0.25	23.1 $\pm$ 1.5	-	-
	0.50	36.1 $\pm$ 1.5	-	-
	0.75	34.2 $\pm$ 1.4	-	-
	1.0	27.5 $\pm$ 1.5	-	-
$LiNbO_3$/graphite	0.25	18.0 $\pm$ 2.0		
	0.75	30.0 $\pm$ 1.5	-	22.2
	1.5	31.5 $\pm$ 1.8	-	25.6
	3.0	33.2 $\pm$ 1.2		
	4.0	35.1 $\pm$ 1.6	-	-
ZrO_2	0.25	5.2 $\pm$ 1.2	-	-
	0.50	8.2 $\pm$ 1.4	-	-
	0.75	-	-	5.3
	4.0	12.1 $\pm$ 1.2	-	-

MGDM = Mass and geometric dimension method, MCTM = micro-CT method, IBM = Immersion-buoyancy method. In second column the amount of two component foaming agent (e.g. 0.1 + 0.75) are: $MgTiO_3$/graphite = 0.1 wt% and $MgCO_3$ = 0.75 wt%

3.4. Results obtained with magnesium carbonate and magnesium carbonate/graphite as foaming agents

We have also tried magnesium carbonate with and without using graphite as reducing component, as foaming agent. Porous Ti structures could be generated with 0.25 wt%-5.0 wt% of $MgCO_3$ as foaming agent. The optical micrographs of the generated polished samples are shown in Fig. 21 (a-c). From the optical micrographs it is apparently observed that pores with various pore diameters and pore shapes are randomly distributed across the whole areas of the generated samples. The porous sample structure generated with 0.25 wt% of $MgCO_3$, deformed spherical (big) pores with average pore diameter of about 690 μm, spherical (medium) pores with average pore diameter of about 320 μm, also spherical (small) pores with average pore diameter of about 220 μm and spherical (smallest) pores with average pore diameter of about 120 μm are observed. Again, in the sample generated with 0.50 wt% of foaming agent, deformed spherical (big) pore with pore diameter of about 1350 μm, also deformed spherical (medium) pores with average pore diameter of about 710 μm, spherical (small) pores with average pore diameter of about 390 μm and also spherical (smallest) pores with average pore diameter of about 130 μm are found. The pores are merging in the sample generated with 1.0 wt% of foaming agent which is clearly observed in Fig. 21 (c). Therefore, with the increasing amounts of foaming agent size and shape of the pores significantly changes. Anyway, for higher percentages of foaming agent unstable foaming process was observed. In the SEM micrograph (Fig. 22 a) it is found that big pores are interconnective whereas small pores are not interconnective. The maximum porosity determined by MGDM is 24.4 $\pm$ 1.5% in this case. Anyway, with electron microprobe, micro-XRF analyses it was not possible to detect residual elements of foaming agent after laser process. Additionally, in laser ablation coupled with MC-ICPMS analysis as Ti^{2+} ions is the main interference on ^{24}Mg, ^{25}Mg and ^{26}Mg therefore, in presence of a high amount of titanium, magnesium could not be determined.
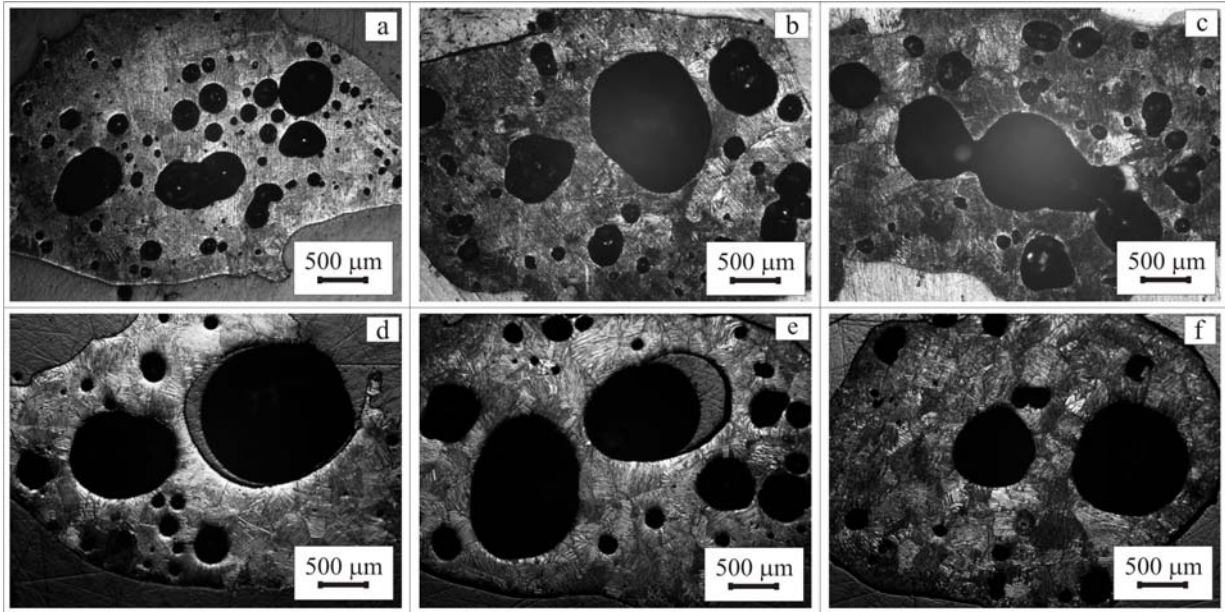
Fig. 21. Optical micrographs of generated Ti samples with: (a) 0.25 wt%, (b) 0.50 wt% and (c) 1.0 wt% MgCO$_3$ as a foaming agent; (d) 0.25 wt%, (e) 0.50 wt% and (f) 1.0 wt% MgCO$_3$/graphite as a foaming agent.

Also a mixture of MgCO$_3$ and graphite (molar ratio of MgCO$_3$:C = 2:1) could be used to generate porous Ti sample with significant porous structures. Optical micrographs of some of the porous Ti structures are shown in Fig. 21 (d-f). Pores are also randomly distributed across the whole areas of samples generated with this foaming agent. In porous sample generated with 0.25 wt% foaming agent ellipsoidal (big) pores with average pore diameter of about 1610 μm, deformed spherical (medium) pores with average pore diameter of about 1005 μm, also deformed spherical (small) pores with average pore diameter of about 375 μm and spherical (smallest) pores with average pore diameter of about 150 μm are observed. For sampled generated with 0.50 wt% of foaming agent, ellipsoidal (big) pores with average pore diameter of about 1300 μm, deformed spherical (medium) pores with average pore diameter of about 580 μm, spherical (small) pores with average pore diameter of about 370 μm and also spherical (smallest) pores with average pore diameter of about 130 μm are found. The pore diameters found in these samples are relatively high compared to the samples generated with corresponding amounts of pure MgCO$_3$ as foaming agent. The pore diameters of generated pores for various foaming agents can be shown in Table 7. Pores with comparably decreasing pore diameter are found for higher percentages (0.75 wt% and 1.0 wt%) of foaming agents which has not been seen in the samples generated with only MgCO$_3$ as foaming agent.

Interconnectivity of pores is found in SEM (Fig. 22 b, c) and micro-CT imaging and analysis. Anyway, in this case maximum total porosity of 43.3 $\pm$ 1.1% has been determined by MGDM.

Table 7: Diameters of different pores in porous Ti sample created with $MgCO_3$ and $MgCO_3$/graphite as foaming agent

Foaming material	Amounts of FA	Pore diameters /μm			
		Big	Medium	Small	Smallest
$MgCO_3$	0.25 wt%	690 (D. sphr)	320 (sphr)	220 (sphr)	120 (sphr)
	0.50 wt%	1350 (D. sphr)	710 (D. sphr)	390 (sphr)	130 (sphr)
	1.0 wt%	Big ellip.	550 (D. sphr)	320 (sphr)	130 (sphr)
$MgCO_3$/graphite	0.25 wt%	1610 (ellip)	1005 (D. sphr)	375 (D. sphr)	150 (sphr)
	0.50 wt%	1300 (ellip)	580 (D. sphr)	370 (sphr)	130 (sphr)
	1.0 wt%	1160 (ellip)	860 (D. sphr)	300 (sphr)	140 (sphr)

Pore shapes are mentioned in parenthesis. ellip = ellipsoidal, D. = deformed, sphr = spherical
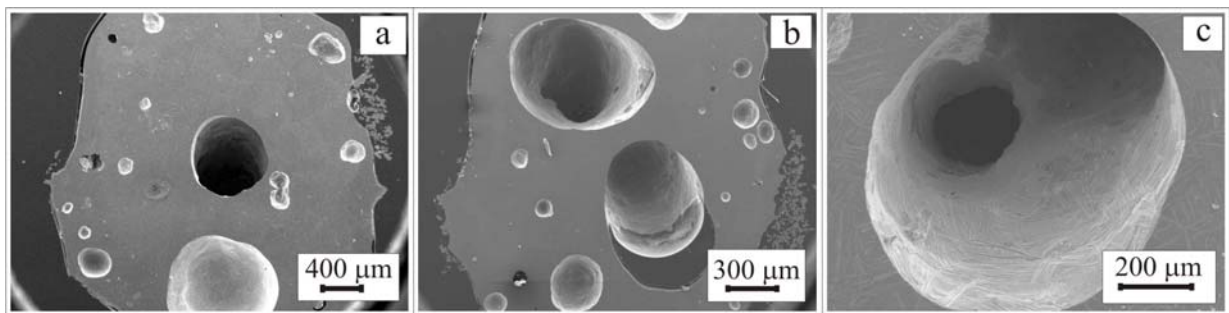
Fig. 22. SEM micrographs of porous Ti sample generated with $MgCO_3$ and $MgCO_3$/graphite as foaming agent: (a) pores interconnectivity, (b) big interconnective pores with rough cell wall and (c) inside environment of big pore.

The electron microprobe and micro-XRF analyses results show as residual material of foaming agent no detectable magnesium present in the material matrix after laser process. Additionally, in laser ablation coupled with MC-ICPMS analysis because of the interfearnce effect (as mentioned earlier) only Ti was found.

3.5. Results obtained with magnesium metatitanate/graphite with magnesium carbonate as foaming agent

In presence of various amounts of $MgCO_3$ porous Ti could be generated with $MgTiO_3$/graphite as foaming agent in laser induced foaming process. In presence of $MgCO_3$ to understand the potentiality of $MgTiO_3$/graphite as a foaming agent various amounts (0.1 wt% to 1.0 wt%) was used to generate the porous Ti structures. The amounts of $MgCO_3$ (0.1 wt%-1.0 wt%) were varying by keeping constant amount of $MgTiO_3$/graphite in each case (e.g. 0.1 wt%, 0.25 wt% etc.). The resulting porous samples were optically inspected and micrographs are shown in Fig. 23. In sample generated with 0.1 wt% $MgTiO_3$/graphite and 0.75 wt% $MgCO_3$, deformed spherical (big) pores with average pore diameter of about 660 μm, spherical (medium) pores with average pore diameter of about 370 μm, also spherical (small) pores with average pore diameter of about 205 μm and also spherical (smallest) pores with average pore diameter of about 50 μm are found. Additionally, deformed ellipsoidal pore with an increased pore diameter are found in this case. For generated Ti sample with 0.25 wt% of $MgTiO_3$/graphite and 0.25 wt% $MgCO_3$ deformed spherical (big) pores with average pore diameter of about 635 μm, deformed spherical (medium) pores with average pore diameter of about 350 μm, spherical (small) pores with average pore diameter of about 230 μm and also spherical (smallest) pores with average pore diameter of about 180 μm are observed. The effect of $MgTiO_3$/graphite and $MgCO_3$ on pores diameter can be visualized in Table 8 and Fig. 24.

It can be seen from the Table 8 and Fig. 24, the pore diameters of different pores increase with the addition of $MgTiO_3$/graphite and $MgCO_3$. The significant changes in pore diameter were found with addition of $MgCO_3$ while a slight change was observed with the increase of $MgTiO_3$/graphite amounts. Therefore, in presence of $MgCO_3$, as a foaming agent $MgTiO_3$/graphite could generate pores with increased pore diameter compared to samples generated with corresponding amount of only $MgTiO_3$/graphite. For higher amounts of the foaming agent materials unstable porous structures were produced. In samples generated with some amounts of foaming materials (e.g. a mixture of 0.50 wt% $MgTiO_3$/graphite and 0.50 wt% $MgCO_3$), the adjacent small pores merging are observed (Fig. 23 a, c, d). Anyway, the maximum total porosity of 23.1% has been calculated by MCTM in this case.
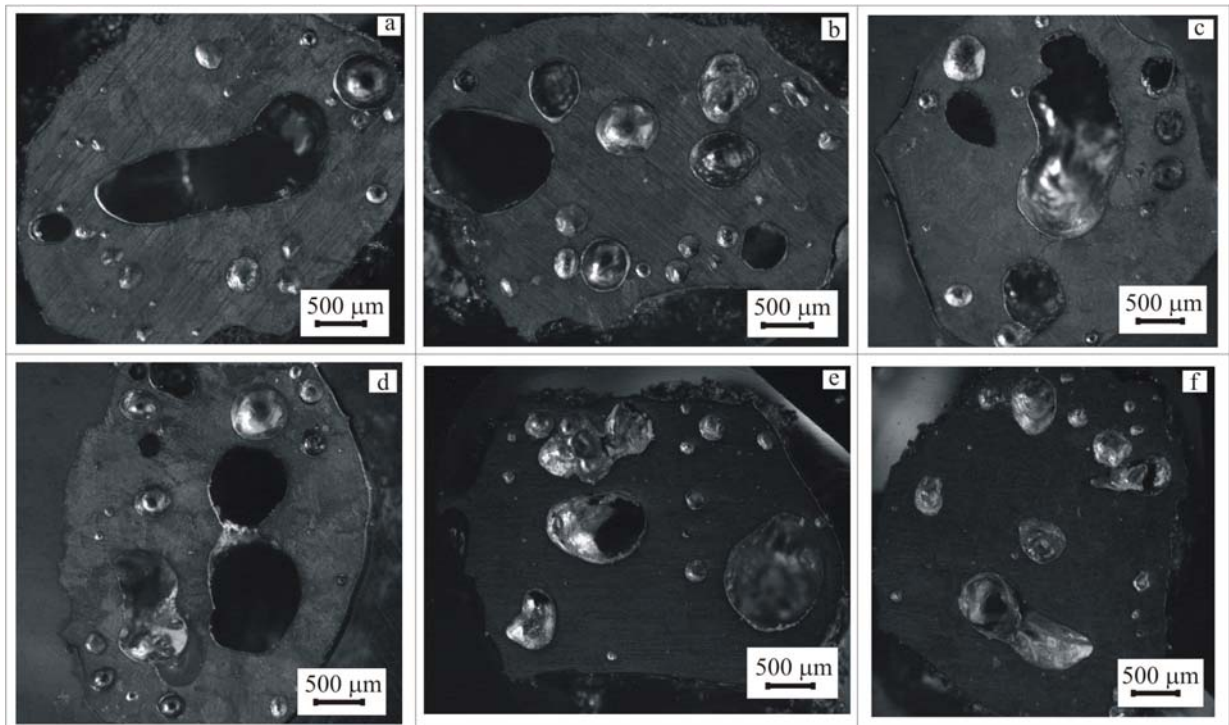
Fig. 23. Optical micrographs of porous Ti metal generated with a mixture of $MgTiO_3$/graphite and $MgCO_3$: (a) 0.1 wt% $MgTiO_3$/graphite and 0.75 wt% $MgCO_3$; (b) 0.25 wt% $MgTiO_3$/graphite and 0.25 wt% $MgCO_3$; (c) 0.50 wt% $MgTiO_3$/graphite and 0.05 wt% $MgCO_3$; (d) 0.50 wt% $MgTiO_3$/graphite and 0.1 wt% $MgCO_3$; (e) 0.75 wt% $MgTiO_3$/graphite and 1.0 wt% $MgCO_3$; (f) 1.0 wt% $MgTiO_3$/graphite and 0.1 wt% $MgCO_3$.

The SEM and micro-CT imaging (Fig. 25) and analysis show that big pores are interconnective while small pores are not interconnective. Anyway, electron microprobe and micro-XRF analyses results show that as residual material of foaming agent no detectable magnesium is present in the specimen after laser process. Moreover, in laser ablation coupled with MC-ICPMS analysis similar interference effect as before is observed. Therefeore, Ti can be detected by the measurement.
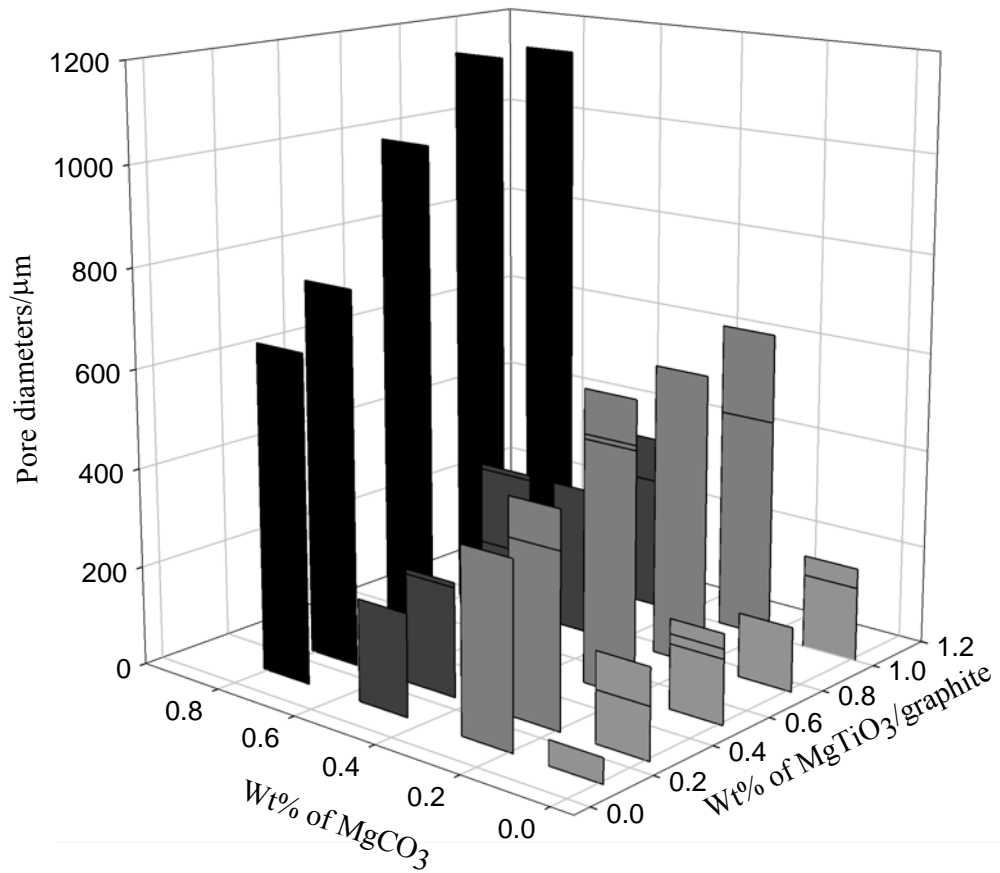
Fig. 24. The effect of the amounts of foaming materials on pore diameter in the porous Ti samples.
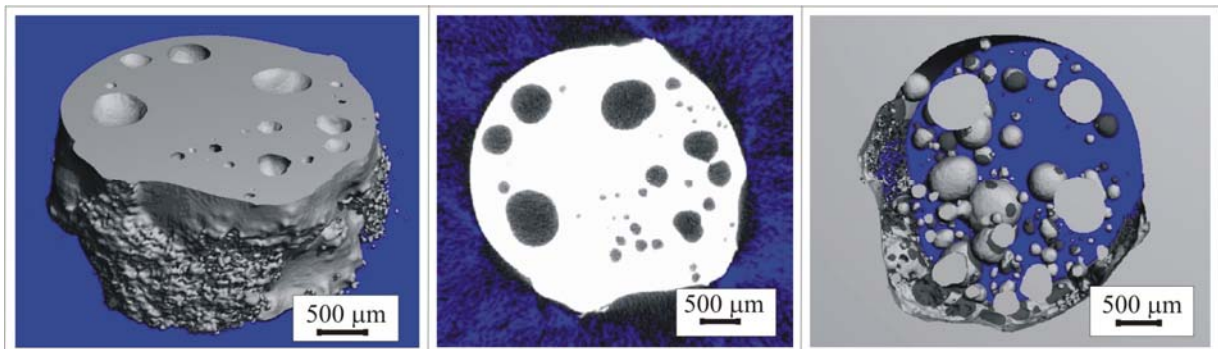
Fig. 25. micro-CT images of porous Ti sample generated with a mixture of $MgTiO_3$/graphite and $MgCO_3$: (a) a 3D-view of a sample compared to (b) 2D-picture and (c) an inverted 3D-picture showing pores as solid structure.

Table 8: Diameters of different pores in porous Ti samples generated with $MgTiO_3$/graphite as foaming agent with various amounts of $MgCO_3$

$MgTiO_3$/graphite	$MgCO_3$	Pore diameters /µm			
		Big	Medium	Small	Smallest
0.1 wt%	0.75 wt%	660 (D. sphr)	370 (sphr)	205 (sphr)	50 (sphr)
0.25 wt%	0.25 wt%	635 (D. sphr)	350 (D. sphr)	230 (sphr)	180 (sphr)
0.25 wt%	0.50 wt%	760 (D. sphr)	430 (D. sphr)	220 (sphr)	105 (sphr)
0.50 wt%	0.05 wt%	780 (D. sphr)	500 (D. sphr)	380 (sphr)	180 (sphr)
0.50 wt%	0.1 wt%	1010 (ellip)	589 (D. sphr)	390 (sphr)	130 (sphr)
0.50wt%	0.75 wt%	820 (D. sphr)	490 (D. sphr)	230 (sphr)	150 (sphr)
0.75 wt%	1.0 wt%	1160 (ellip)	590 (D. sphr)	300 (sphr)	130 (sphr)
1.0 wt%	0.1 wt%	600 (D. sphr)	450 (sphr)	270 (sphr)	150 (sphr)
1.0 wt%	0.75 wt%	1150 (ellip)	630 (D. sphr)	360 (sphr)	190 (sphr)

In parenthesis pore shapes are expressed. The elaboration of abbreviated forms of pore shapes is mentiond before.

3.6. Results obtained with lithium titanate and lithium titanate/graphite as foaming agents

We have also tried lithium titanate with and without using graphite as reducing component, as foaming agent. Porous Ti structures could be generated with 0.25 wt% to 5.0 wt% of Li_2TiO_3 as foaming agent. Optical micrographs of the polished porous samples are shown in Fig. 26 (a-c). It is apparently found that the pores are randomly distributed across the whole areas of the specimen. In sample generated with 0.25 wt% of Li_2TiO_3 as foaming agent, ellipsoidal (big) pores with average pore diameter of about 750 µm, deformed spherical (medium) pores with average pore diameter of about 450 µm, spherical (small) pores with average pore diameter of about 250 µm and also spherical (smallest) pores with average pore diameter of about 130 µm are observed. Again, ellipsoidal (big) pores with average pore diameter of about 750 µm, deformed spherical (medium) pores with average pore diameter of about 450 µm, also deformed spherical (small) pores with average pore diameter of about 240 µm and spherical (smallest) pores with average pore diameter of about 130 µm are found in sample created with

0.50 wt% of foaming agent. Altogether increased diameters of pores are found for samples generated with higher amounts of Li_2TiO_3. Nevertheless, in this case relatively homogeneous pore distribution is found. The pores diameter of Ti samples generated with Li_2TiO_3 as foaming agent are shown in Table 9.
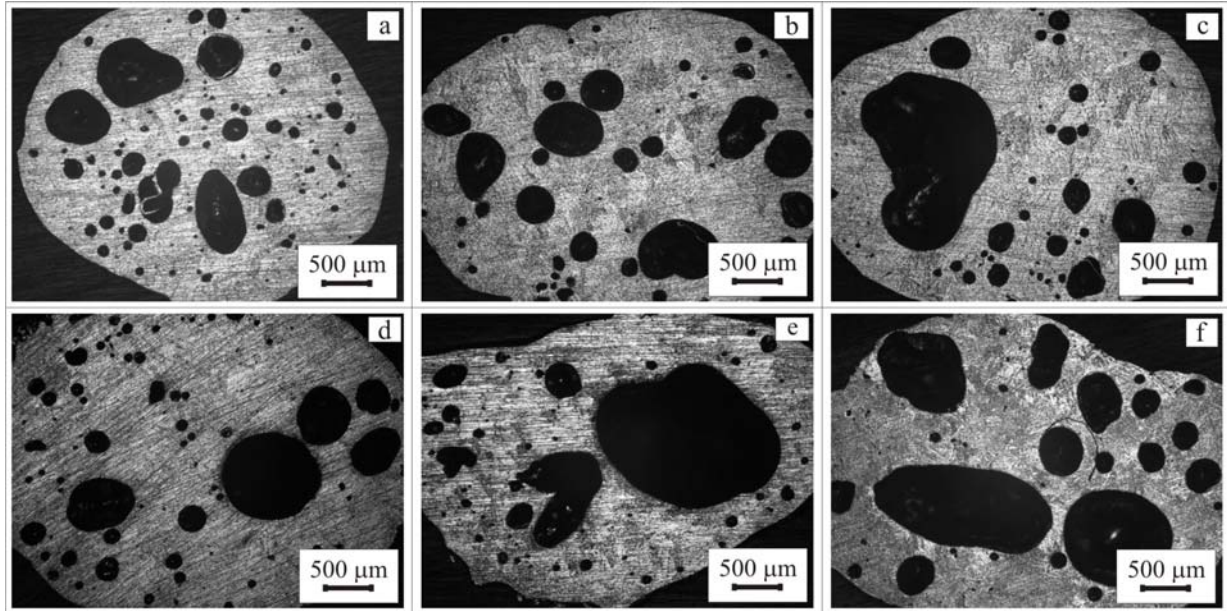
Fig. 26. Optical micrographs of generated porous Ti samples with pure Li_2TiO_3 and Li_2TiO_3/graphite: (a) 0.25 wt% (b) 0.75 wt% and (c) 1.0 wt% of Li_2TiO_3; (d) 0.25 wt%, (e) 0.50 wt% and (f) 1.0 wt% of Li_2TiO_3/graphite as foaming agents.

The SEM (Fig. 27) and micro-CT imaging and analysis confirm that the pores with increased diameter are interconnective while small pores are not interconnective with each other. Nevertheless, maximum total porosity calculated by MGDM in this case is $32.4 \pm 1.4\%$.

Laser ablation coupled with MC-ICPMS has been employed to determine the residual material of the foaming agent in Ti sample matrix with the use of a secondary electron multiplier (SEM). In the case of the mass 7 a low signal was observed but its instability and the shape of the peak can not point on [7]Li alone. Therefore, Li could not be deciphered either with certainty. With careful experiments producing Ti matrix with different amounts of Li, Li content in the sample may be deciphered. Due to lack of sufficient Li standard, additional experiments could not be carried out.

Fig. 27. SEM micrographs of porous Ti samples generated with Li_2TiO_3 as foaming agent: (a) overview of the porous surface, (b) surface morphology and (c) big interconnective pore.

Table 9: Pore diameters of pores in samples generated with pure Li_2TiO_3 and Li_2TiO_3/graphite

Foaming materials	Amounts of FA	Pore diameters /μm			
		Big	Medium	Small	Smallest
Li_2TiO_3	0.25 wt%	750 (ellip)	450 (D. sphr)	250 (sphr)	130 (sphr)
	0.50 wt%	750 (ellip)	450 (D. sphr)	240 (D. sphr)	130 (sphr)
	0.75 wt%	720 (ellip)	400 (sphr)	250 (sphr)	130 (sphr)
	1.0 wt%	Big void	460 (D. sphr)	260 (D. sphr)	130 (sphr)
Li_2TiO_3/graphite	0.25 wt%	850 (D. sphr)	520 (D. sphr)	250 (sphr)	150 (sphr)
	0.50 wt%	1450 (ellip)	800 (D. sphr)	330 (sphr)	140 (sphr)
	0.75 wt%	1200 (ellip)	500 (D. sphr)	300 (sphr)	150 (sphr)
	1.0 wt%	1000 (ellip)	520 (D. sphr)	280 (sphr)	190 (sphr)

In parenthesis shapes of generated pore in various porous samples are mentioned. The elaboration of abbreviated forms is mentiond before.

Also a mixture of Li_2TiO_3 and graphite (molar ratio of Li_2TiO_3:C = 2:3) could be used to generate porous Ti with significant porous structures. In this case, 0.25 wt%-5.0 wt% foaming agent could be provided to generate Ti sample. Optical micrographs of some of the porous Ti structures are shown in Fig. 26 (d-f). From optical micrographs of generated polished sample surfaces it is apparently observed that pores with different pore diameters and pore shapes are randomly distributed across the whole areas of specimen. In porous sample generated with 0.25 wt% of foaming agent deformed spherical (big) pores with average pore diameter of about 850 μm, also deformed spherical (medium) pores with average pore diameter of about 520 μm,

spherical (small) pores with average pore diameter of about 250 μm and also spherical (smallest) pores with average pore diameter of about 150 μm are observed. Again, big ellipsoidal (big) pore with pore diameter of about 1450 μm, deformed spherical (medium) pores with average pore diameter of about 800 μm, spherical (small) pores with average pore diameter of about 330 μm and also spherical (smallest) pores with average pore diameter of about 130 μm are found in sample created with 0.50 wt% of foaming agent. In general, for higher amounts of foaming agent pores with increasing pore diameters were observed. The generated pore diameter for various samples is given in Table 9. The pore diameters found in these samples generated with Li_2TiO_3/graphite as foaming agent are relatively high compared to the samples generated with corresponding amounts of pure Li_2TiO_3 as foaming agent.
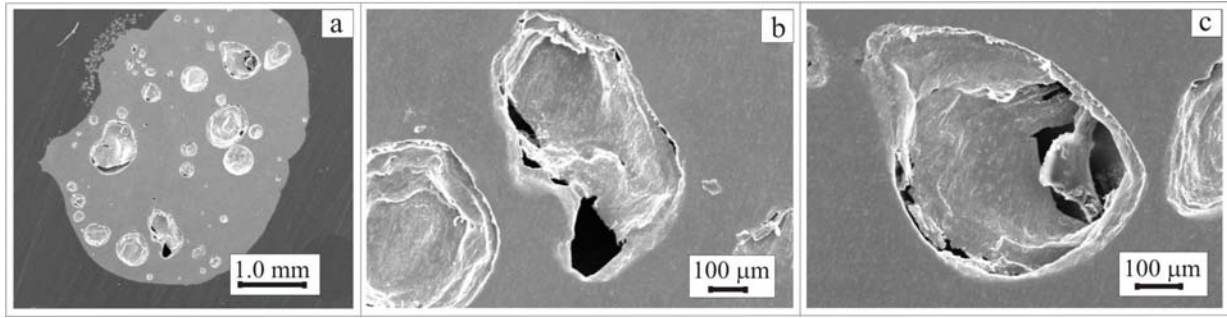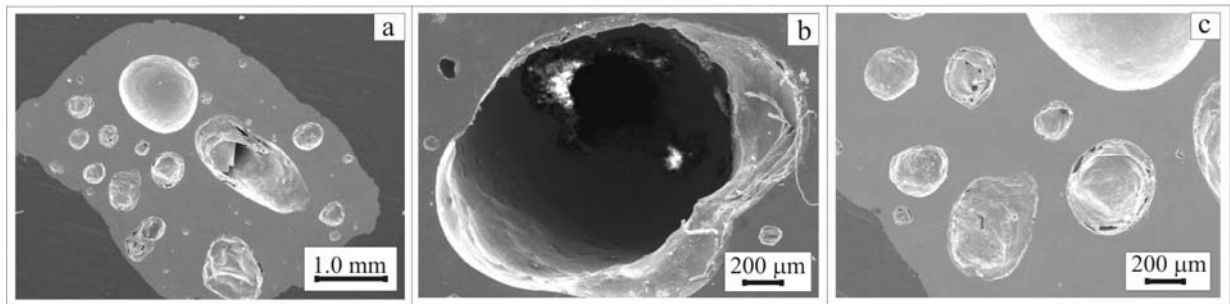

Fig. 28. SEM micrographs of porous Ti samples generated with Li_2TiO_3/graphite as foaming agent: (a) overview of the porous surface, (b) a big and a small interconnective pores (c) porous surface structure showing more pores.

The SEM (Fig. 28) and micro-CT image and analysis reveal that the pores with increasing pore diameter are interconnective within the sample while the small pores are not interconnective. Anyway, the obtained total porosity found for this foaming agent is $36.1 \pm 1.5\%$ (calculated by MGDM). To determine the residual material of foaming agent by laser ablation coupled with MC-ICPMS similar observation as before was realized.

3.7. Results obtained with lithium niobate/graphite as foaming agent

In our investigation lithium niobate and graphite (molar ratio of $LiNbO_3$: graphite = 2:3) as a foaming agent was also provided to generate Ti structure in laser induced foaming process. Anyway, porous Ti sample could be produced with this foaming agent from 0.25 wt% to 5.0 wt%. The porous samples were mechanically divided and polished and finally optically

inspected. The optical micrographs of generated samples are shown in Fig. 29. From optical investigation it is apparently found that the generated pores are randomly distributed across the whole areas of specimen. From the apparent view of the samples generated with lower percentages of foaming agent it is observed that the pores are nearly homogeneously distributed across the sample area.

Fig. 29. Optical micrographs of generated porous Ti samples with: (a) 0.25 wt%, (b) 0.75 wt% and (c) 3.0 wt% of LiNbO$_3$/graphite as foaming agent in laser induced foaming process.

In sample generated with 0.25 wt% of LiNbO$_3$/graphite, big ellipsoidal (big) pore with pore diameter of about 1350 μm, deformed spherical (medium) pores with average pore diameter of about 420 μm, also deformed spherical (small) pores with average pore diameter of about 260 μm and spherical (smallest) pores with average pore diameter of about 130 μm are found. Again, deformed ellipsoidal (big) pores with average pore diameter of about 1440 μm, deformed spherical (medium) pores with average pore diameter of about 500 μm, also deformed spherical (small) pores with average pore diameter of about 320 μm and spherical (smallest) pores with average pore diameter of about 130 μm are observed in sample generated with 0.75 wt% of foaming agent. Altogether in samples generated with higher percentages of foaming agents pores with relatively increasing pore diameters are found. The pore diameters of created pores can be shown in Table 10. Anyway, due to the shortage of LiNbO$_3$, the potentiality of only LiNbO$_3$ has not been investigated in the laser induced foaming process.

The SEM micrographs as in Fig. 30 show the pore distribution and surface structures of the generated porous Ti samples. The orientation of pores formation is quite [80] different compared to porous metal generated with other foaming agent. Additionally, in most cases both small and large pores are interconnective with each other. Again, micro-CT images show that

both of the small and big pores are interconnective within the sample. Anyway, the maximum total porosity obtained for this foaming agent is 35.1 $\pm$ 1.6% (determined by MGDM).

Table 10: The pore diameter of pores in porous Ti samples generated with LiNbO$_3$/graphite

Foaming material	Amounts of FA	Pore diameters /µm			
		Big	Medium	Small	Smallest
LiNbO$_3$/graphite	0.25 wt%	1350 (ellip)	420 (D. Sphr)	260 (D. sphr)	130 (sphr)
	0.50 wt%	1300 (ellip)	450 (D. Sphr)	250 (D. sphr)	130 (sphr)
	0.75 wt%	1440 (D. ellip)	500 (D. Sphr)	320 (D. Sphr)	130 (sphr)
	1.0 wt%	1400 (D. ellip)	530 (D. Sphr)	350 (D. Sphr)	130 (sphr)
	3.0 wt%	1450 (D. ellip)	650 (D. Sphr)	430 (D. Sphr)	180 (sphr)
	4. wt%	1420 (D. ellip)	600 (D. Sphr)	420 (sphr)	180 (sphr)

Laser ablation coupled with MC-ICPMS has been employed to determine the residual material of the foaming agent in porous Ti samples. Due to low signal Li could not be deciphered either with certainty. With careful experiments producing Ti matrix with different amounts of Li, the amount of Li in the sample may be deciphered. Because of interference effect trace amount of niobium content could not also be determined.
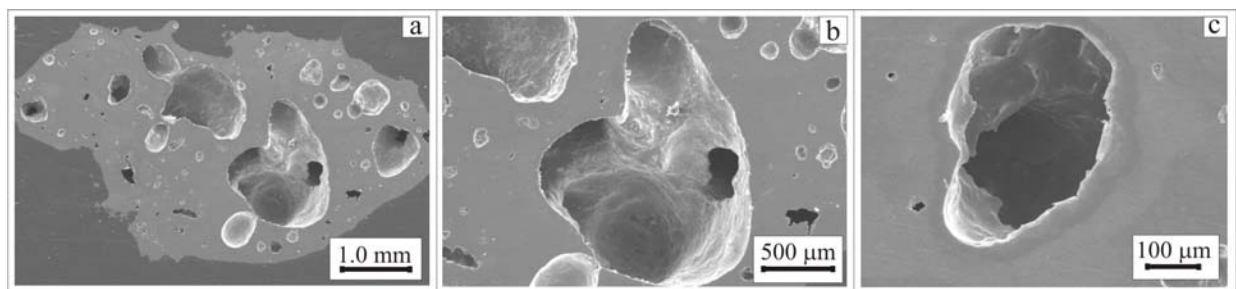
Fig. 30. SEM micrographs of porous Ti metal generated with LiNbO$_3$/graphite as foaming agent: (a) overview of the porous surface, (b) big interconnective pore showing rough cell wall and (c) small interconnective pore.

3.8. Results obtained with zirconium oxide and zirconium oxide/graphite as foaming agents

Zirconium oxide with and without using graphite as reducing agent, as foaming agents has been used to generate Ti porous structure in laser induced foaming process. Both of the cases, 0.25 wt% to 5.0 wt% foaming agents were provided to understand the potentiality of the foaming agents. Optical micrographs of sample generated with ZrO_2 as foaming agent are shown in Fig. 31. It is apparently visualized that the pores are randomly distributed across the whole areas of specimen. For lower percentages (e. g. 0.25 wt%-1.0 wt% of foaming agent) generally spherical pores with decreased pore diameters are found. In sample generated with 4.0 wt% of ZrO_2 big ellipsoidal pore (Fig. 31 c) with pore diameter of about 950 μm, also ellipsoidal (medium) pores with average pore diameter of about 420 μm, spherical (small)pores with average pore diameter of about 250 μm and also spherical (smallest) pores with average pore diameter of about 120 μm are observed. In this foaming agent case, small spherical pores are generated by various amounts of foaming agent. Anyway, similar pore formation behavior is also observed in the samples generated with ZrO_2/graphite as a foaming agent. The Table 11 shows pores diameters of different pores in the samples generated with ZrO_2 and ZrO_2/graphite as foaming agents.
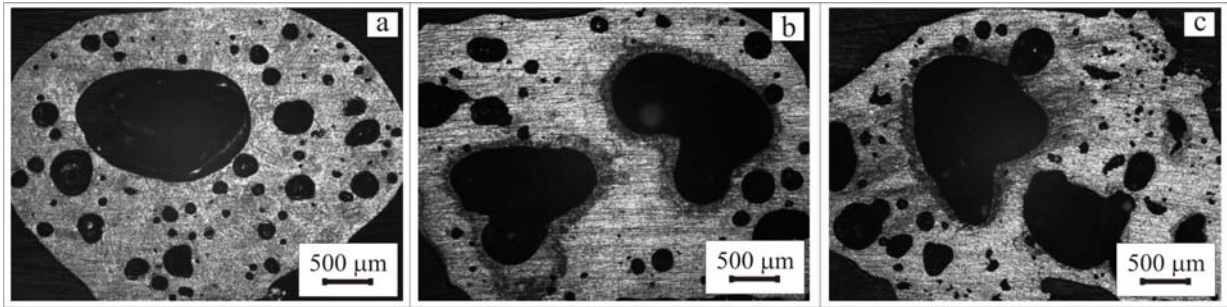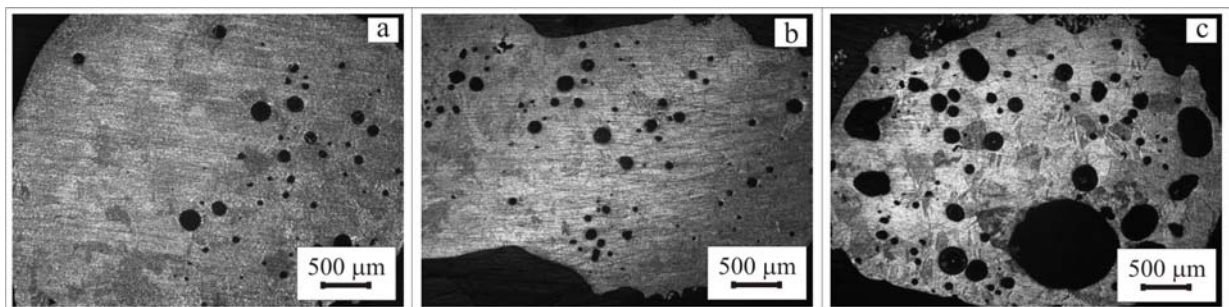

Fig. 31. Optical micrographs of generated porous Ti samples with: (a) 0.25 wt%, (b) 1.0 wt% and (c) 4.0 wt% of ZrO_2 as foaming agent in the laser induced foaming process.

The SEM (Fig. 32) and micro-CT images show that the pores with increased pore diameters are partially interconnective within the samples whereas small pore are not interconnective. Maximum total porosity of samples generated with ZrO_2 is $12.1 \pm 1.2\%$ while with ZrO_2/graphite is $13.1 \pm 1.6\%$. Microanalysis results show as a residual material of foaming agent no detectable zirconium was found in the Ti matrix.

Table 11: The pore diameter of pores in various porous Ti samples generated with ZrO_2 and ZrO_2/graphite

Foaming materials	Amounts of FA	Pore diameters /μm			
		Big	Medium	Small	Smallest
ZrO_2	0.25 wt%	-	210 (sphr)	120 (sphr)	70 (sphr)
	0.50 wt%	-	230 (sphr)	130 (sphr)	70 (sphr)
	1.0 wt%	-	170 (sphr)	90 (sphr)	60 (sphr)
	4.0 wt%	950 (ellip)	420 (ellip)	250 (sphr)	120 (sphr)
ZrO_2/graphite	0.25 wt%	-	220 (sphr)	120 (sphr)	70 (sphr)
	0.50 wt%	-	230 (sphr)	135 (sphr)	80 (sphr)
	1.0 wt%	-	250 (sphr)	140 (sphr)	80 (sphr)
	3.0 wt%	1000 (ellip)	450 (D. sphr)	280 (sphr)	130 (sphr)
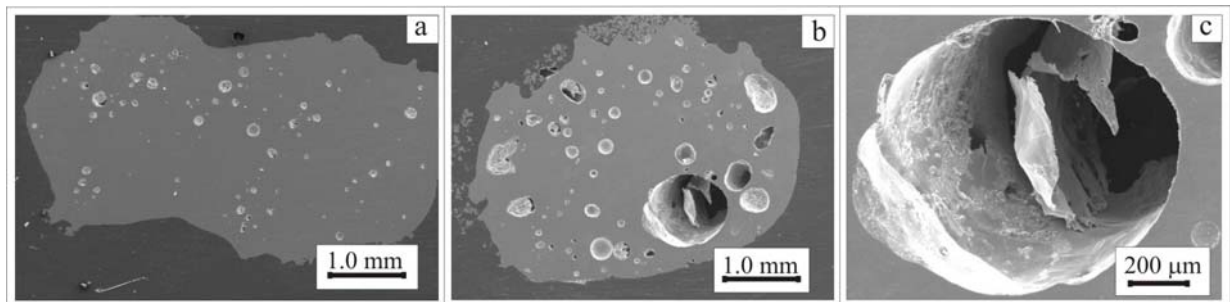
Fig. 32. SEM micrographs of porous Ti sample generated with pure ZrO_2 and ZrO_2/graphite as foaming agents: (a) overview of the porous surface generated with ZrO_2, (b) surface morphology of porous Ti metal generated with ZrO_2/graphite and (c) big interconnective pore with rough cell wall.

3.9. Results obtained with a mixture of MgTiO₃/graphite and Li₂TiO₃/graphite (MgT) as foaming agent

A mixture of $MgTiO_3$/graphite and Li_2TiO_3/graphite (mass ratio between MgTiO3/graphite and Li_2TiO_3/graphite is 1 to 1) was considered as a foaming agent for the generation of porous Ti structures in laser induced foaming process. To understand the potentiality of this system 0.25

wt% to 5.0 wt% of the foaming mixtures could be used in this case. The optical micrographs are shown in Fig. 33 after optical investigation of the mechanically divided polished samples. It is apparently visualized that the pores with different shapes and sizes are randomly distributed across the whole areas of specimen. In samples generated with 0.50 wt% of foaming agent ellipsoidal (big) pores with average pore diameter of about 1000 μm, deformed spherical (medium) pores with average pore diameter of about 630 μm, also deformed spherical (small) pores with average pore diameter of about 330 μm and spherical (smallest) pores with average pore diameter of about 130 μm are found. For lowest amount of foaming agent (e.g. 0.25 wt%) a big void (Fig. 33a) is produced in the sample surface. Addition to that spherical or deformed spherical pore with decreased pore diameters is also found in this case. Furthermore, sample generated with 1.0 wt% of foaming agent pores with decreasing pore diameters are produced while for higher percentages of foaming agents (e. g. 3.0 wt%) again pores with increasing diameters are observed. The pore diameters of pores in various generated samples can be shown in Table 12. Nevertheless, for higher amounts (>5.0 wt%) of foaming agents unstable foaming process was occurred.

Fig. 33. Optical micrographs of generated porous Ti samples with: (a) 0.25 wt%, (b) 0.50 wt% and (c) 1.0 wt% of a mixture of $MgTiO_3$/graphite and Li_2TiO_3/graphite as foaming agent.

The SEM micrographs as in Fig. 34 show the interconnectivity of the porosity in the specimen. Moreover, micro-CT images confirm that the pores are interconnected within the specimen. Anyway, maximum porosity determined for this porous Ti sample is $38.8 \pm 1.1\%$. Electron microprobe and micro-XRF analyses show no detectable magnesium as residual element of foaming agent is present in the Ti sample matrix. Additionally, regarding magnesium and lithium contents in the specimens after foaming process, laser ablation coupled with MC-ICPMS analysis shows similar effect as previously mentioned.

Table 12: The pore diameter of pores in Ti samples generated with a mixture of MgTiO₃/graphite and Li₂TiO₃/graphite as a foaming agent

Foaming material	Amounts of FA	Pore diameters /μm			
		Big	Medium	Small	Smallest
MgTiO$_3$/graphite and Li$_2$TiO$_3$/graphite	0.25 wt%	Big void	500 (D. sphr)	300 (sphr)	130 (sphr)
	0.50 wt%	1000 (ellip)	630 (D. sphr)	330 (D. sphr)	130 (sphr)
	1.0 wt%	-	480 (D. sphr)	270 (sphr)	130 (sphr)
	3.0 wt%	Big ellip.	500 (D. sphr)	320 (sphr)	140 (sphr)
	4.0 wt%	1300 (ellip)	550 (D. sphr)	330 (D. sphr)	150 (sphr)
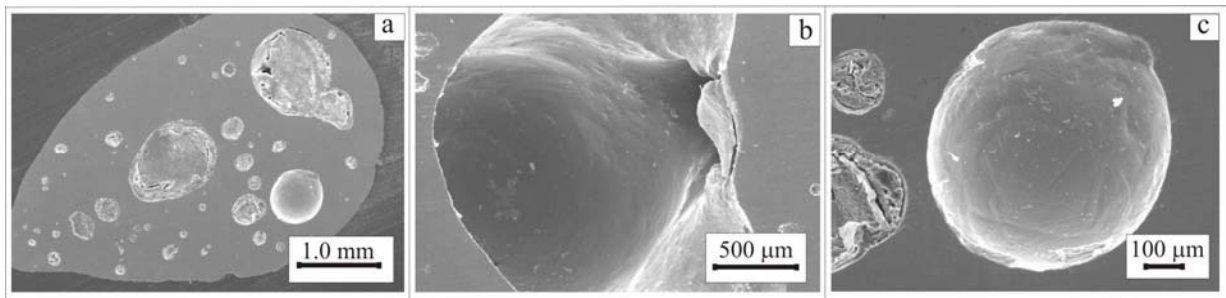
Fig. 34. SEM micrographs of porous Ti samples generated with a mixture of MgTiO$_3$/graphite and Li$_2$TiO$_3$/graphite as foaming agent: (a) overview of the porous sample surface, (b) big interconnective pore and (c) big pore showing rough cell wall.

3.10. Results obtained with a mixture of MgTiO₃/graphite, Li₂TiO₃/graphite and MgCO₃ (MTM) as foaming agent

For laser experiments 0.002 g of MgCO$_3$ was mixed with an equal amount mixture of MgTiO$_3$/graphite and Li$_2$TiO$_3$/graphite (mass ratio of MgTiO$_3$/graphite and Li$_2$TiO$_3$/graphite is 1 to 1) for considering it as a foaming agent. Porous Ti structure could be generated with 0.25 wt% to 5.0 wt% of MTM as foaming agent. The optimal energy per length unit input 1750 Wm/min was used in laser induced foaming process. Optical microscopic observation was carried out with generated porous structures and micrographs are shown in Fig. 35. It is apparently observed from the optical micrograph that pores with different size and shapes are randomly distributed across the whole areas of specimen. In sample generated with 0.25 wt% of

foaming agent ellipsoidal (big) pores with average pore diameter of about 720 μm, deformed spherical (medium) pores with average pore diameter of about 470 μm, spherical (small) pores with average pore diameter of about 200 μm and also spherical (smalles) pores with average pore diameter of about 100 μm are found. Again, ellipsoidal or deformed spherical (big) pores with average pore diameter of about 930 μm, deformed spherical (medium) pores with average pore diameter of about 450 μm, also deformed spherical (small) pores with average pore diameter of about 250 μm and spherical (smallest) pores with average pore diameter of about 100 μm are observed in sample generated with 0.50 wt% of MTM as foaming agent. Altogether pores with increasing pore diameter are found in the samples generated with higher amounts of foaming agent. The pore diameters of pores of generated samples can be shown in Table 13. For lower percentages (e. g. 0.25 wt%) of foaming agent pores with small size and nearly homogeneous pore distribution is observed. While for higher percentages (e.g. 1.0 wt%) of foaming agent ellipsoidal or deformed ellipsoidal pores with inhomogeneous pore distribution is found. Nevertheless, for higher amounts of foaming agents (>5.0 wt%) unstable porous structures was observed.
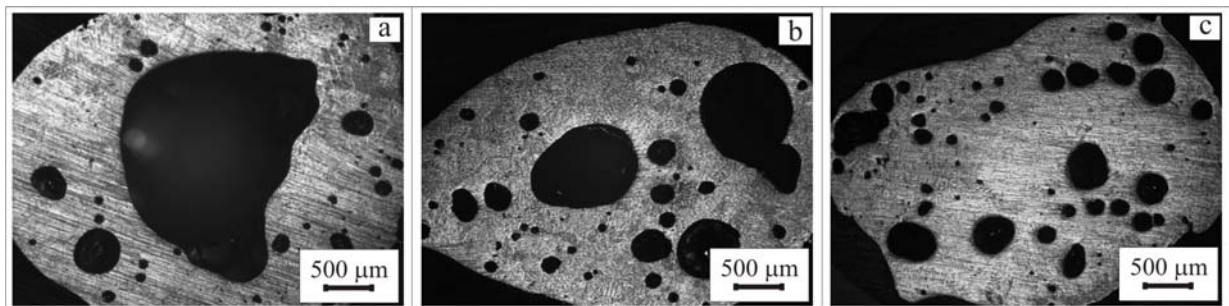

Fig. 35. Optical micrographs of porous Ti sample generated with: (a) 0.25 wt%, (b) 0.50 wt% and (c) 1.0 wt% of a mixture of MgTiO$_3$/graphite, Li$_2$TiO$_3$/graphite and MgCO$_3$ as foaming agent.

From SEM micrographs as in Fig. 36 it is found that in some cases both small and large pores are interconnective within the sample. Additionally, increased pore diameter with rouch cell wall is observed in a few cases. Moreover, micro-CT images show that pores are interconnective with each other in most of the cases. Maximum total porosity calculated by MGDM is 41.4 $\pm$ 1.5%. Ti samples were employed for compositional analysis by electron microprobe, micro-XRF and laser ablation coupled with MC-ICPMS. It was not possible to detect any other residual element except Ti of the foaminga gent.

Table 13: The pore diameter of pores in porous Ti samples generated with a mixture of MgTiO$_3$/graphite, Li$_2$TiO$_3$/graphite and MgCO$_3$ as a foaming agent; and a mixture of MgTiO$_3$/graphite, Li$_2$TiO$_3$/graphite and MgCO$_3$/graphite as foaming agent

Foaming materials	Amounts of FA	Pore diameters /μm			
		Big	Medium	Small	Smallest
MgTiO$_3$/graphite,	0.25 wt%	720 (ellip)	470 (D. sphr)	200 (sphr)	100 (sphr)
Li$_2$TiO$_3$/graphite	0.50 wt%	930 (ellip)	450 (D. sphr)	250 (D. sphr)	100 (sphr)
& MgCO$_3$	1.0 wt%	Very big	-	250 (sphr)	<50 (sphr)
	2.0 wt%	Very big	500 (D. sphr)	280 (D. sphr)	120 (sphr)
MgTiO$_3$/graphite,	0.25 wt%	1000 (D. sphr)	620 (D. sphr)	320 (sphr)	140 (sphr)
Li$_2$TiO$_3$/graphite	0.50 wt%	930 (ellip)	450 (D. sphr)	230 (sphr)	100 (sphr)
&	1.0 wt%	Very big	600 (D. sphr)	200 (sphr)	70 (sphr)
MgCO$_3$/graphite	2.0 wt%	Very big	630 (D. sphr)	300 (D. sphr)	140 (sphr)

Fig. 36. SEM micrographs of porous Ti sample generated with a mixture of MgTiO$_3$/graphite, Li$_2$TiO$_3$/graphite and MgCO$_3$ as foaming agent: (a) Overview of the porous surface, (b) big pore showing rough cell wall and (c) interconnective pores.

3.11. Results obtained with a mixture of MgTiO$_3$/graphite, Li$_2$TiO$_3$/graphite and MgCO$_3$/graphite (MTMC) as foaming agent

A small amount (0.002 g) of MgCO$_3$/graphite was mixed with an equal amount mixture of MgTiO$_3$/graphite and Li$_2$TiO$_3$/graphite (mixture following same ratio as before) and considered it as a foaming agent for laser induced Ti foaming process. With 0.25 wt% to 5.0 wt% of this

foaming agent could be used for the generation of Ti structure. Optical inspections of the mechanically divided porous samples were carried out and micrographs are shown in Fig. 37. From optical observations it is apparently visualized that pores with various shapes and sizes are randomly distributed across the whole sample areas. Anyway, in sample generated with 0.25 wt% of this foaming agent deformed spherical (big) pores with average pore diameter of about 1000 μm, also deformed spherical (medium) pores with average pore diameter of about 620 μm, spherical (small) pores with average pore diameter of about 320 μm and also spherical (smallest) pores with average pore diameter of about 140 μm are found. Again, a very big ellipsoidal pores and additionally, deformed spherical (big) pores with average pore diameter of about 930 μm, also deformed spherical (medium) pores with average pore diameter of about 450 μm, spherical (small) pores with average pore diameter of about 230 μm and also spherical (smallest) pores with average pore diameter of about 100 μm are found in sample generated with 0.50 wt% of MTMC. Altogether pores with increasing pore diameter are found for higher percentages of foaming agent. The pore size of various pores in generated porous samples is tabulated in Table 13. Nevertheless, for higher percentages of foaming agent unstable foaming process was observed. The porosity was determined and maximum total porosity found is 36.2 ± 1.5% for this sample.
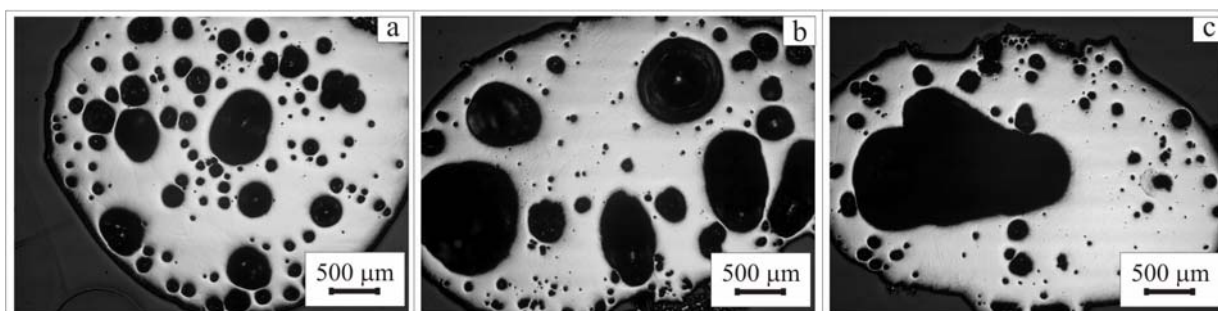

Fig. 37. Optical micrographs of generated porous Ti sample with: (a) 0.25 wt%, (b) 0.50 wt% and (c) 1.0 wt% of a mixture of $MgTiO_3$/graphite, Li_2TiO_3/graphite and $MgCO_3$/graphite as foaming agent.

SEM micrographs of the Ti samples as in Fig. 38 show that both of the small and large pores in a few cases are interconnective with each other. Additionally, micro-CT images showed that the interconnectivity of pores within the samples. In electron microprobe, micro-XRF and MC-ICPMS analyses no detectable magnesium or lithium is found in the porous samples after laser process.
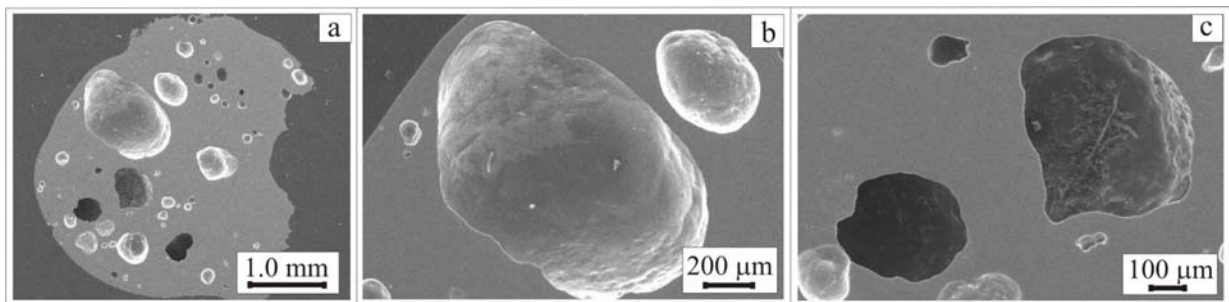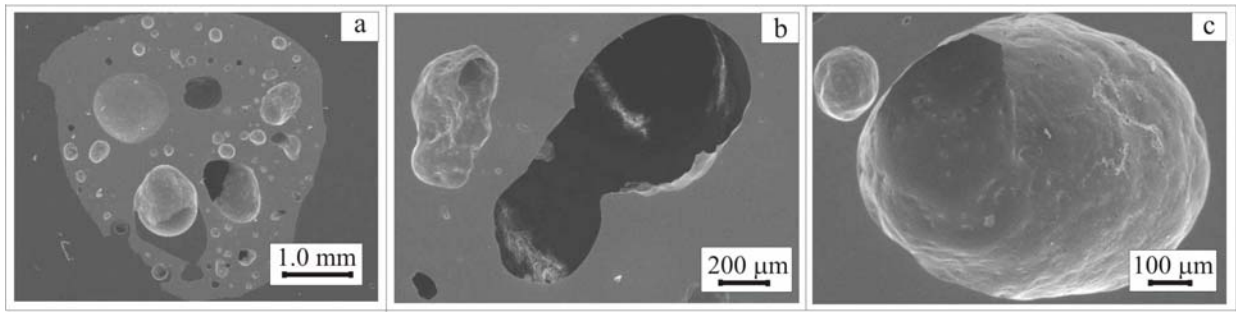
Fig. 38. SEM micrographs of porous Ti sample generated with a mixture of MgTiO$_3$/graphite, Li$_2$TiO$_3$/graphite and MgCO$_3$/graphite as foaming agent: (a) Overview of the porous surface, (b) deformed ellipsoidal interconnective pore and (c) a pore showing rough cell wall.

3.12. Results obtained with a mixture of MgTiO$_3$/graphite and LiNbO$_3$/graphite (MLN) as foaming agent

A mixture of MgTiO$_3$/graphite and LiNbO$_3$/graphite (mass ratio of MgTiO$_3$/graphite and Li$_2$TiO$_3$/graphite = 1:1) as foaming agent was used for the laser induced Ti foaming process. In this case, 0.25 wt% to 5.0 wt% of this foaming agent could be provided to generate Ti structure. The optimal energy per length unit input 1750 Wm/min can be used to get porous structures. After laser experiments the specimens were mechanically divided and optical investigations were carried out. Optical micrographs of generated Ti samples are shown in Fig. 39. It is apparently observed that pores with different shapes and sizes are randomly distributed across the whole sample areas. In sample generated with 0.25 wt% of MLN deformed spherical (big) pores with average pore diameter of about 550 μm, spherical (medium) pores with average pore diameter of about 300 μm, spherical (small) pores with average pore diameter of about 180 μm and also spherical (smallest) pores with average pore diameter of about 100 μm are found. Again, deformed spherical (big) pores with average pore diameter of about 600 μm, also deformed spherical (medium) pores with average pore diameter of about 430 μm, also deformed spherical (small) pores with average pore diameter of about 280 μm and spherical (smallest) pores with average pore diameter of about 150 μm are observed in porous Ti sample generated with 0.50 wt% of foaming agent.
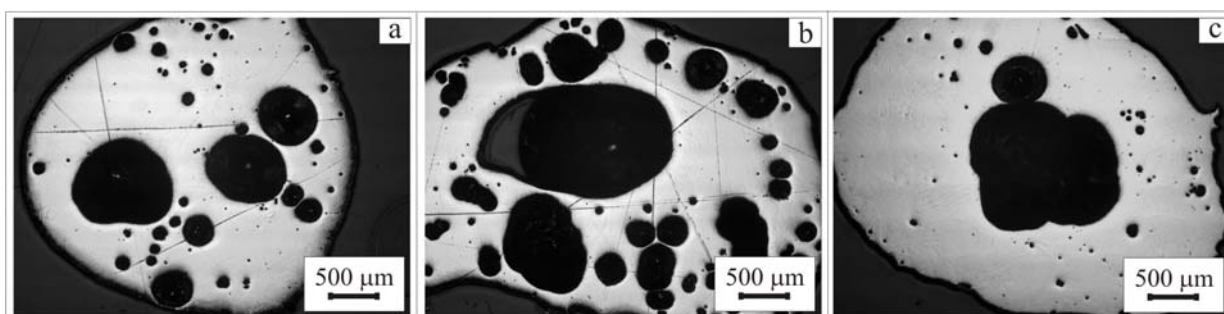
Fig. 39. Optical micrographs of generated porous Ti samples with: (a) 0.25 wt%, (b) 0.50 wt% and (c) 1.0 wt% of a mixture of MgTiO$_3$/graphite and LiNbO$_3$/graphite as foaming agent.

For higher amounts of foaming agent additionally deformed ellipsoidal or ellipsoidal pores with very high pore diameter are found. The pore diameters of various pores found in the samples generated with different percentages of foaming agents are shown in Table 14. Nevertheless, unstable foaming process was observed for higher amounts of foaming agent. The maximum total porosity has been calculated by MGDM and which is $49.8 \pm 1.0\%$.

Pore interconnectivity of the porous samples was observed in the SEM micrographs as shown in Fig. 40. From the SEM micrographs it is observed that pore coalescence effect is small compared to the sample generated with other foaming agents. Additionally, micro-CT images confirm that the porous Ti samples generated with this foaming agent has pore interconnecting behavior. The compositional analysis has been carried out by electron microprobe, micro-XRF and laser ablation coupled with MC-ICPMS. As a residual material of foaming agent no detectable magnesium, lithium and niobium is found in Ti matrix.
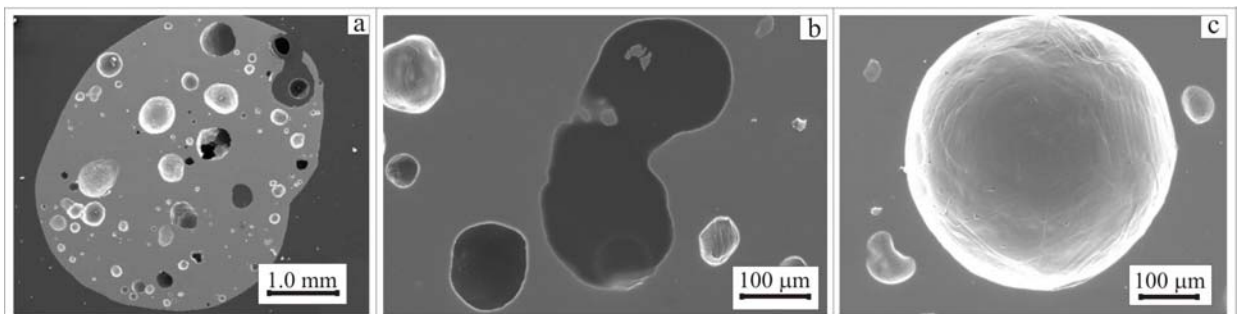
Fig. 40. SEM micrographs of porous Ti sample generated with a mixture of MgTiO$_3$/graphite, LiNbO$_3$/graphite as foaming agent: (a) Overview of the porous surface, (b) interconnecting small pore and merging of small pores and (c) a big pore showing rough cell interior.

Table 14: The pore diameter of pores in Ti samples generated with a mixture of MgTiO$_3$/graphite, LiNbO$_3$/graphite as a foaming agent; and a mixture of MgTiO$_3$/graphite, LiNbO$_3$/graphite and MgCO$_3$ as foaming agent

Foaming materials	Amounts of FA	Pore diameters /μm			
		Big	Medium	Small	Smallest
MgTiO$_3$/graphite	0.25 wt%	550 (D. sphr)	300 (sphr)	180 (sphr)	100 (sphr)
&	0.50 wt%	600 (D. sphr)	430 (D. sphr)	280 (D. sphr)	150 (sphr)
LiNbO$_3$/graphite	1.0 wt%	Big ellip.	580 (D. sphr)	230 (sphr)	120 (sphr)
	2.0 wt%	Big void	550 (D. sphr)	300 (D. sphr)	150 (sphr)
MgTiO$_3$/graphite,	0.25 wt%	1150 (ellip)	580 (D. sphr)	250 (D. sphr)	150 (sphr)
LiNbO$_3$/graphite	0.50 wt%	1250 (D. ellip)	650 (ellip)	260 (D. sphr)	130 (sphr)
&	1.0 wt%	1250 (D. ellip)	550 (ellip)	310 (D. sphr)	150 (sphr)
MgCO$_3$	2.0 wt%	Big ellip.	670 (ellip)	350 (D. sphr)	150 (sphr)

3.13. Results obtained with a mixture of MgTiO$_3$/graphite, LiNbO$_3$/graphite and MgCO$_3$ (MLNM) as foaming agent

A small amount (0.002 g) of pure MgCO$_3$ powder was carefully mixed with an equal amount mixture of MgTiO$_3$/graphite and LiNbO$_3$/graphite (mixing ratio as before) and considered it as a foaming agent in the laser induced Ti foaming process. In this case, 0.25 wt% to 5.0 wt% of foaming agent could be provided to generate porous Ti structures. The generated porous Ti samples have been analyzed by optical microscopy and micrographs are shown in Fig. 41. From optical investigation it is apparently visualized that a mixture of various shapes and sizes of pores are randomly distributed across the whole regions of sample. In sample generated with 0.25 wt% of MLNM as foaming agent ellipsoidal (big) pores with average pore diameter of about 1150 μm, deformed spherical (medium) pores with average pore diameter of about 580 μm, also deformed spherical (small) pores with average pore diameter of about 250 μm and spherical (smallest) pores with average pore diameter of about 150 μm are found. Again, deformed ellipsoidal (big) pores with average pore diameter of about 1250 μm, ellipsoidal (medium) pores with average pore diameter of about 650 μm, deformed spherical (small) pores with average pore diameter of about 260 μm and spherical (smallest) pores with average pore

diameter of about 130 μm are observed in sample produced with 0.50 wt% of foaming agent. For higher amounts (e.g. 1.0 wt%) of foaming agent additionally, deformed ellipsoidal pores with increasing pore diameters are found. The pore diameters of different pores created in various Ti samples are shown in Table 14. Porous Ti sample generated with every percentage of MLNM as foaming agent pores with increased pore diameters are found compared to samples generated with corresponding amount of MLN as foaming agent. Anyway, the maximum total porosity of $57.0 \pm 1.0\%$ has been found for this Ti sample generated with MLNM as foaming agent.
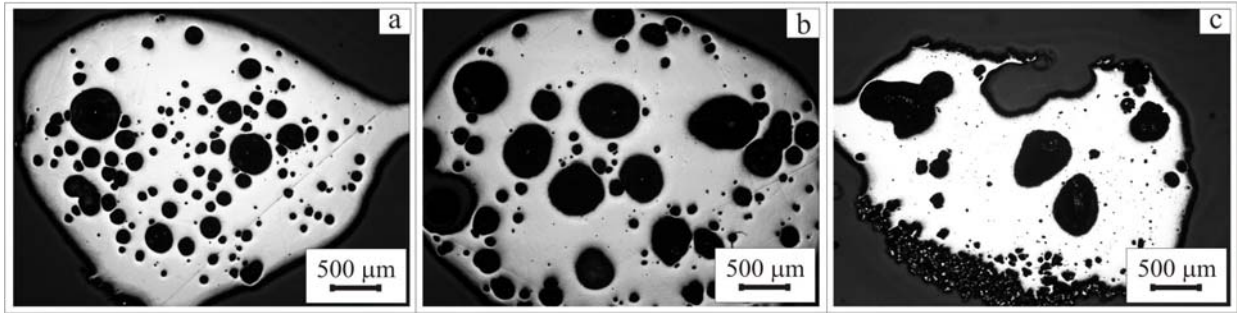

Fig. 41. Optical micrographs of generated porous Ti samples with: (a) 0.25 wt%, (b) 0.50 wt% and (c) 1.0 wt% of a mixture of $MgTiO_3$/graphite, $LiNbO_3$/graphite and $MgCO_3$ as foaming agent.
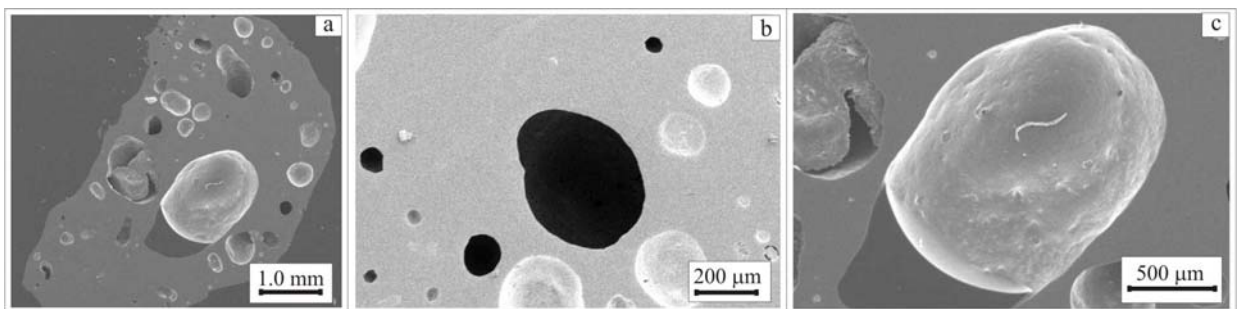
Fig. 42. SEM micrographs of porous Ti sample generated with a mixture of $MgTiO_3$/graphite, $LiNbO_3$/graphite and $MgCO_3$ as foaming agent: (a) Overview of the porous surface, (b) small and large interconnected pores and (c) big pore with rough pore wall.

In SEM micrographs as in Fig 42, it was observed that pores are interconnective within the sample area. Moreover, micro-CT image and analysis also shows the pores are interconnective to each other. Anyway, compositional analysis has been carried out by electron microprobe,

micro-XRF and laser ablation coupled with MC-ICPMS. However, as residual elements of foaming agent no detectable magnesium, lithium or niobium is found in the Ti matrix after laser process

3.14. Results obtained with a mixture of MgTiO$_3$/graphite, Li$_2$TiO$_3$/graphite, BaCO$_3$ and MgCO$_3$ (MTBM) as foaming agent

A small amount (0.001g) of BaCO$_3$ and (0.001g) MgCO$_3$ powder was carefully mixed with an equal mixture of MgTiO$_3$/graphite and Li$_2$TiO$_3$/graphite (mass ratio of 1:1) for employing it as a foaming agent in laser induced Ti foaming process. Here 0.25 wt% to 4.0 wt% of foaming agent could be provided for the generation of Ti porous structures. After foaming process the samples were mechanically divided and optical inspections have been carried out. Anyway, optical micrographs of polished samples are shown in Fig. 43. It is apparently observed from the generated porous Ti samples that pore with different sizes and shapes are randomly distributed across the whole regions of specimens. In sample generated with 0.25 wt% of MTBM as foaming agent deformed spherical (big) pores with average pore diameter of about 450 μm, spherical (medium) pores with average pore diameter of about 250 μm, also spherical (small) pore with average pore diameter of about 150 μm and also spherical (smallest) pores with average pore diameter of about 80 μm are found. Again, ellipsoidal (big) pores with average pore diameter of about 1160 μm, deformed spherical (medium) pores with average pore diameter of about 650 μm, spherical (small) pores with average pore diameter of about 370 μm and also spherical (smallest) pores with average pore diameter of about 150 μm are observed in Ti sample generated with 0.50 wt% of this foaming agent. With the increased amounts of foaming agent the pores with increased pore diameters are visualized. The dependency of pore diameters on percentages of foaming agent can be shown in Table 15. Although the pore diameters of pores are decreased in size for lower amounts of foaming agent (e.g. 0.25 wt%) however, for higher amounts (e.g. 1.0 wt%) big void with high pore diameters are observed. Here the dependency of amounts of foaming agent on pore diameter is significant compared to previous case. Anyway, the maximum total porosity 29.5 $\pm$ 1.2% has been determined in this case.

SEM micrographs as in Fig. 44 show that pores with increased pore diameter are interconnective within the sample whereas small pores are not interconnective. Additionally,

micro-CT images prove that there is interconnectivity of pores in the sample. Anyway, Ti samples were employed to determine the composition after laser process by various micro-analytical methods. Nevertheless, as residual materials of the foaming agent no detectable magnesium, lithium, barium has been found in the Ti matrix.
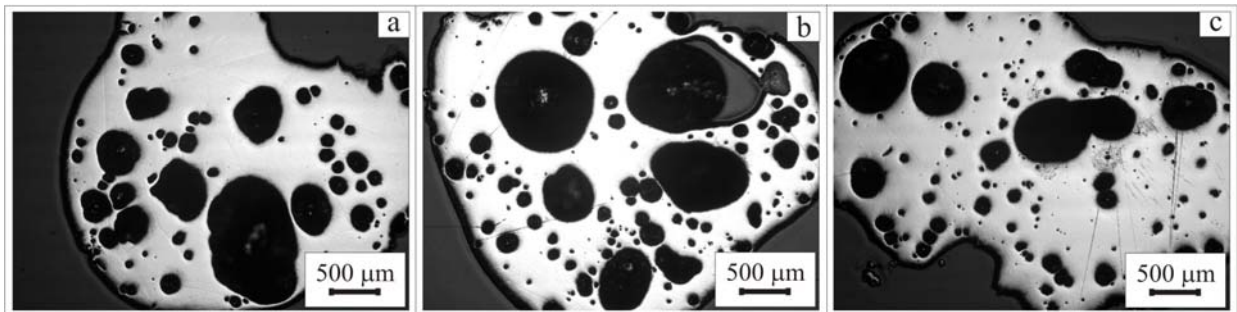

Fig. 43. Optical micrographs of porous Ti sample generated with: (a) 0.25 wt%, (b) 0.50 wt% and (c) 1.0 wt% of a mixture of $MgTiO_3$/graphite, Li_2TiO_3/graphite, $BaCO_3$ and $MgCO_3$ as foaming agent.

Table 15: The pore diameter of pores in porous Ti metals generated with a mixture of $MgTiO_3$/graphite, Li_2TiO_3/graphite, $BaCO_3$ and $MgCO_3$ as foaming agent; and a mixture of $MgTiO_3$/graphite, Li_2TiO_3/graphite, $BaCO_3$ and $MgCO_3$/graphite as foaming agent

Foaming materials	Amounts of FA	Pore diameters /μm			
		Big	Medium	Small	Smallest
$MgTiO_3$/graphite,	0.25 wt%	450 (D. sphr)	250 (sphr)	150 (sphr)	80 (sphr)
Li_2TiO_3/graphite,	0.50 wt%	1160 (ellip)	650 (D. sphr)	370 (sphr)	150 (sphr)
$BaCO_3$ &	1.0 wt%	Very big ellip	450 (D. sphr)	280 (sphr)	130 (sphr)
$MgCO_3$	2.0 wt%	Very big ellip	600 (D. sphr)	350 (sphr)	160 (sphr)
$MgTiO_3$/graphite,	0.25 wt%	700 (D. ellip)	520 (D. sphr)	250 (sphr)	120 (sphr)
Li_2TiO_3/graphite,	0.50 wt%	1220 (ellip)	530 (ellip)	250 (sphr)	130 (sphr)
$BaCO_3$ &	1.0 wt%	1260 (D. ellip)	700 (ellip)	250 (sphr)	130 (sphr)
$MgCO_3$/graphite	2.0 wt%	Very big ellip	720 (ellip)	300 (sphr)	150 (sphr)
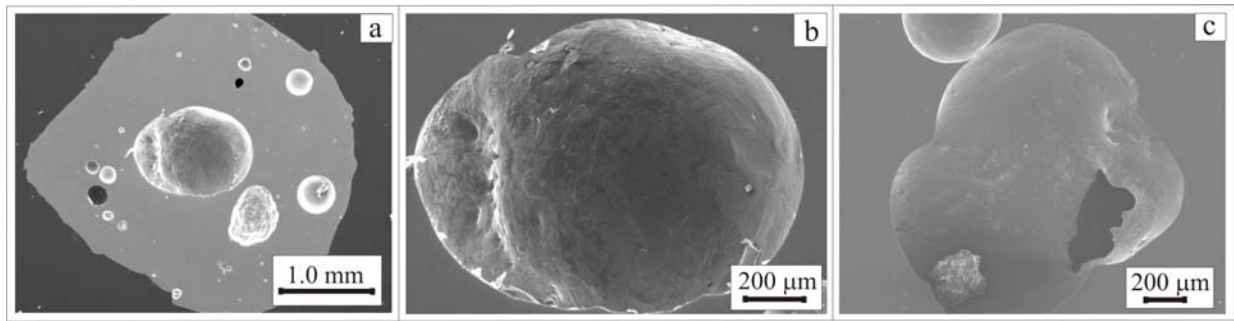
Fig. 44. SEM micrographs of porous Ti sample generated with a mixture of MgTiO$_3$/graphite, Li$_2$TiO$_3$/graphite, BaCO$_3$ and MgCO$_3$ as foaming agent: (a) Overview of the porous surface, (b) big pore with rough cell wall and (c) interconnective pore.

3.15. Results obtained with a mixture of MgTiO$_3$/graphite, Li$_2$TiO$_3$/graphite, BaCO$_3$ and MgCO$_3$/graphite (MTBMC) as foaming agent

For investigation the potentiality of foaming agent, a small amount (0.001g) of BaCO$_3$ and (0.001g) MgCO$_3$/graphite were mixed with an equal amount mixture of MgTiO$_3$/graphite and Li$_2$TiO$_3$/graphite (mass ratio mentioned earlier) and considered it as a foaming agent. For this foaming agent also 0.25 wt% to 4.0 wt% could be used to generate porous Ti structures. The generated samples were optically investigated and micrographs are shown in Fig. 45. From optical observation it is apparently found that pores with various shapes and sizes are randomly distributed across the whole regions of specimens. Anyway, in sample generated with 0.25 wt% of MTBMC as foaming agent deformed ellipsoidal (big) pores with average pore diameter of about 700 μm, deformed spherical (medium) pores with average pore diameter of about 520 μm, spherical (small) pores with average pore diameter of about 250 μm and also spherical (smallest) pores with average pore diameter of about 120 μm are observed. Again, ellipsoidal (big) pores with average pore diameter of about 1220 μm, also ellipsoidal (medium) pores with average pore diameter of about 530 μm, spherical (small) pores with average pore diameter of about 250 μm and also spherical (smallest) pores with average pore diameter of about 130 μm are observed in the Ti sample produced with 0.50 wt% of this foaming agent. Pores with ellipsoidal shapes and very high pore diameters are additionally found in the sample generated with higher amounts of foaming agent (e.g. 1.0 wt%). The pore diameter of various pores generated with different amounts of foaming agents can be shown in Table 15. Nevertheless, for higher amounts of foaming agent (>5.0 wt%) unstable foaming process was observed.

Actually in this case intermediate amount of foaming agent (e.g. 0.50 wt%) creates a good number of homogenous pores in the sample. Nevertheless, maximum total porosity of 37.3 $\pm$ 1.3% has been determined in this case.

Table 16: The obtained porosity of porous samples generated with various foaming agents

Foaming materials	Wt% of FA	Obtained total porosity /vol%		
		By MGDM	By MCTM	By IBM
ZrO_2/graphite	0.25	-	-	5.9
	0.50	8.2 $\pm$ 1.4	-	-
	4.0	13.1 $\pm$ 1.6	-	5.1
MgT	0.25	28.1 $\pm$ 2.1	-	23.4
	0.50	32.3 $\pm$ 1.5	-	28.2
	0.75	38.8 $\pm$ 1.1	-	-
	1.0	33.5 $\pm$ 1.6	-	24.6
MTM	0.25	41.4 $\pm$ 1.5	-	26.8
	0.50	26.4 $\pm$ 1.8	-	26.3
	1.0	23.8 $\pm$ 1.6	-	-
MTMC	0.25	31.2 $\pm$ 1.4	-	18.7
	0.50	36.2 $\pm$ 1.5	-	28.8
	1.0	15.4 $\pm$ 1.9	-	25.8
	2.0	-	-	15.4
MLN	0.25	-	-	-
	0.50	49.8 $\pm$ 1.0	-	36.1
	0.75	-	-	-
	1.0	-	-	35.2
MLNM	0.25	28.2 $\pm$ 1.6	-	17.1
	0.50	44.9 $\pm$ 1.2	-	-
	1.0	57.0 $\pm$ 1.0	-	-
	1.5	39.1 $\pm$ 1.5	-	-
	2.0	30.0 $\pm$ 1.8	-	-
MTBM	0.25	-	-	8.7
	0.50	9.0 $\pm$ 1.5	-	-
	1.0	29.5 $\pm$ 1.2	-	-
MTBMC	0.25	-	-	4.6
	0.50	24.1 $\pm$ 1.5	-	11.7
	1.0	37.3 $\pm$ 1.3	-	21.0

By MCTM no sample is emplyed to calculate the porosity (mentioned in Table 16).

SEM and micro-CT images show that pores with increased pore diameter are interconnective within the sample. Again microanalysis of this sample show that no detectable residual element except Ti of foaming agent is present in the sample after laser induced foaming process.

Nevertheless, porosity obtained in the Ti porous samples generated with various foaming agents can be shown in detailed in Table 16.

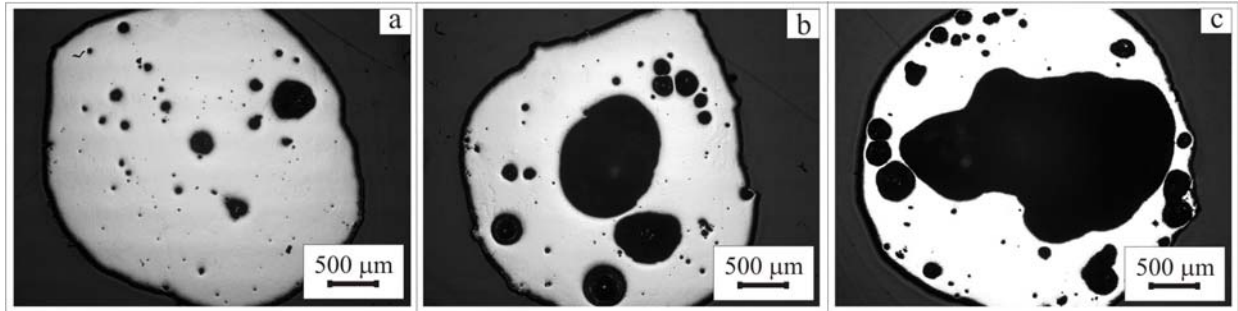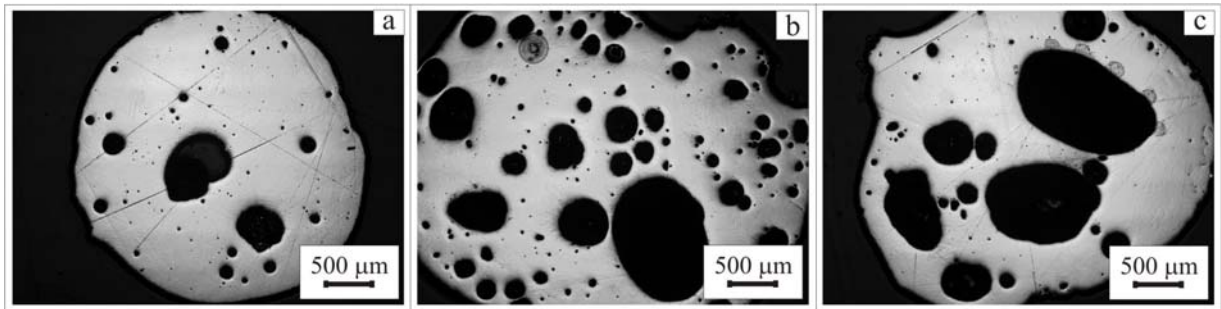Fig. 45. Optical micrographs of porous Ti samples generated with: (a) 0.25 wt%, (b) 0.50 wt% and (c) 1.0 wt% of a mixture of $MgTiO_3$/graphite, Li_2TiO_3/graphite, $BaCO_3$ and $MgCO_3$/graphite as foaming agent.

4. DISCUSSIONS

The illustrated pore formation in the titanium matrix is based on chemical reactions which occur in the melt as a result of the laser induced interaction of the gas producing foaming agent and the titanium powder. For this reason, the gas production from the foaming agent is chemically considered. Titanium in the liquid state can dissolve oxygen by reacting with carbon dioxide according to following reaction.

$$n\ Ti + CO_2 = (n\text{-}1)\ Ti + 2\ O_{(dissolved)} + TiC \qquad\qquad (7)$$

The contamination from oxygen in the material matrix might make the porous Ti sample brittle. However, the amounts of different elements present in the foaming agents are quite small. Therefore, these dissolved elements are expected to have negligible effect on the embrittlement of the porous materials. Moreover, it is theoretically found that if we start with 0.50 wt% of foaming agent the Ti grade 1 powder material would become Ti grade 4 materials after foaming process. Therefore, the mechanical property of the generated porous Ti sample especially brittleness, is not significantly affected by the incorporation of a small amount of oxygen contained in the foaming agents. It, however, was not possible to generate large Ti porous matrix samples with layered structures within the stipulated time of this PhD dissertation (Which is not the part of this thesis). Therefore, mechanical properties such as, brittleness and Young's modulus are yet to be determined.

As the quality of the porous sample somehow depends on the oxygen contamination, therefore, emphasis has been given to generate the sample with lower amount of foaming agents. Compositional analysis almost in every cases were carried out for samples generated with lower amount of foaming agents (e.g. 0.25 wt%). Small spot size is used in the micro-XRF measurement, therefore, as a light element; a trace amount of magnesium could not be determined. As Ti^{2+} is the major interference on ^{24}Mg, ^{25}Mg and ^{26}Mg, it is difficult to determine low concentration of magnesium in a matrix consisting of high concentration of Ti. Due to this interference magnesium has not been determined. Ways to determine magnesium would have been ICP-OES (Inductively coupled plasma-Optical emission spectroscopy) or ICP-MS (Inductively coupled plasma-Mass spectroscopy) after chromatographic separation of Ti from the system. With careful production of Ti matrix having different amounts of Li, the

quantity of Li in the sample may be deciphered. By this way lithium content can be determined. By ICP-OES the trace amount of barium in the sample would have also been determined by careful experiment.

4.1. Discussion of the results obtained with anatase or rutile/graphite as foaming agents

At a high temperature (>2000 K) the expected decomposition reaction together with competitive reactions for anatase (rutile) and graphite are:

$$TiO_{2(s)} + C_{(s)} \rightarrow Ti_{(s)} + CO_{2(g)} \tag{8}$$

$$TiO_{2(s)} + 3C_{(s)} \rightarrow TiC_{(s)} + 2CO_{(g)} \tag{9}$$

$$TiC_{(s)} + TiO_{2(s)} \rightarrow 2Ti_{(s)} + CO_{2(g)} \tag{10}$$
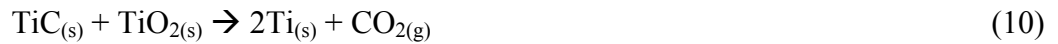
In laser beam it is speculative that besides the main decomposition reaction competitive reactions resulting to titanium carbide formation occured. While the emerging carbon dioxide was gaseous, the generated high temperature resisting ceramic like particle (TiC) increase the viscosity [3, 84, 85] of the Ti melt. The gas pressure resulting from the development of carbon dioxide was not sufficient to expand the Ti matrix because of this increased viscosity of the melt which is observed previously [3]. The atmosphere inside the growing pores regarding pressure and concentration may even cause the inhibition of the above described decomposition reactions. Nevertheless, ceramic particles show an effect as nucleating agents and induce the development of pores in the melt [86]. Anyway, pores are randomly distributed in the sample that might be due to the formation of closed-cell pore structures. In closed-cell pore morphology, the pore size, shape and location of pores within the sample varies, depending on the process parameters which can be seen in previous studies [22, 83]. In porous Ti sample generated with anatase or rutile/graphite as foaming agents found less amount of porosity. This is probably due to the big differences of melting temperature of Ti and anatase or rutile samples. As the size and shapes of the pores in the samples generated with anatase (rutile)/graphite varies with the average crystal size of the foaming agents, therefore average crystal size of anatase (rutile) has significant influence on pore formation in Ti matrix.

4.2. Discussion of the results obtained with calcium tungstate/graphite as foaming agent

The expected decomposition reaction of $CaWO_4$ in presence of pure graphite powder in the proper stoichiometry of the titanium foaming process is:

$$CaWO_{4(s)} + 2C_{(s)} \rightarrow Ca/W_{(s)} + 2CO_{2(g)} \qquad (11)$$
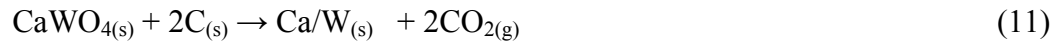
In presence of Ti powder the competitive reactions additional to Eq[n]. (9) are

$$CaWO_{4(s)} + C_{(s)} + Ti_{(s)} \rightarrow Ca/W_{(s)} + CO_{2(g)} + TiO_{2(s)} \qquad (12)$$
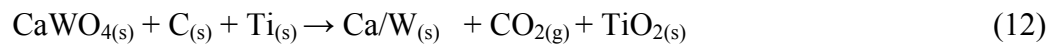
In the laser beam, during decomposition reaction, escapable gaseous carbon dioxide was produced together with solidus ceramic like particles (Ca/W, TiC and TiO_2). The ceramic like particles were expected to act as a stabilizing agent so that the growing bubble does not collapse immediately [3, 85, 86]. From the previous studies [86] it is found that the presence of oxides particles in the melt hindered the melt drainage by increasing the viscosity of the system. This effect also suppressed the coalescence of the pores during their formation time. As the decomposition reaction temperature of $CaWO_4$ (1893 K) is close to the melting temperature of titanium, a stable porous structure is formed. Anyway, at lower percentages of foaming agent, the amount of gas produced was not sufficient to generate a high amount of pores with increased diameter. The generation of a few pore of increased pore diameter resulting from this test series with higher amounts of foaming agent (0.75 wt%-1.5 wt%) can be ascribed to the production of an adequate amount of gas on the one hand as well as to the presence of a higher amount of stabilizing particles on the other hand. Moreover, competitive gaseous reaction products (more CO_2 evolves) at higher percentages of foaming agent have an effect on formation of pores with increased pore diameters.

4.3. Discussion of the results obtained with magnesium metatitanate/graphite as foaming agent

Graphite powder in a pure form with proper stoichiometry was expected to reduce [83] the decomposition temperature of the foaming agent and titanium powder according to the following reaction scheme together with similar competitive reactions described previously:

$$2MgTiO_{3(s)} + 3C_{(s)} \rightarrow 2(Mg/Ti)_{(s)} + 3CO_{2(g)} \tag{13}$$
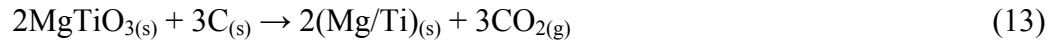
Due to high buoyancy forces of the high-density liquid the growing gas bubbles in a metallic melt normally tend to rise quickly towards its surface. The rise can be hindered by increasing the viscosity of the molten metal either by adding alloying elements to form stabilizing particles in the melt or by adding a viscosity increasing agent. In the present case pure graphite powder acted both as a reducing agent and a viscosity increasing material during the foaming process. Anyway, out of the reactants and products of the decomposition reaction carbon dioxide is only gaseous substance which has a quick escaping tendency from the melt. Compared to other foaming agents the decomposition temperature of $MgTiO_3$ (1883 K) is much closer to the melting temperature of titanium and therefore, the leaking of gas from the un-molten matrix powder is less likely to occur. The core area of the sample cools more slowly compared to the outer region and remains molten longer. This phenomenon probably allowed more time for pore coarsening in center zone of a few samples because of the gas pressure in the pores. In the case of lower percentages of foaming agent (0.25 wt% and 0.50 wt%) carbon dioxide gas production is presumably not sufficient to create a high number of pores with big pore diameters in the porous structure. The pore formation governed with intermediate amounts of foaming agent offers an increased quantity of gas production and facilitates the formation of a high number of spherical or ellipsoidal pores in the sample. For higher percentages of foaming agent, some pores which have been formed immediately merge with each other (Fig. 18 c, d and e) during the foaming stage. Therefore, the ultimate shape of the pores transforms to ellipsoidal or deformed ellipsoidal or deformed spherical from their original spherical shape. Furthermore, it is found that longitudinal axis of tube-like connected pores is directed to the feed rate of the laser process. Therefore, the laser based foaming process offers the possibility to generate directed porosity.

The porosity of porous Ti samples determined by different porosity calculating methods which can be compared and shown in Table 6 and Fig. 46. The porosity determined by MGDM (mentioned earlier) of the porous samples shows slightly increasing order with the increased amounts of foaming agent initially and after certain point it is linear. Again, porosity calculated by MCTM (mentioned earlier) also follows similar increasing order with the increased percentages of this foaming agent. While porosity estimated by IBM (mentioned earlier) initially impressive increase of the porosity with the foaming agent amount up to 0.75 wt% and then a little bit decrease and then straight with the increased amount of foaming agent. Altogether, with increase of the amount of foaming agent the porosity of the samples increases. Anyway, maximum total porosity of 22.10% is calculated by MCTM in this case for sample generated with 1.5 wt% of foaming agent. As the values of porosity calculated by three different porosity determining methods are comparable, therefore, porosity calculation for the rest of the Ti sample could be carried out by MGDM and IBM.
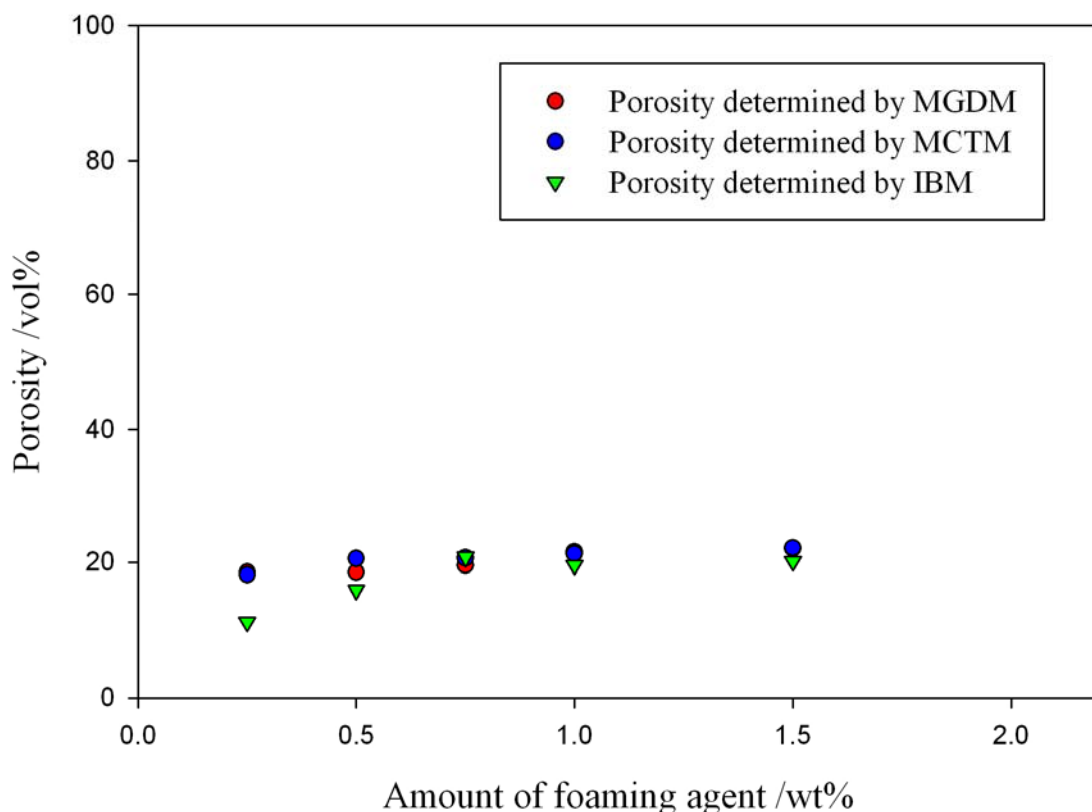
Fig. 46. A plot of foaming agent amounts against obtained total porosity in porous Ti samples generated with $MgTiO_3$/graphite as foaming agent.

4.4. Discussion of the results obtained with magnesium carbonate and magnesium carbonate/graphite as foaming agents

At high temperature as in the laser beam the expected decomposition reaction of $MgCO_3$ starts at about 623 K in this laser induced foaming process. Here also a few other competitive reactions might occur.

$$MgCO_{3(s)} \rightarrow MgO_{(s)} + CO_{2(g)} \tag{14}$$

$$MgO_{(s)} + Ti_{(s)} \rightarrow Mg/Ti_{(s)} + TiO_{2(s)} \tag{15}$$

In the laser beam, gaseous carbon dioxide was produced together with solidus ceramic like particles (e.g. TiO_2) during decomposition reaction. Like previous case the ceramic like particles perform as a stabilizing agent so that the growing pore does not collapse immediately [3, 85, 86]. Moreover, generated magnesium based alloy has a vital role for the escalating of the viscosity of the system. Although the generated oxides particle could be stabilized the pore structures however, for higher amounts of foaming agent the adjacent bubble merges and produced big ellipsoidal pores as shown in Fig. 21 (b) and (c). The merging or coalescence of pores was occurred by the reunion of adjacent pores due to the rupture of liquid film that separated them. The production of a huge amount of gasses during the interactions of different materials at high temperature somehow escalates this rupture of cell walls. In samples generated with lower (e.g. 0.25 wt%) and intermediate (e.g. 0.75 wt%) amounts of foaming agent nearly homogeneous pores with lesser pore diameters are found. This is most probably because of lesser amount of cell wall rupture occurs. While for higher amounts the pores are merging and big void is produced. The maximum total porosity (24.4 $\pm$ 1.5%) calculated by MGDM is found for the sample generated with 1.0 wt% of foaming agent. Therefore, achieving homogeneous pores with maximum porosity relatively intermediate amounts of foaming agent is functioning effectively.

For the samples generated with magnesium carbonate and graphite the expected decomposition reaction [Eq^n. (14)] of $MgCO_3$ starts at about 623 K in this process. Additionally, at high temperature as laser beam the interaction of *in-situ* produced magnesium oxide and graphite in presence of Ti can be represented by the following reactions [additional to Eq^{ns}. (9), (10)].

Direct reduction reaction:

$$MgO_{(s)} + C_{(s)} \rightarrow Mg_{(g)} + CO_{(g)} \tag{16}$$

Indirect reduction reaction:

$$MgO_{(g)} + CO_{(g)} \rightarrow Mg_{(g)} + CO_{2(g)} \tag{17}$$

$$CO_{2(g)} + C_{(s)} \rightarrow 2CO_{(g)} \tag{18}$$

$$2MgO_{(g)} + C_{(s)} + 2Ti_{(s)} \rightarrow 2Mg/Ti_{(s)} + CO_{2(g)} \tag{19}$$

$$2MgO_{(s)} + 2MgCO_{3(s)} + C_{(s)} + 5Ti_{(s)} \rightarrow 4Mg/Ti_{(s)} + 3CO_{2(g)} + TiO_{2(s)} \tag{20}$$
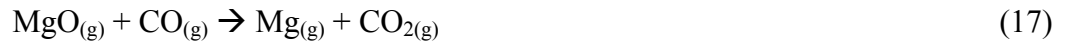
A substantial amount of gaseous particles were evolved which are potential enough to create pores with increased pore diameters in the material matrix. Moreover, ceramic like particles could be potential entities for the stabilization of the porous structures. Additionally, presence of several oxides (e. g. MgO) particles in the melt slowed down drainage effect by increasing the viscosity of the melt which is in good agreement with previously published results [86]. Compared to the samples resulting by pure $MgCO_3$, pores with increased pore diameters are found in this case. This is due to the generation of several additional gaseous oxides in presence of graphite. The production of gaseous magnesium by reduction reaction could have additional effect on pore morphology. The coalescence of the several adjacent pores in the material matrix is probably due to the production of several gaseous species by the reduction reactions. This behavior additionally, clearly indicates the reduction of the foaming material with graphite. Therefore, in this case in samples generated with all amounts of foaming agent pores with comparably increased pore diameters are observed. Additionally, porous metal generated with $MgCO_3$/graphite exhibit more spherical pore compared to that of with $MgCO_3$. Anyway, Ti sample created with $MgCO_3$/graphite has a relative density (ρ_{foam}/ρ_{solid}) of 0.56 (maximum porosity) and comarably increased pore diameters, while sample generated with $MgCO_3$ has relative density of 0.75 (for maximum porosity) and comparably decreased pore diameter. These results are in good agreement with previously published paper [83]. As huge amount of gases produced by the reduction reactions the pressure differences between the adjoining cells give rise to cell wall curvature as previously found [87]. Here the pores coarsening were occurred additionally, probably due to the diffusion of entrapped gases through the cell walls. Nevertheless, maximum total porosity ($43.3 \pm 1.1\%$) calculated by MGDM is found in the sample generated with 0.75 wt% of $MgCO_3$/graphite as foaming agent.

Anyway, from SEM micrographs, as in Fig. 22, it can be assumed that interconnecting pores with obtained porosity can be advantage for the reduction of the stiffness of the generated porous materials. Therefore, this foaming agent can be a good candidate for the generation of Ti porous sample with required stiffness for implants.

4.5. Discussion of the results obtained with magnesium metatitanate/graphite with magnesium carbonate as foaming agent

Besides decomposition reactions of $MgTiO_3$ and $MgCO_3$ several reductions (as previously shown) and competitive reactions (as previously mentioned) were also occurred at high temperature in laser beam. Because of various reactions increasing amounts of ceramic like particles are generated. These ceramic like particles might stabilize the porous structures more effectively compared to previous case. Moreover, presence of *in-situ* produced several oxides particles (e. g. MgO) slowed down drainage effect by increasing the viscosity of the melt which is also described before. Anyway, due to production of huge amounts of various gases, pores with increased pore diameters are found in the samples generated with these foaming materials. From Table 8 and Fig. 23, it seems that amount of $MgCO_3$ is more effective on pore formation compared to the amounts of $MgTiO_3$/graphite. In almost all percentages of foaming materials generate porous Ti sample with increased pore diameter which is not found in samples generated with only $MgTiO_3$/graphite. The dependency of pore diameters on amounts of foaming agent (from Fig. 24) clearly indicates that both of $MgTiO_3$/graphite and $MgCO_3$ have significant influences on pore diameters of pores. Among them it is apparently observed that $MgCO_3$ has comparably higher influence on pore diameter than that of $MgTiO_3$/graphite. This is due to the production of MgO from decomposition of $MgCO_3$ and additionally, reduction of MgO by graphite. Furthermore, for every amount of foaming materials pore coalescence have been observed which is unlikely in porous Ti samples generated with lower amounts (e.g. 0.25 wt%) of other foaming agents. Moreover, homogeneity of pore distribution is not always present in Ti sample generated with these foaming materials. Nevertheless, maximum total porosity (23.1%) is calculated in Ti sample generated with a mixture of 0.1 wt% of $MgTiO_3$/graphite and 0.75 wt% of $MgCO_3$ as foaming agent.

4.6. Discussion of the results obtained with lithium titanate and lithium titanate/graphite as foaming agents

According to Nakagawa *et al.* [88] vaporization behavior of lithium titanate has been occurred in the temperature range of 1180-1628 K across the order-disorder transition temperature of $Li_2TiO_{3(s)}$. In the laser beam volatilization reaction may be written as:

$$Li_2TiO_{3(s)} \rightarrow Li_2O_{(g)} + TiO_{2(g)} \qquad (21)$$

$$TiO_{2(g)} \rightarrow TiO_{(g)} + \tfrac{1}{2} O_{2(g)} \qquad (22)$$

$$TiO_{2(g)} \rightarrow Ti_{(s)} + O_{2(g)} \qquad (23)$$

Due to the generation of various gaseous species in the reaction porous Ti samples are created with only lithium titanate as foaming agent in this laser induced foaming process. At lower percentages of foaming agent spherical/ellipsoidal pore with decreasing pore diameters are found because of the production of relatively less amount of escapable gas in this process. For higher amounts of foaming agent predominantly deformed spherical or ellipsoidal pores with increased pore diameters were produced. This is due to the generation of huge amounts of gaseous species in the reaction. Anyway in a few cases, pores are merged by the reunion of adjacent pores because of the rupture of the liquid thin film which separated them. The pore coalescence was occurred probably due to the presence of high amounts of escapable gases in the melt for higher percentages of foaming agents.

The phase diagram of Li_2O-TiO_2 system shows four known stable compounds of lithium such as Li_4TiO_4, Li_2TiO_3, $Li_4Ti_5O_{12}$, and $Li_2Ti_3O_7$ [89]. Among them, Li_2TiO_3 has two polymorphs such as ordered polymorph with a rock salt super structure (stable form) and disordered polymorph with a metastable cubic structure. The later (disordered) form is stable above the order-disorder transition temperature of 1486 K and melts at 1820 K. Anyway, the monoclinic β-phase (ordered polymorph) of this lithium titanate is stable at low temperature while cubic form (disordered polymorph) exists at high temperature. The density of β-phase is 3.43 g/cm^3 [90]. The transition in lattice type at this reversible phase change is accompanied by a large volume change. This drastic volume and crystallographic change results might be indirectly influencing for the generation pores in the Ti material matrix. Therefore, both of vaporization reactions and phase transition phenomena were responsible for the generation of pores in the Ti

material matrix in this laser induced foaming process. Among various percentages intermediate amount of pure Li_2TiO_3 (0.50 wt%) generated sample with maximum total porosity of $32.4 \pm 1.4\%$. For higher amounts of foaming agent (e.g. 1.0 wt%) less amounts of pore with increased pore diameters are present therefore, less porosity is obtained.

For the samples generated with lithium titanate and graphite the expected decomposition and reduction reactions can be shown as:

$$2Li_2TiO_{3(s)} + 3C_{(s)} \rightarrow 2Li/Ti_{(s)} + 3\ CO_{2(g)} + Li_2O_{(g)} \qquad (24)$$
$$Li_2O_{(g)} + C_{(s)} \rightarrow 2Li_{(s)} + CO_{(g)} \qquad (25)$$
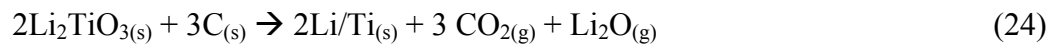
In-situ produced ceramic like particles and oxides species, respectively, stabilize the porous Ti metal and prevent the excessive melt drainage by maintaining the viscosity and surface tension of the system. The generations of several escapable gasses were responsible for the creation of pores with various pore diameters in the porous Ti samples. In samples generated with lower amounts (0.25 wt%) of foaming agent pores with decreasing pore diameters are found. This is probably due to the generation of lesser amounts of gases in the process. For intermediate amounts of foaming agents predominantly deformed spherical or ellipsoidal pores with increased pore diameters were created. This is because of the production of high amounts of escapable gaseous species. The pores merging or pore coalescence was occurred by the reunion of adjacent pores due to the rupture of the thin liquid film that separated them as a cell wall. The cell rupturing was occurred probably due to the presence of a huge amount of gases during reaction in the melt. Because of the presence of huge amounts of gases during reactions for higher amounts (>5.0 wt%) of foaming agents unstable pores structures were found. Anyway pores with comparably increased pore diameters are found in the samples generated with lithium titanate and graphite than that of with corresponding amount of only Li_2TiO_3. This behavior is due to the presence of additional reduction reactions as above for the mixing of graphite in the Ti foaming process. Nevertheless, in the samples generated with lower percentages of foaming agents both of the cases nearly homogenous small pores are visualized. Anyway, intermediate amount of foaming agent (0.50 wt%) generates porous Ti sample with maximum porosity ($36.1 \pm 1.5\%$). With such amount of porosity this foaming agent can also be a good candidate for the manufacture of Ti implants with required stiffness.

4.7. Discussion of the results obtained with lithium niobate/graphite as a foaming agent

The expected decomposition reaction of lithium niobate with graphite at the high temperature as laser beam can be written as:

$$2LiNbO_{3(s)} + 3C_{(s)} \rightarrow 2Li/Nb_{(s)} + 3CO_{2(g)} \tag{26}$$
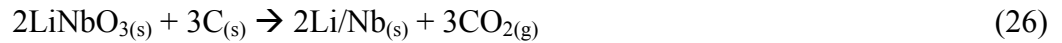
According to previous study [91] at high temperature above 1273 K readily causes weight loss of $LiNbO_3$ due to the lithium oxide volatilization. The volatilized lithium oxide can have potentiality to generate pore in Ti matrix. Additionally, this gaseous Li_2O can be a good candidate to react with graphite as bellow:

$$Li_2O_{(g)} + C_{(s)} \rightarrow 2Li_{(s)} + CO_{(g)} \tag{27}$$

Besides theses decomposition, volatilization and reduction reactions other competitive reactions produced a substantial amounts of evolving gases and additionally ceramic like particles as before. The various non-metal and metal gaseous oxides are responsible for the generation of pores in the Ti material matrix. Except a big void as a foaming agent, 0.25 wt% of $LiNbO_3$/graphite can generate porous sample of spherical pores with nearly similar pore diameter. While intermediate and relatively higher foaming agent amounts generated samples with deformed spherical or deformed ellipsoidal pores shapes and higher pore diameters. This increased pore diameters is probably due to the huge amounts of evolving gas for higher amounts of foaming agent at very high temperatures. Additionally, reduction of Li_2O by graphite has another cause for the creation of pores with increased pore diameter in porous samples. Moreover, previous studies [92] suggest that there is a phase transition occurs in hot-pressed $LiNbO_3$ ceramics at elevated temperature. This phase transition is associated with volume change of the system. This phenomenon is probably additional influence for the generation of big void in the Ti samples. Although a few ceramic like and oxide particles were produced during reaction, the coalescence of pores by the reunion of adjacent bubbles, and simultaneously pores drainage is responsible for inhomogeneous pore size and shape and pore distribution in the specimen produced by higher amounts of foaming agent.

Although the lower amounts of foaming agent generated sample with small pore diameter and homogenous distribution of pores, the intermediate and higher amounts of foaming agent created sample with high porosity. The maximum porosity of 35.1 $\pm$ 1.6% was found in the sample generated with 4.0 wt% of foaming agent. The influence of foaming agent percentages on the generation of the porosity amounts can be shown in Fig. 47.
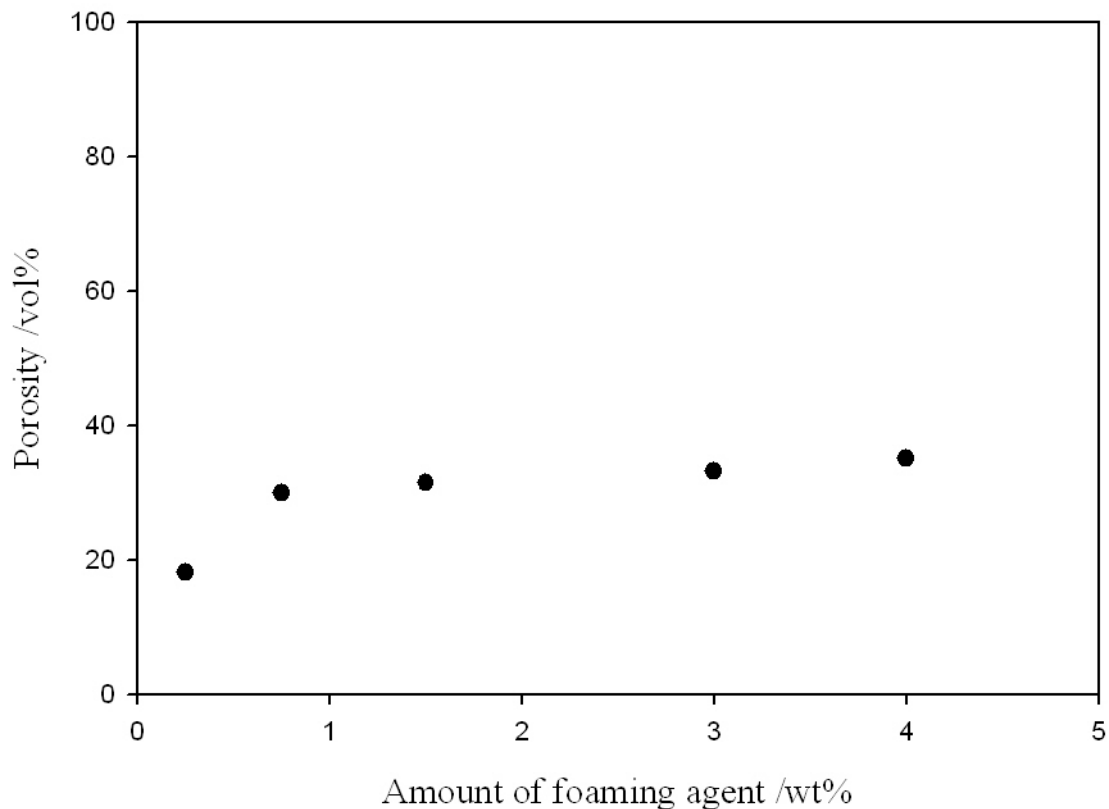
Fig. 47. Influence of the percentage of foaming agent on amount of porosity of the porous Ti sample generated with $LiNbO_3$/graphite as foaming agent.

It is clearly observed from Fig. 47 that with the increasing amounts of foaming agent the porosity of the Ti porous sample increases. For higher amounts of foaming agent pore coalescence was significantly occurred. Therefore, adjacent small pores were merged and produced big void in the sample. Due to this effect inhomogeneous pore distribution is observed in samples generated with higher percentages of foaming agent. Furthermore, from SEM micrographs (Fig. 30 a, b) it is assumed that the especial type of internally widely extended and interconnective pores can be a good reason for the reduction of the stiffness of the generated porous materials. As a result of the high potentiality for the generation of pores with

nearly homogeneous pore distribution LiNbO$_3$/graphite can also be a potential candidate for this foaming process.

4.8. Discussion of the results obtained with zirconium oxide and zirconium oxide/graphite as foaming agents

It is well known that oxides such as SiO$_2$, CaO, MgO, Fe$_2$O$_3$, TiO$_2$, etc. can stabilize the tetragonal or cubic phase of zirconia by formation of solid solutions [93, 94] during synthesis. Due to the presence of these oxides as impurities, volatilization or decomposition reactions occurred during laser process. Because of this reactions small pores with decreased pore diameters were created in the samples generated with lower (0.25 wt%) amount of foaming agent. The number of pores and pore diameters increases with the increasing amounts of foaming agent as shown in Fig. 31. In the presence of increasing amounts of impurities more gaseous substances are produced and escaped from the melts. Consequently, pores with increasing pore diameters are found in the Ti sample generated with 4.0 wt% of ZrO$_2$ as a foaming agent.

Again at ambient pressure, pure zirconium oxide possesses three crystallographic polymorphs such as monoclinic at temperature below 1446 K, tetragonal stable between 1446 and 2643 K, and cubic at temperatures from 2643 K to the melting point at approximately 2900 K [95-97]. With the transformation from monoclinic to the tetragonal polymorph, ZrO$_2$ undergoes a considerable volume contraction of the order of 3-4% [98]. The phase transformation of ZrO$_2$ can be shown as below.

$$\text{ZrO}_{2(monoclinic)} \longrightarrow \text{ZrO}_{2(tetragonal)} \longrightarrow \text{ZrO}_{2(cubic)}$$
$$<1446\ \text{K} \qquad\qquad 1446\text{-}2643\ \text{K} \qquad\qquad 2643\text{-}2900\ \text{K}$$

Phase transformation sequence of ZrO$_2$

This volume change phenomenon is an additionally information for further investigation of the suitability of foaming agent. Anyway, samples generated with higher percentages of foaming agent (e.g. 4.0 wt%) create comparably increasing number of pores compared to lower percentages. Maximum porosity of 12.1 $\pm$ 1.2% has been determined in the sample generated with 4.0 wt% of foaming agent.

At laser beam expected decomposition reaction of ZrO_2 and pure graphite can be written as:

$$ZrO_{2(s)} + C_{(s)} \rightarrow Zr_{(s)} + CO_{2(s)} \qquad (28)$$

$$Zr_{(s)} + C_{(s)} \rightarrow ZrC_{(s)} \qquad (29)$$

At high temperature due to the production of gaseous carbon dioxide in the decomposition reaction pores were formed in the Ti material matrix. Moreover, in the presence of impurities in ZrO_2 has additional influence for the creation of porous materials in the laser beam. For lower percentages of foaming agent the generated gas were not sufficient to produced pore with increased diameters. Samples generated with higher amounts of foaming agent (e.g. 4.0 wt%) increasing number of pores with higher pore diameters are found. This is due to the presence of high amounts of escapable gases in the melts. Here maximum porosity (13.1 $\pm$ 1.6%) was calculated in the sample generated with 4.0 wt% of foaming agent.

4.9. Discussion of the results obtained with a mixture of MgTiO$_3$/graphite and Li$_2$TiO$_3$/graphite (MgT) as foaming agent

In laser beam several decomposition products as well as volatilized species (e.g. Li_2O) can be produced from the foaming mixture of $MgTiO_3$/graphite and $LiTiO_3$/graphite. As earlier described the production of various ceramic like (e.g. TiC) and alloy like (e.g. Mg/Ti) particles can be a potential entities for the stabilization of the Ti structures. Moreover, produced oxides particles slows down the melt drainage effect as described previously. Anyway, according to described decomposition and reduction reactions (13), (24), (25) in this case, a substantial amount of gaseous species generated in the melt. Even for the lower amount of foaming agent (e.g. 0.25 wt%) a big void is produced which can be found in Fig. 33 (a) and Table 12. For intermediate amount of foaming agent pores with almost similar shapes and sizes are found. Again, for higher amounts, pores with ellipsoidal or deformed ellipsoidal shapes and increased pore diameters are visualized. These pores with increased pore diameter is formed may be due to the volatilization of huge amounts of Li_2O in one hand and generation of substantial amounts of escapable gaseous products in the other hand.

The dependency of the percentages of foaming agent on the amounts of calculated porosity can be shown in Fig. 48. It is found that the porosity initially increases with increasing amounts of

foaming agent up 0.75 wt%. Then again, it falls down with increasing amounts of foaming agent. The fall down of porosity for higher percentages of foaming agent is presumably due to the partially break down of the porous structure because of high gaseous pressure. The determined porosity of every sample generated with MgT is high (Table 16). However, among various samples, 0.75 wt% of foaming agent generated total maximum porosity of $38.8 \pm 1.1\%$. The pore size and shape found here is different compared to porous Ti metal generated with either only $MgTiO_3$/graphite or Li_2TiO_3/graphite. Moreover, determined porosity is comparably higher than those calculated in the sample generated either with $MgTiO_3$/graphite or with Li_2TiO_3/graphite individually. These characteristics are probably either due to the volatilization of lithium oxide in the laser beam or evolving of several gaseous substances in the melts. As a result of a high amount of porosity formation, a mixture of $MgTiO_3$/graphite and Li_2TiO_3/graphite as a foaming agent can be a suitable candidate for the manufacture of Ti implant.
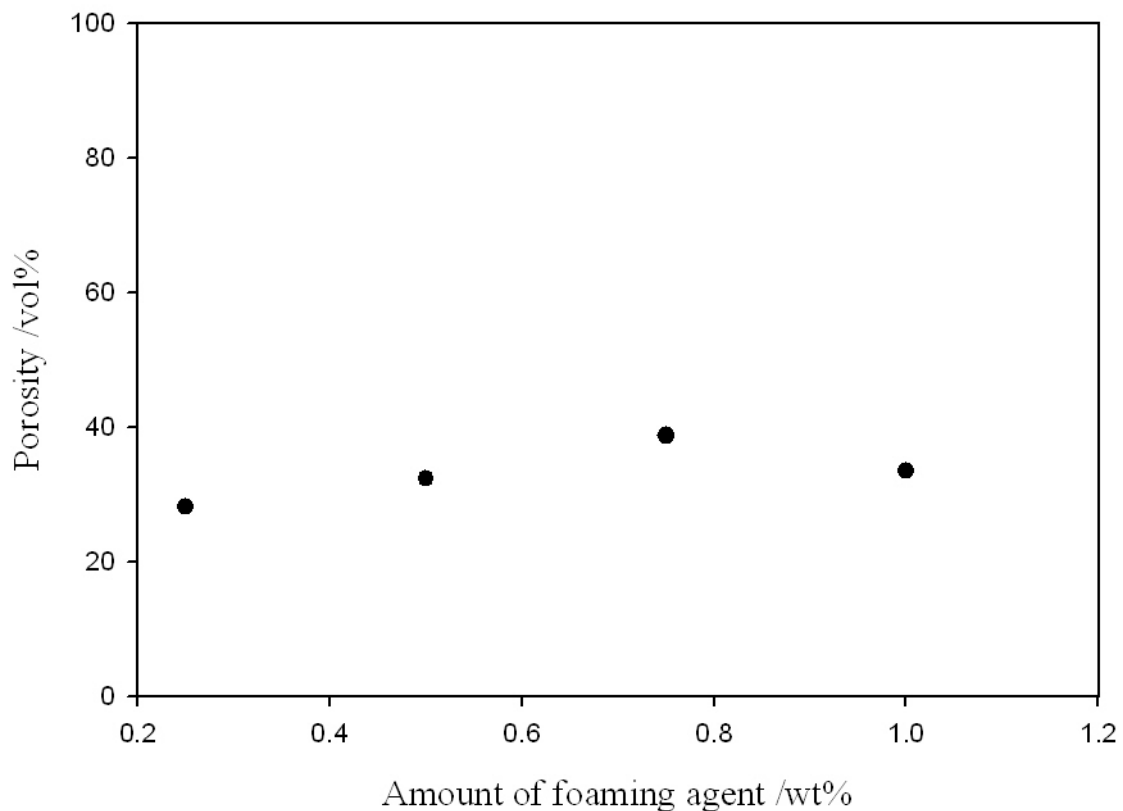

Fig. 48. Influence of the percentages of foaming agent on the amounts of porosity of porous Ti structure generated with a mixture of $MgTiO_3$/graphite and Li_2TiO_3/graphite.

4.10. Discussion of the results obtained with a mixture of MgTiO$_3$/graphite, Li$_2$TiO$_3$/graphite and MgCO$_3$ (MTM) as foaming agent

In presence of Ti for this foaming mixture at high temperature as laser beam various decomposition reactions [e.g. Eq^{ns}. (13), (14) and (24)] together with reduction reactions [e.g. Eq^{ns}. (16), (17), (18) and (25)] and additionally volatilization [e.g. Eq^{n}. (21)] were occurred. During the various reactions gaseous oxides were produced together with substantial amounts of solidus ceramic and alloy like particles. Anyway, generated oxides particles in the melt slows down more effectively the melt drainage compared to previous case. For lower percentages (e.g. 0.25 wt%) of foaming agent exerted gas pressure in the melt was not too high to be coalescence or merging of pores during their formation. Therefore, pores with decreasing pore diameter and nearly homogeneous pore distribution are found in sample generated with lower amounts of foaming agent. With the increasing amounts of foaming agent exerted gas pressure in the melt was high enough to merge several adjacent pores by rupturing of cell walls. The pore coalescence by the reunion of several adjacent pores due to cell wall rupture was significantly occurred in sample generated with higher amount of foaming agent (e.g. 1.0 wt%). This is also due to the presence of various reduction reactions because of increasing amounts of graphite and MgO in the melt.

Among different methods, porosity in this case has been calculated by IBM and MGDM. The maximum total porosity (41.4 $\pm$ 1.5%) is found in sample generated with 0.25 wt% of MTM as foaming agent. Therefore, lower amounts of foaming agent can be used for the generation of high amounts of porosity with homogeneous pore distribution in the specimens. Anyway, from SEM (Fig. 36) and micro-CT images it is observed that pores with increasing pore diameter and in some cases additionally pore with decreasing pore diameter are interconnective within the specimen.

4.11. Discussion of the results obtained with a mixture of MgTiO$_3$/graphite, Li$_2$TiO$_3$/graphite and MgCO$_3$/graphite (MTMC) as foaming agent

At high temperature as laser beam different decomposition reactions (as descried previously) and several reduction reactions (mentioned earlier) together with various competitive reactions and more importantly Li$_2$O volatilization were taken place during Ti foaming process. During

these chemical reactions various gaseous species along with high amount of ceramic and alloy like particles were produced more freequently compared to previous case. These different gaseous species produced by volatilization and other chemical reactions are responsible for the generation of pores in the Ti samples. As described previously these ceramic or alloy particles can be performed as stabilizing agent so that generated pore structures might be stable. In sample generated with lower amounts (e.g. 0.25 wt%) of MTMC as foaming agent pores with comparably decreasing pore diameters are found. This is probably due to the creation of lower amounts of escape able gases in the melt. For higher amounts of foaming agent pores with high pore diameter are found and additionally pore coalescence is occurred. These behaviors are most probably due to the presence of huge amounts of gaseous species that exerted pressure to create pore with increasing pore diameter. In sample generated with every amount of foaming agent pores with increased pore diameters are found (Table 13) compared to Ti sample generated with the corresponding amount of MTM as foaming agent. Due to the presence of additional amount of graphite the reduction reactions [e.g. Eq^{ns}. (16)-(18)] was more pronouncedly occurred here compared to previously described case. Therefore, pores coalescence is significant here by the reunion of several adjacent pores. Anyway the pore distribution is not homogeneous in all cases. This is also due to the merging of pores by the rupture of cell walls during formation of pores in the presence of increasing quantity of evolving gases.

Although pore merging is observed in sample generated with every amounts of foaming agent however, the coalescence of pores is significantly occurred in sample generated with higher amounts (e.g. 1.0 wt%) of foaming agent. This is due to the presence of a huge amount of escape able gases produced by various reactions. Nevertheless, maximum total porosity $36.2 \pm 1.5\%$ is calculated for sample generated with 0.50 wt% of MTMC as foaming agent.

The influence of percentages of foaming agent on the generated amounts of porosity can be shown in Fig. 49. It is found that the porosity increases primarily with the increasing amounts of foaming agent up to 0.50 wt% and then again decreases. Due to partial break down of porous structures in presence of a huge amount of gases, for higher amounts of foaming agent lesser amount of porosity is found.
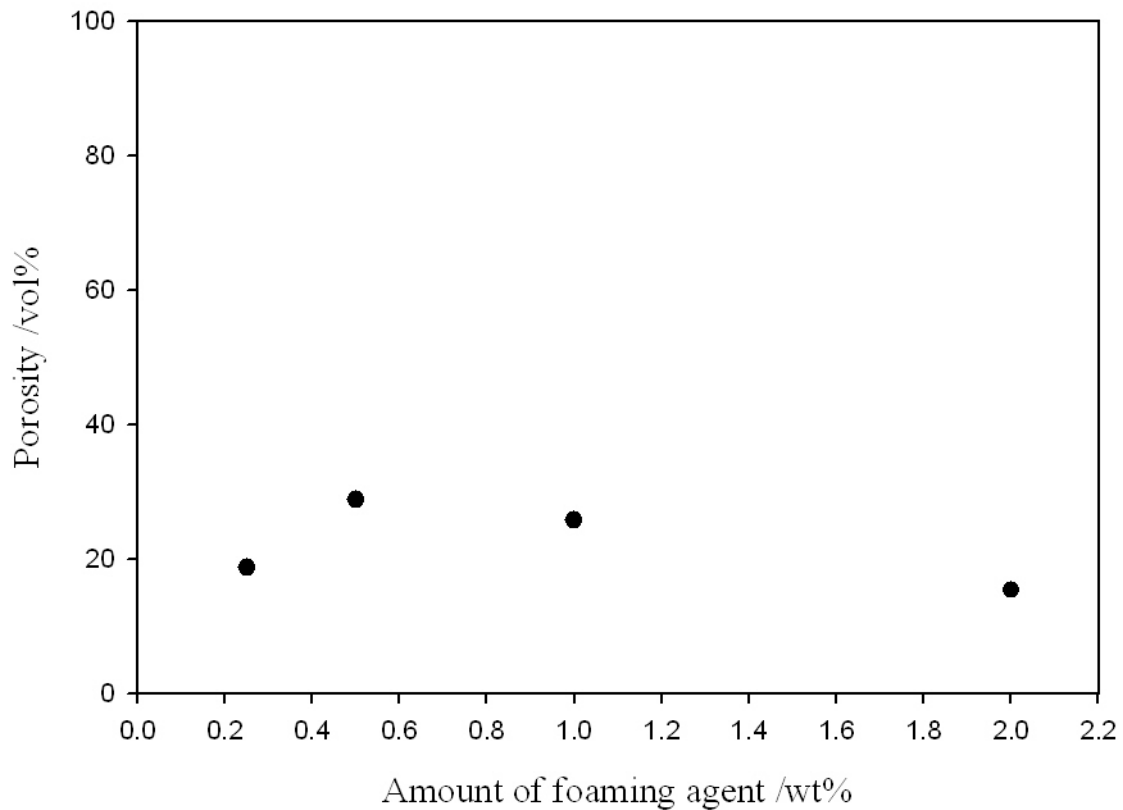
Fig. 49. Variation of amounts of porosity on the percentages of a mixture of $MgTiO_3$/graphite, Li_2TiO_3/graphite and $MgCO_3$/graphite as a foaming agent.

4.12. Discussion of the results obtained with a mixture of $MgTiO_3$/graphite and $LiNbO_3$/graphite (MLN) as foaming agent

The expected decomposition reactions of $MgTiO_3$ and graphite, and $LiNbO_3$ and graphite at high temperature as laser beam has been descried previously in Eq[ns]. (13) and (26) respectively. Additionally, reduction reaction in Eq[n]. (27) could be occurred at temperature around 1473 K in presence of graphite. It is also speculative that due to the presence of $LiNbO_3$ in foaming mixture, an Mg-Nb intermetallic might be formed in presence of $MgTiO_3$ during laser process. The produced several ceramic like and alloy like or intermetallic particles ccould be acted as stabilizing agent so that the growing pore dose not collapse immediately which is described before [3, 86]. Moreover, *in-situ* produced different oxides species prevent the porous structure from melt drainage [3, 86] more effectively than previous case. Anyway, in samples generated with lower amounts of foaming agent (e.g. 0.25 wt%) small pore size and nearly homogeneous

pore formation is observed. This is due to production of lesser amounts of gaseous species in the system. Additionally, due to the absence of an increased amount of graphite for lower percentages of foaming agent reduction of Li_2O is less likely occured. Also homogeneous and increasing pore diameter (Table 14) of generated pores are found in sample created with intermediate percentages of foaming agent (0.50 wt%). This is due to the production of increasing amount of escape able gaseous particles in the melt. A negligible number of pore coalescence was occurred by the reunion of several adjacent pores. This is most possibly due to the presence of Mg-Nb alloy particle in the matrix. In both of the lower and intermediate amounts of foaming agent generate Ti sample with homogeneous pore distribution. This is most likely because of the presence of several ceramic like, alloy like and intermetallic like particles. This particle presumably has especial characteristics to act as a viscosity increasing agent so that the growing bubble can be stabilized effectively. Due to the presence of an increased amount of gases, for higher amounts of foaming agent pores with increasing pore diameters are found. Although the various percentages of foaming agent created a high number of pores in the Ti sample however, 0.50 wt% of foaming agent provides a maximum total porosity of 49.8 $\pm$ 1.0% in this case.

Furthermore, SEM images shows that both of the pores with increased and decreased pore diameters are interconnective within the specimens. This interconnective pores can be good advantage for the reduction of the stiffness of the porous material. With this high amount of porosity and pore homogeneity as a foaming agent, a mixture of $MgTiO_3$/graphite and $LiNbO_3$/graphite is a suitable candidate for themanufacture of Ti implant.

4.13. Discussion of the results obtained with a mixture of $MgTiO_3$/graphite, $LiNbO_3$/graphite and $MgCO_3$ (MLNM) as foaming agent

At a high temperature as laser beam the possible decomposition reactions of $MgTiO_3$ and graphite, $LiNbO_3$ and graphite and additionally $MgCO_3$ are described previously in Eq^{ns}. (13), (26), and (14) respectively. The produced lithium oxide could be reduced in presence of graphite according to previously described reaction (27). Additionally, in presence of $MgCO_3$ in the foaming mixture *in-situ* MgO could be reduced by graphite [Eq^{ns}. (16)-(18)] and evolved gaseous magnesium and oxides of carbon in the system during laser process. The generated various gaseous species were responsible for the creation of pores in the material matrix.

Anyway, in samples generated with lower percentages of foaming agent (e.g. 0.25 wt%), a high number of pores with decreased pore diameter and a small number of pores with increased pore diameter are found. This is perhaps due to the formation of less amount of escape able gas in the system. Again, for intermediate amount of foaming agent (e.g. 0.50 wt%), a high number of pores with increased pore diameter were formed. This is because of the exerted pressure by a high amount of gaseous specie in the melt during laser process. Due to higher gaseous pressure for higher amounts of foaming agent pore with increasing pore diameter were dominated. Anyway, in Ti samples generated with every percentages of MLNM as foaming agent created pores with increasing pore diameters compared to the samples generated with corresponding amount of MLN as foaming agent. This behavior is due to the presence of additional amounts of $MgCO_3$ in the foaming mixture. Its presence not only decomposition reaction occurs but also additional reduction reaction took place in the system. The reduction of MgO by graphite produced gaseous magnesium and oxides of carbon which has a greate influence to generate pores with increasing pore diameter in the Ti samples.

The influence of percentages of foaming agent on the amounts of porosity in the samples can be shown in Fig. 50. It is observed that amount of porosity increases with the increasing amount of foaming agent up to 1.0 wt%. Again, porosity amount decreases with the increasing amounts of foaming agent. Therefore, maximum total porosity is found in the sample generated with 1.0 wt% of foaming agent. Initially total porosity is less it is probably due to the production of lower amount of gaseous species by less amount of foaming agent. As the foaming agent amount increases the exerting gas pressure increases and total porosity goes up to 57.0 $\pm$ 1.0%. Again, total porosity decreases with the increasing amounts of foaming agent. This is due to partially break down of the porous structure because of huge amounts of gaseous species in the melt. Nevertheless, among all foaming agents, highest total porosity has been found in the sample generated with 1.0 wt% of MLNM as foaming agent. Anyway, this foaming mixture can be a potential candidate for the production of a good amount of well defined homogeneous porosity in the samples.
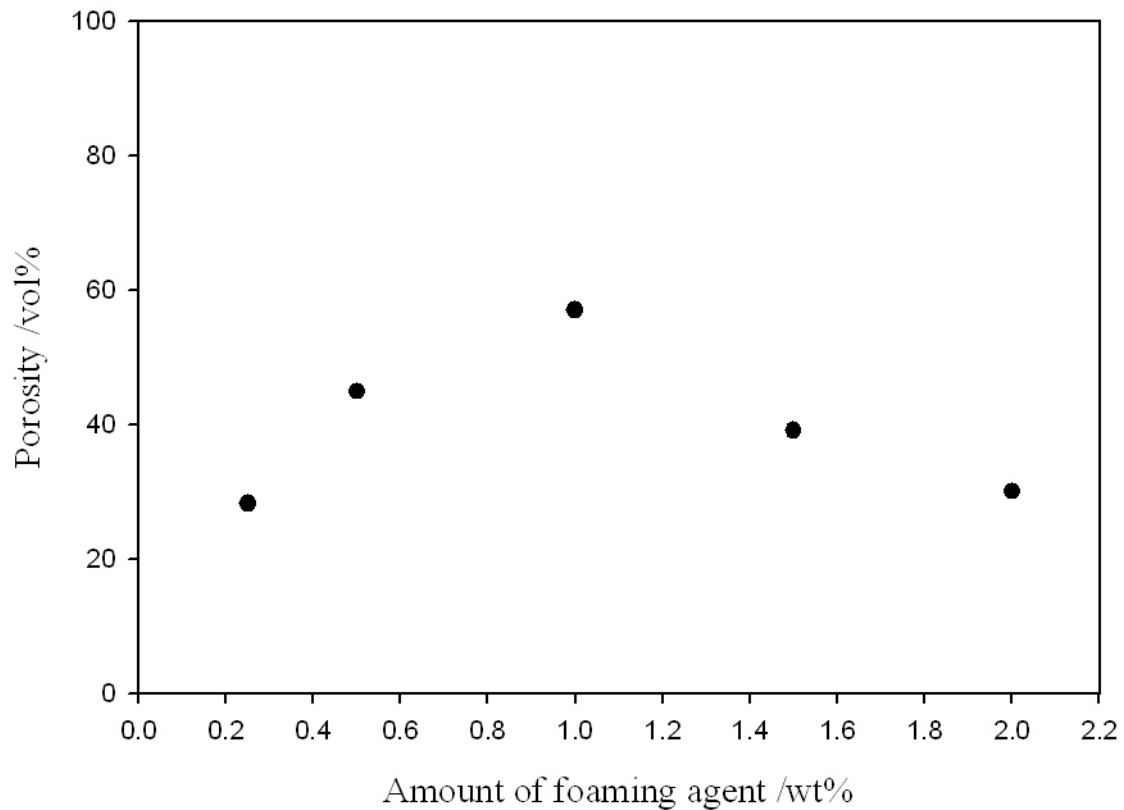
Fig. 50. Dependency of the amounts of foaming agent on total porosity of porous Ti sample generated with a mixture of MgTiO₃/graphite, LiNbO₃/graphite and MgCO₃ as foaming agent.

4.14. Discussion of the results obtained with a mixture of MgTiO$_3$/graphite, Li$_2$TiO$_3$/graphite, BaCO$_3$ and MgCO$_3$ (MTBM) as foaming agent

At a high temperature as laser beam, a number of chemical reactions took place such as decomposition reactions of MgTiO₃ and graphite (as described earlier); Li₂TiO₃ and graphite (as mentioned earlier); and MgCO₃ (as described before) and together with various reduction reactions which is shown before. In addition to those reactions decomposition of BaCO₃ and reduction [99-101] of *in-situ* produced BaO in presence of graphite was taken place at 1223 K.

$$BaCO_{3(s)} \rightarrow BaO_{(s)} + CO_{2(g)} \tag{30}$$

$$BaO_{(s)} + C_{(s)} \rightarrow Ba_{(s)} + CO_{(g)} \tag{31}$$

Due to the production of a huge amount of various gaseous species in the melt, it is expected that substantial number of pores should be created in the porous Ti samples. Furthermore, different oxides species (such as MgO, BaO) could be good candidates to slow down the melt drainage which has already been discussed. Anyway, in the sample generated with lower amount of foaming agent (e.g. 0.25 wt%), a very few pore with decreasing pore diameter are found. This is due to the presence of insufficient amount of gas pressure in the melt which was unable to create a good number of pores with considerable pore diameters. Although intermediate amount of foaming agent (e.g. 0.50 wt%) created some small and a few big pores (Table 15) the higher amounts of foaming agent (e.g. 1.0 wt%) created pore with very high pore diameter like a big void (Fig. 43). This very big deformed ellipsoidal pore has been generated probably due to the presence of additional reduction reaction of BaO besides other decomposition and reduction reactions in the melt. Because of a high amount of gaseous species for higher amount of foaming agent (>5.0 wt%) unstable foaming process was observed. Anyway, maximum total porosity of 29.5 + 1.2% is determined in the sample created with 1.0 wt% of this foaming agent.

4.15. Discussion of the results obtained with a mixture of MgTiO$_3$/graphite, Li$_2$TiO$_3$/graphite, BaCO$_3$ and MgCO$_3$/graphite (MTBMC) as foaming agent

In the case of MTBMC as foaming agent at a high temperature a number of chemical reactions has been taken place during foaming process. Besides the decomposition and reduction reactions (described just before), reductions MgO and BaO were more pronounced here because of the presence of additional amounts of graphite in the foaming mixture. Like previous case with lower amount of foaming agent decreased number of pores with relatively small pore diameter is generated. This is due to the presence of insufficient amount of escape able gases in the melt. The intermediate amounts of foaming agent (e.g. 0.50 wt%) created a high number of pores with an increased pore diameter and nearly homogeneous pore distribution. This is due to the generation of a sufficient amount of gases by different reactions to provide an increased number of pores and homogeneous pore distribution in the specimens. Because of a substantial amount of evolving gaseous species, for higher percentages of foaming agent pores with higher pore diameter are found. In general pores with increasing pore diameters are observed in Ti samples generated with this foaming agent compared to the sample generated with corresponding amount of MTBM as foaming agent (Table 15). The increasing

pore diameter is due to the additional reduction reactions of MgO and BaO in presence of added graphite in the foaming mixture. Therefore, in most cases it is observed that added graphite has a significant contribution for the generation more pore with increasing pore diameter. Nevertheles, maximum total porosity of 37.3 $\pm$ 1.3% has been determined by MGDM in the sample created with 1.0 wt% of foaming agent.

Table 17: Maximum porosity calculated by various methods for the different porous Ti samples

Foaming materials	Material codes	Foaming agent /wt%	Maximum porosity /vol%
CaWO$_4$/graphite	-	1.0	10.4
MgTiO$_3$/graphite	-	1.5	22.1
MgCO$_3$	-	1.0	24.4 $\pm$ 1.5
MgCO$_3$/graphite	-	0.75	43.3 $\pm$ 1.1
MgTiO$_3$/graphite + MgCO$_3$	-	0.10 + 0.75	23.1
Li$_2$TiO$_3$	-	0.50	32.4 $\pm$ 1.4
Li$_2$TiO$_3$/graphite	-	0.50	36.1 $\pm$ 1.5
LiNbO$_3$/graphite	-	4.0	35.1 $\pm$ 1.6
ZrO$_2$	-	4.0	12.1 $\pm$ 1.2
ZrO$_2$/graphite	-	4.0	13.1 $\pm$ 1.6
MgTiO$_3$/graphite + Li$_2$TiO$_3$/graphite	MgT	0.75	38.8 $\pm$ 1.1
MgTiO$_3$/graphite + Li$_2$TiO$_3$/graphite + MgCO$_3$	MTM	0.25	41.4 $\pm$ 1.5
MgTiO$_3$/graphite + Li$_2$TiO$_3$/graphite + MgCO$_3$/graphite	MTMC	0.50	36.2 $\pm$ 1.5
MgTiO$_3$/graphite + LiNbO$_3$/graphite	MLN	0.50	49.8 $\pm$ 1.0
MgTiO$_3$/graphite + LiNbO$_3$/graphite + MgCO$_3$	MLNM	1.0	57.0 $\pm$ 1.0
MgTiO$_3$/graphite + Li$_2$TiO$_3$/graphite + BaCO$_3$ + MgCO$_3$	MTBM	1.0	29.6 $\pm$ 1.2
MgTiO$_3$/graphite + Li$_2$TiO$_3$/graphite + BaCO$_3$ + MgCO$_3$/graphite	MTBMC	1.0	37.3 $\pm$ 1.3

Error in porosity has been shown only the porosity of porous samples calculated by mass and geometric dimension method (MGDM)

The maximum porosity of various porous Ti samples otained by using different porosity calculating methods can be shown in Table 17. Among them LiNbO$_3$/graphite based foaming agent provides higher poristy compared to other foaming agents. Moreover, theis foaming agent mixtures create porous Ti sample with nearly homogeneous pore distribution and additionally, considerable pore shapes and sizes. Again, Li$_2$TiO$_3$/graphite based foaming agent also provides porous Ti metal with a high number of pores and considerable amounts of porosity. Nevertheless, amongst the entire foaming agent a mixture of MgTiO$_3$/graphite, LiNbO$_3$/graphite and MgCO$_3$ has been produced a maximum porosity of $57.0 \pm 1.1\%$.
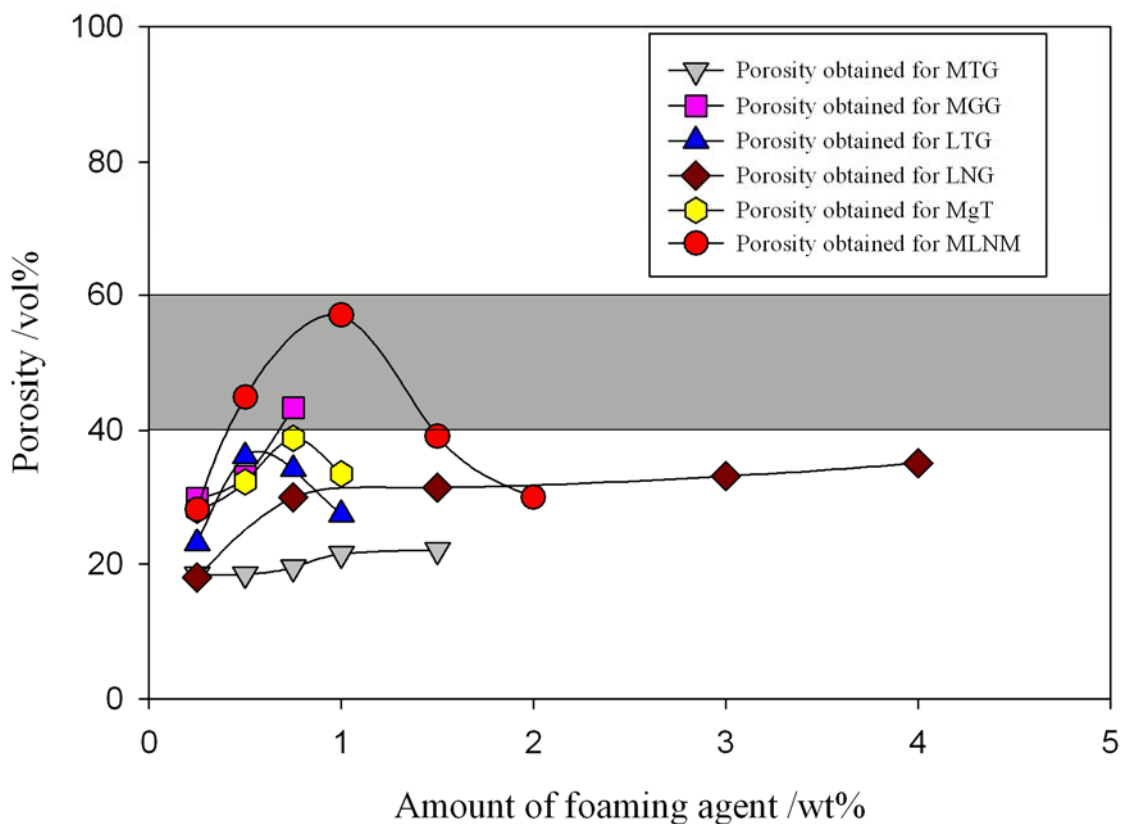
Fig. 51. Comparison of the influences of foaming agent on porosities of various porous Ti samples generated with different foaming agents. MTG = MgTiO$_3$/graphite, MGG = MgCO$_3$/graphite, LTG = Li$_2$TiO$_3$/graphite, LNG = LiNbO$_3$/graphite, MgT = MgTiO$_3$/graphite + Li$_2$TiO$_3$/graphite, MLNM = MgTiO$_3$/graphite + LiNbO$_3$/graphite + MgCO$_3$.

A comparison of the influence of amount of foaming agent on porosity generation can be shown in Fig. 51. Most of the cases, it is observed that with the increasing of foaming agent amount porosity of the samples increases. After certain point it again decreses with the

increasing amount of foaming agent. The marked area of the Fig. 51 is our present interest. Nevertheless, $MgTiO_3$ and $LiNbO_3$ based foaming agent provides high porosity compared to other foaming agents. Therefore, this foaming mixture can be a suitable candidate for the generation of porous Ti matrix for the manufacture of hip or knee prosthesis.

For the determination of mechanical properties of the porous Ti sample, a large specimen with layered structure is nessesary to generate. It was not the aim of this thesis to create such kind of big sample. Therefore, the correlation between porosity and mechanical properties of the presently generated samples has not been established. Total compositional analysis is another important parameter that has to be determined in detailed for recognizing the quality of the material.

5. MICROSTRUCTURAL INVESTIGATIONS

The microstructure of porous Ti sample has a substantial role for the influence on the mechanical properties of this material [63, 102-105]. For the conventional Ti alloys the microstructure is primarily descrived by the size, shape and arrangement of the two phases such as α and β-Ti. Upon cooling from the β phase field one of the extreme cases of phase arrangements lamellar microstructure is produced. On the other hand equiaxed microstructure is produced by recrystallization process. Both categories of the microstructures can have a fine and a coarse arrangement of their two phases. The influences of the different microstructures on the mechanical properties of titanium can be found elsewhere [63].

The microstructural observation of the porous Ti metal generated with various foaming agents has been carried out. The results of microstructural investigation of Ti samples generated with some specific foaming agents are described for understanding. The varied microstructural morphologies observed in the presently generated Ti sample with different amounts of MgTiO$_3$/graphite content as a foaming are shown in Fig. 52. The hexagonal pure Ti exhibits a typical air cooled metastable feather-like microstructure (Fig. 52 a). In the presence of a small amount (0.25%) of foaming agent, the alloy exhibits lamellar martensite (ά) microstructure with a small amount of α-Ti. Moreover, plate-like region of parallel laths and additionally region showing a more un-oriented lamellar behavior. As the foaming agent content is low the α lath formation occurs due to creation of much diluted alloys. Laths of about 5-6 μm width are found. A few irregular regions without any clear internal feathers are also visible. When foaming agent content is 0.50% or higher, ά martensite microstructures also are found. With the increasing amount of foaming agents, widths of laths as well as colony size are decreased as given in Table 18. Both colony and laths size reduction is continuing up the 1.5% of the foaming agent content and then increases again with foaming agent amounts [Fig. 52 (c-f)]. For higher percentages of foaming agent, the microstructures are also dominated by ά martensite lamellar structure together with a few dendritic microstructures.

From microstructural investigation of the porous material it is found that for an intermediate amounts of foaming agent, small grain size with small thin α laths is found while for the higher and lowest amounts laths coarsening are observed. The grain size influences on the formation of pores is shown in Fig. 53.
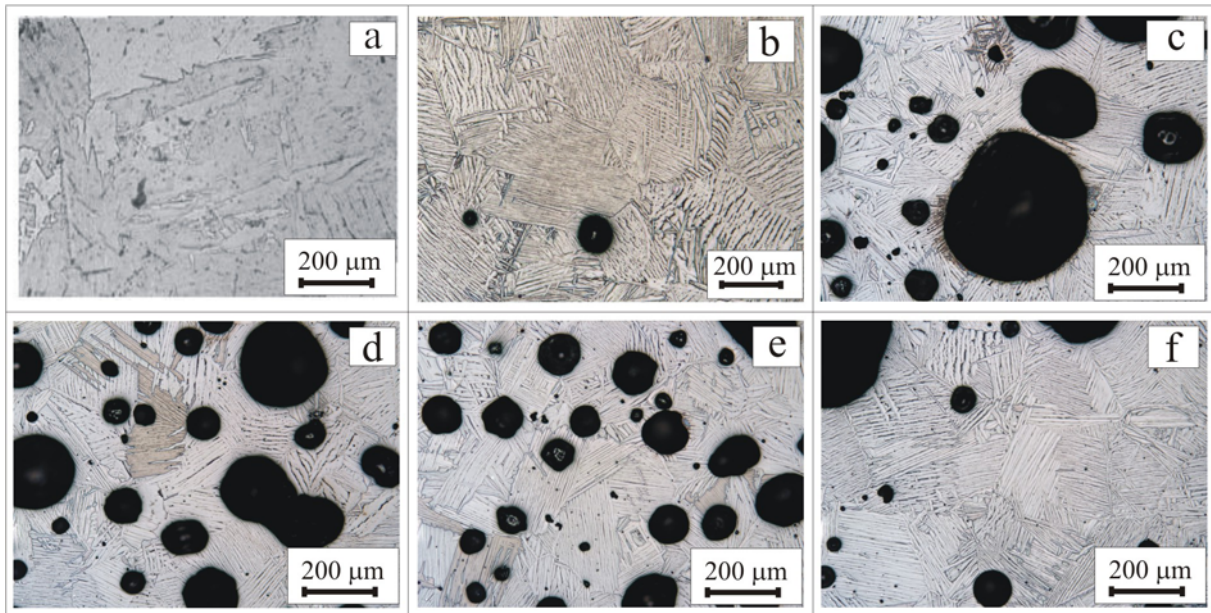
Fig. 52. Optical micrographs of porous Ti structures: (a) pure Ti and (b) Ti-0.25 wt%, (c) Ti-0.50 wt%, (d) Ti-1.0 wt%, (e) Ti-1.5 wt%, (f) Ti-2.0 wt% of MgTiO₃/graphite as foaming agent.
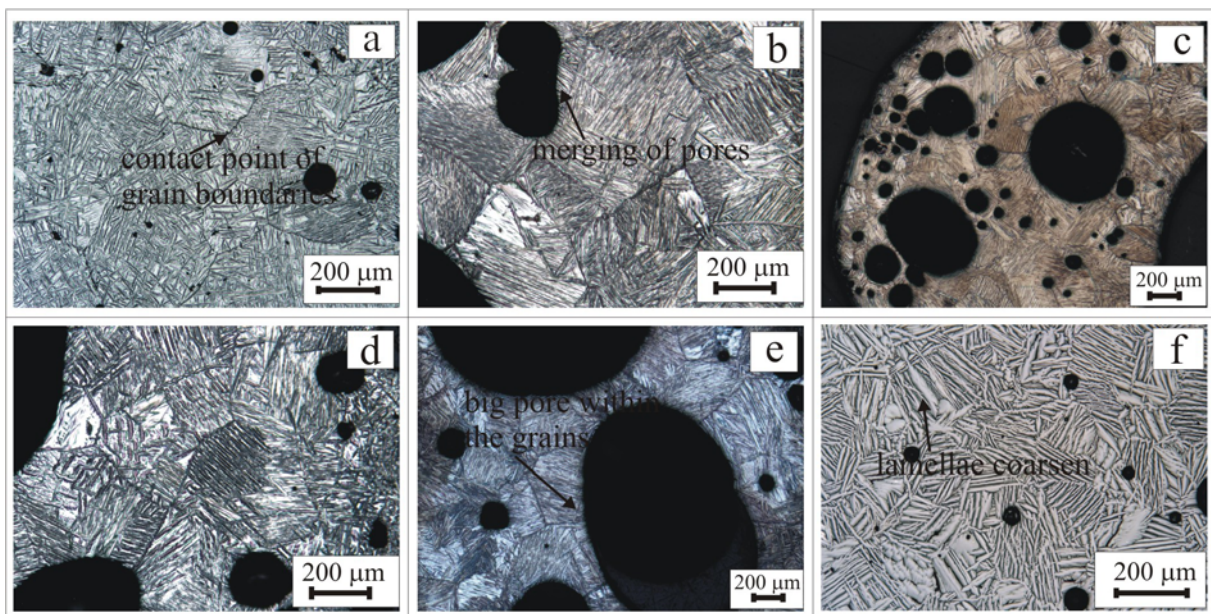
Fig. 53. Optical micrographs of porous Ti-metal with MgTiO₃/graphite: (a) small pore at the contact point of the grain boundaries, (b) pores merging, (c) more pores with small grain boundary, (d) laths separation, (e) big pores form within the grains and (f) laths coarsening.

Table 18: Details of the respective microstructural features of generated porous Ti samples

Foaming agent	Amounts of foaming agent	Lath width /μm	Grain size
MgTiO$_3$/graphite	0.25%	5-6	medium
	0.50%	4-4.5	small
	1.0%	3-4.5	smallest
	1.5%	2.5-4	small
	2.0%	5.5-6.5	largest
Anatase/graphite	0.50%	4.5-5	small
Rutile/graphite	0.50%	5-5.5	small
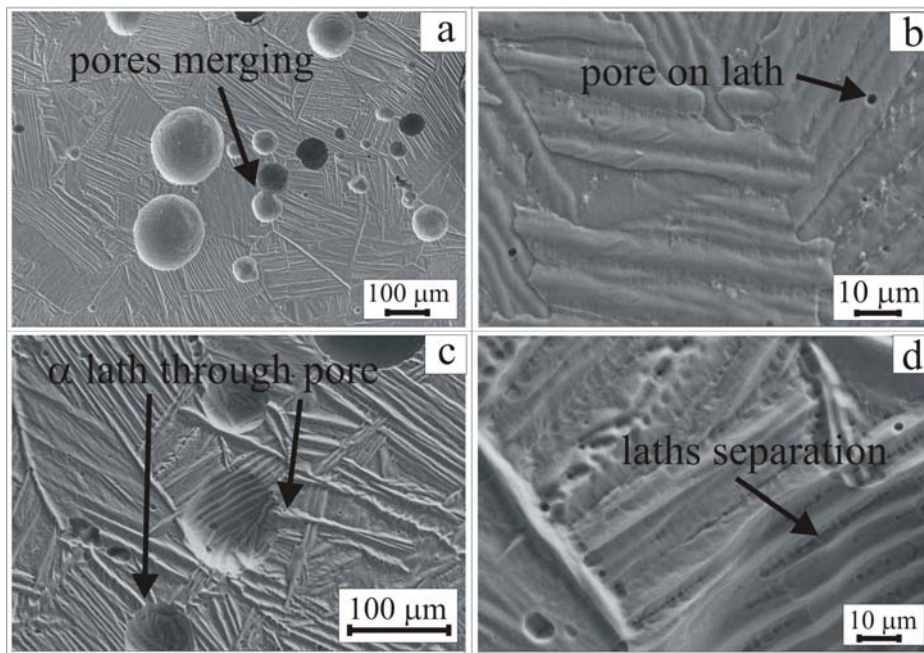
Fig. 54. SEM micrographs of Ti sample generated with MgTiO$_3$/graphite as foaming agent: (a) pores merging within grains boundary, (b) small pore on coarse lath, (c) lath grows through pore and (d) separation of course laths.

From the SEM investigation it is found that for lower percentages of foaming agent small pores are created all over the grains while for higher amounts of foaming agents big pores are dominated within the grains. The big pores are presumably created due the merging of the small pores during the process. Additionally, increased amounts of pores are found within the small

grain size. SEM investigation also reveals that small pores are created either on the laths or anywhere in the grains (Fig. 54).

Similar microstructural features have been found for the generated Ti metal with anatase/graphite and rutile/graphite as foaming agents. With the addition of increasing amount of foaming agent for both of the lath and colony size decrease initially and after certain amounts of foaming agent increase again. The microstructural features are shown in Fig. 55.
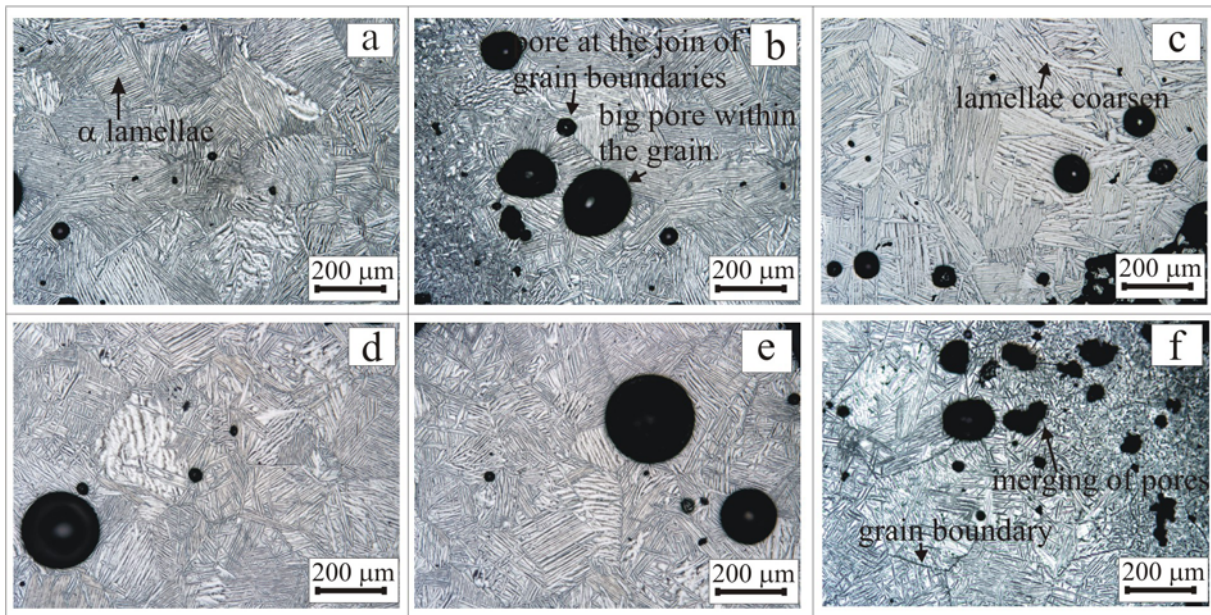
Fig. 55. Optical micrographs of porous Ti sample generated with anatase/graphite: (a)-(c); rutile/graphite: (d)-(f) showing microstructural features of specimens.

The XRD result of the samples generated with MgTiO$_3$/graphite and pure Ti is shown in Fig. 56. It is apparently found that hexagonal close packed α-Ti is only present after the laser process. The peak of [002] at 38.22 2θ angle of α-Ti and that of [011] at 38.38 of β-Ti overlap each other. Due to the overlapping the peak broadening is observed in the refinement of XRD data for sample generated with higher percentages of foaming agent. Therefore, from this observation it is speculative that at least a trace amount of β-Ti phase is present besides α-Ti in the Ti sample generated with high amounts of foaming agent. The XRD result indicates that crystal structure of the Ti sample with MgTiO$_3$/graphite is remained same with considerable amount of foaming agent content (e.g. 0.25-1.0 wt%). This is presumably due to the presence of graphite which acts as α stabilizing agent in this process. Samples generated with anatase and

rutile demonstrates similar results. EDX analysis also reveals that only α- Ti is present in the specimens. Further investigations are necessary for the details micro-chemical analysis.

Fig. 56. X-ray diffraction patterns for Ti samples generated with pure Ti and with 0.25 wt% MaTiO₃/graphite as a foaming agent.
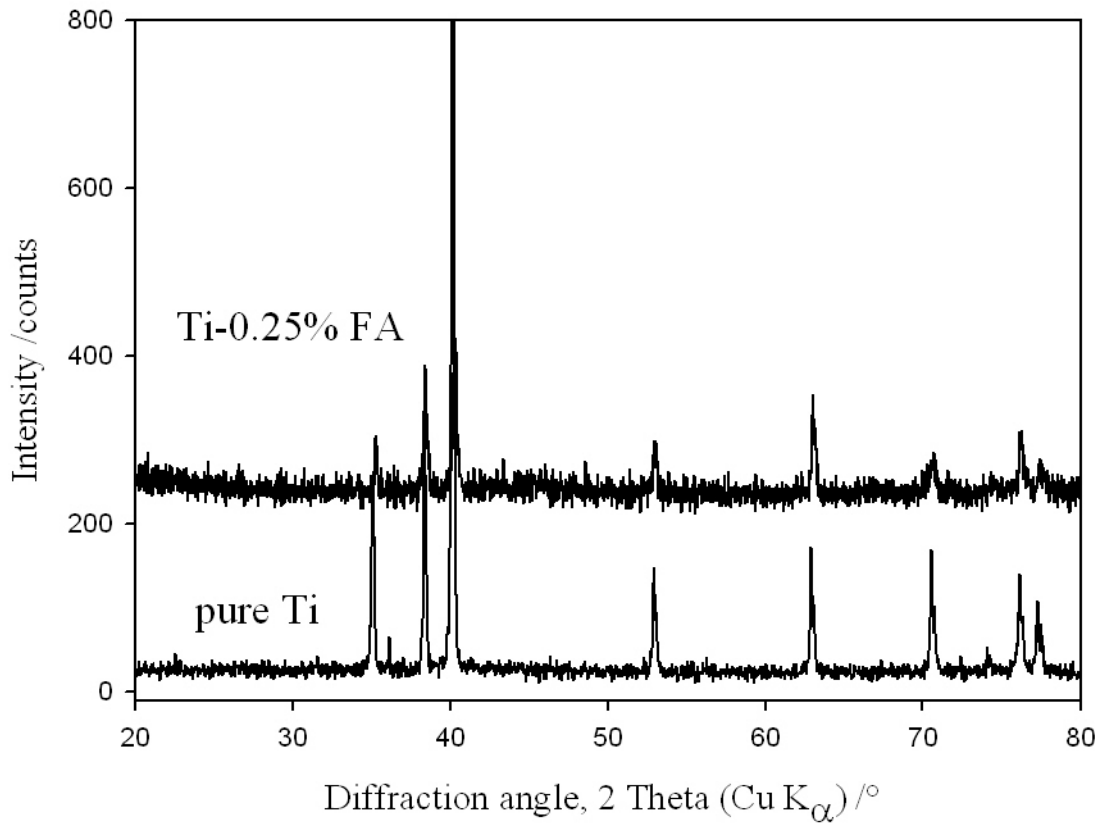
6. SUMMARY AND OUTLOOK

Metals and alloys have been widely used as implants for hard tissue replacement. Among various implant materials, pure Ti and its alloys are employed in place of human bone because of their excellent biocompatibility, outstanding resistance to corrosion reaction, high strength-to-weight ratio, and light weight. However, the mismatch of Young's modulus between the bone and metallic implants is one of the major problems concerning metallic implants for medical applications. Although the Young's modulus of Ti (110 GPa) is relatively low compared to that of stainless steel (about 210 GPa), there is a huge difference in elasticity between the titanium implant and the tissue (30 GPa) in which it is inserted. Due to this mismatch in mechanical properties bone is insufficiently loaded which is known as "stress-shielding". As most of the load is borne by the titanium implant, the surrounding bone degrades. In order to minimize the risk of implant loosening caused by these factors there is a high demand for endoprostheses with adapted macroscopic elasticity to human bone. One way of increasing the elasticity of titanium material is to introduce pores which reduce the Young's modulus in the implant materials. To achieve this goal, a simple idea is to create a hollow endoprosthesis scaffold which is filled up with porous metal. By this way the implant elasticity can be adapted to bone elasticity by controlling the amount of porosity of the material. Biocompatible foaming agents, such as, titanium dioxide (anatase/rutile)/graphite, calcium tungstate/graphite, magnesium metatitanate/graphite, magnesium carbonate/graphite, lithium titanate/graphite, lithium niobate/graphite, zirconium oxide/graphite and their mixture, etc., have been investigated which allow a laser induced foaming of titanium without leaving the toxic degradation products in the remaining titanium porous matrix. In order to adapt the elasticity of a closed cell Ti porous material to that of bone based on Eq^n (4), it is assumed that porosities of 40%-60%, depending on the pore morphology, are required.

The total porosity, distribution, shape and size of the pores in the porous samples have been investigated by taking micrographs and micro-CT images and analysis. It has been found that magnesium metatitanate/graphite, lithium titanate with and without graphite, and lithium niobate/graphite as foaming agents generate porous Ti structures with high amount of porosity, considerable pore shape and size and nearly homogeneous pore distribution in the porous matrix. As a foaming agent, $MgTiO_3$/graphite creates nearly homogeneous pore with maximum porosity of 22% while a mixture of $MgTiO_3$/graphite and $MgCO_3$ create a porosity of 23% and

cause inhomogeneous pore distribution in the porous sample. In samples generated with $MgCO_3$/graphite as foaming agent a maximum porosity of 43% is found while only $MgCO_3$ creates porous samples with a maximum porosity of 24%. The pore distribution in samples generated with $MgCO_3$ is nearly homogeneous whereas pore distribution in samples generated with $MgCO_3$/graphite is inhomogeneous. It has been found that higher percentages (e.g. 4.0 wt%) of $LiNbO_3$/graphite can produce a maximum porosity of 35.1%, while lower (e.g. 0.50 wt%) or intermediate percentages of Li_2TiO_3 with and without graphite generate porous sample with maximum porosity of 36%. In most cases, due to the partial break down of porous structures, comparably lesser amount of porosity were found in the samples generated with higher percentages of foaming agents. Nevertheless, ZrO_2 and ZrO_2/graphite did not create samples with high porosity. Similar results are also observed in samples generated with TiO_2/graphite and $CaWO_4$/graphite. A mixture of $MgTiO_3$/graphite, Li_2TiO_3/graphite and $MgCO_3$ or $MgCO_3$/graphite and a mixture of $MgTiO_3$/graphite, $LiNbO_3$/graphite and $MgCO_3$ as foaming agents generate porous Ti samples with significant amounts of porosity. Among them $LiNbO_3$/graphite based foaming mixture generate porous samples with well defined distribution of pores and high porosity while Li_2TiO_3/graphite based foaming mixture create lesser amount of porosity. Nevertheless, the mixture of $MgTiO_3$/graphite, $LiNbO_3$/graphite and $MgCO_3$ as foaming agent generates porous sample with highest porosity (57%) and well defined pore distribution in the sample. Therefore, these $MgTiO_3$/graphite, Li_2TiO_3/graphite and $LiNbO_3$/graphite based materials could be potential candidates for the generation of porous Ti material with required elasticity for the generation of implant.

Moreover, the porous materials were analyzed by EDX, electron microprobe, micro-XRF and laser ablation coupled with MC-ICPMS in order to detect and quantitate the residues of the foaming agent after laser experiments. With EDX, electron microprobe and micro-XRF no other element except Ti were found. In case of laser ablation coupled with MC-ICPMS analysis it is very difficult to determine such a low concentration of magnesium in a matrix consisting of high amount of Ti because of the interference of Ti^{2+} with ^{24}Mg, ^{25}Mg and ^{26}Mg. It is, however, possible to determine such a low concentration of magnesium by ICP-OES or ICP-MS after chromatographic separation of Ti from the system. In the case of the mass 7, a low signal was observed which could not be ascribed to ^7Li alone because of its instability and the shape of the peak. With careful production of Ti matrix having different amounts of Li, the quantity of Li in the sample may be deciphered. Due to the lack of sufficient Li standard, additional investigations could not be carried out.

Titanium in the liquid state can dissolve oxygen by reacting with carbon dioxide according to previously described chemical reaction [Eq^n. (7)]. The contamination from oxygen in the material matrix might make the porous sample brittle. However, the amounts of different elements present in the foaming agents are quite small. Therefore, these dissolved elements are expected to have negligible effect on the embrittlement of the porous materials. Moreover, it is theoretically found that Ti grade 1 powder with 0.50 wt% of foaming agent would be Ti grade 4 after foaming process. Therefore, the mechanical property of the generated Ti porous sample, especially brittleness, is not significantly affected by the incorporation of a small amount of oxygen contained in the foaming agents. It, however, was not possible to generate large Ti porous matrix samples with layered structures within the stipulated time of this PhD dissertation. Therefore, mechanical properties such as, brittleness and Young's modulus are yet to be determined.

In order to understand the quality of the generated porous Ti material for implants the following steps must be taken:

(a) Generation of big porous Ti sample for the determination of mechanical properties such as elasticity, mechanical strength, brittleness, etc. This would allow correlating porosity with the mechanical properties of the porous sample.

(b) Hot gas extraction method can be a suitable technique to determine oxygen content of the porous samples

7. REFERENCES

[1]   F. Simancik, in: H.P. Degischer, B. Kriszt (Eds.), Handbook of Cellular Metals: Production, processing and applications, Wiley-VCH, Weinheim, 2002.

[2]   L.J. Gibson, M.F. Ashby, Cellular Solids: Structure and properties, Cambridge University Press, Cambridge, 1997, p 175-213.

[3]   J. Banhart, Manufacruring routes for metallic foams, JOM. 52 (12) (2000) 22-27.

[4]   V.C. Mow, R. Huiske, Basic orthopaedic biomechanics and mechano-biology, Lippincott Williams & Wilkins, Philadelphia, 2005.

[5]   D.M. Robertson, L. Pierre, R. Chahal, Preliminary observations of bone ingrowth into porous materials, J. Biomed. Mater. Res. 10 (1976) 335-44.

[6]   H.U. Cameron, I. Macnab, R.M. Pilliar, A porous metal system for joint replacement surgery, Int. J. Artif. Organs, 1 (1978) 104-9.

[7]   W.C. Head, D.J. Bauk, R.H. Jr. Emerson, Titanium as the material of choice for cementless femoral components in total hip arthroplasty, Clin. Orthop. Relat. Res. 311 (1995) 85-90.

[8]   B.V. Krishna, S. Bose, A. Bandyopadhay, Low stiffness porous Ti structures for load-bearing implants, Acta Biomaterialia, 3 (2007) 997-1006.

[9]   R.M. Pillar, Porous-surfaced metallic implants for orthopaedic applications, J. Biomed. Mater. Res-Appl. Biomater. 21(A1) (1987) 1-33.

[10]   K. Asaoka, N. Kuwayama, O. Okuno, I. Miura, Mechanical properties and biomechanical compatibility of porous titanium for dental implants, J. Biomed. Mater. Res. 19 (1985) 699-713.

[11]   F.A. Young, M. Spector, C.H. Kresch, Porous titanium endosseous dental implants in Rhesus monkeys: microradiography and histological evaluation, J. Biomed. Mater. Res. 13 (1979) 843-56.

[12]   H. Hahn, W. Palich, Preliminary evaluation of porous metal surfaced titanium for orthopedic implants, J. Biomed. Mater. Res. 4 (1970) 571-7.

[13]   J.B. Park, R.S. Lakes, Biomaterials: An introduction, 2nd ed, Plenum press, New York, 1992.

[14]   M.J. Walt, E.G. Lamprecht, Bone ingrowth into an open porous surface, Trans. 38th Ortho. Res. Soc. 1992, 360.

[15] M. Jasty, C.R. Bragdon, T. Haire, R.D. Mulroy, H. Harris, Comparison of bone ingrowth into cobalt chrome sphere and titanium fiber mesh porous coated cementless canine acetabular components, J. Biomed. Mater. Res. 27 (1993) 639-44.

[16] A. Fujisawa, I. Noda, Y. Nishio, H. Okimatsu, The development of the new titanium arc-sprayed artificial joints, Mater. Sci. Eng. C 2 (1995) 151-7.

[17] R.D. Bloebaum, N.L. Mihalopolulus, J.W. Jensen, L.D. Dorr, Postmortem analysis of bone growth into porous-coated acetabular components, J. Bone. Joint. Surg. 79 (1997) 1013-22.

[18] S. D. Cook, F.S. Georgette, H.B. Skinner, R.J. Haddad Jr., Fatigue properties of carbon and porous-coated Ti-6Al-4V alloy, J. Biomed. Mater. Res. 18 (1984) 497-512.

[19] S. Yue, R. Pilliar, G. Weatherly, The fatigue strength of porous-coated Ti-6%Al-4%V implant alloy, J. Biomed. Mater. Res. 18 (1984) 1043-58.

[20] I.H. Oh, N. Nomura, N. Masahashi, S. Hanada, Mechanical properties of porous titanium compacts prepared by powder sintering, Scripta Mater. 49 (2003) 1197-202.

[21] C.E. Wen, M. Mabuchi, Y. Yamada, K. Shimojima, Y. Chino, T. Asahina, Processing of biocompatible porous Ti and Mg, Scripta Mater. 45 (2001) 1147-53.

[22] G. Ryan, A. Pandit, D.P. Apatsidis, Fabrication methods of porous metals for use in orthopaedic applications, Biomater. 27 (2006) 2651-2670.

[23] M. Niinomi, Recent metallic materials for biomedical applications, Metal. Mater. Trans. A33 (2002) 477-486.

[24] M. Long, H.J. Rack, Review: Titanium alloys in total joint replacement-a materials science perspective, Biomater. 19 (1998) 1621-1639.

[25] K.S. Katti, Biomaterials in total joint replacement, Colloid Surf. B: Biointerfaces, 39 (2004) 133-142

[26] C. Körner, R.F. Singer, Foaming process for aluminium, H.P. Degischer, B. Kriszt, editors, Handbook of cellular metals, Wiley-VCH Verlag, Weinheim, 2002, p. 8-14.

[27] H. Haugen, J. Will, A. Köhler, U. Hopfner, J. Aigner, E. Wintermantel, Ceramic TiO_2-foams: characterisation of a potential scaffold, J. Eur. Cer. Soc. 24 (2004) 661-668.

[28] S.K. Hyun, H. Nakajima, Effect of solidification velocity on pore morphology of lotus-type porous copper fabricated by unidirectional solidification, Mat. Lett. 57 (2003) 3149-3154.

[29] S. Yamamura, H. Shiota, K. Murakami, H. Nakajima, Evaluation of porosity in porous copper fabricated by unidirectional solidification under pressurized hydrogen, Mater. Sci. Eng. A318 (2001) 137-143.

[30] C. Körner, R. Singer, Processing of metal foams- challenges and opportunities, Adv. Eng. Mater. 2 (2000) 159-65.

[31] J. Banhart, Manufacture, characterization and application of cellular metals and metal foams, Progr. Mater. Sci. 46 (2001) 559-632.

[32] J. Bobyn, S. Hacking, S. Chan, K. Toh, J. Krygier, M. Tanzer, Characterization of a new porous tantalum biomaterial for reconstructive orthopaedics, A scientific exhibit at the Annual AAOS, Anahein, CA, 1999.

[33] M. Thieme, K.P. Wieters, F. Bergner, D. Scharnweber, H. Worch, J. Ndop, T.J. Kim, W. Grill, Titanium powder sintering for preparation of a porous functionally graded material destined for orthopaedic implants, J. Mater. Sci. Mater. Med. 12(3) (2001) 225-231.

[34] R. Banerjee, S. Nag, J. Stechschulte, H.L. Fraser, Strengthening mechanisms in Ti-Nb-Zr-Ta and Ti-Mo-Zr-Fe orthopaedic alloys, Biomater. 25 (2004) 3413-3419.

[35] D.W. Hoeppner, V. Chandrasekarn, Fretting in orthopaedic implants: a review, Wear, 173 (1994) 189-97.

[36] D.F. Williams, The Williams Dictionary of Biomaterials, Liverpool University Press, Liverpool, 1999.

[37] T. Thomsen, L.M. Bjursten, L.E. Ericson, Implants in the abdominal wall of the rat, Scand. J. Plast. Reconstr. Surg. 20 (1986) 173-182.

[38] T.N. Salthouse, B.F. Matlaga, In evaluation of biomaterials (Eds Winter, Leray and DeGroot), John Wiley, New York, 1980, p. 295-305.

[39] P. Tengvall, I. Lundström, L. Sjöqvist, H. Elwing, L.M. Bjursten, Titanium-hydrogen peroxide interaction: model studies of the influence of the inflammatory response on titanium implants, Biomater. 10 (1989) 166-175.

[40] D.A. Puleo, A. Nanci, Understanding and controlling the bone-implant interface, Biomater. 20 (1999) 2311-2321.

[41] P. Tengvall, H. Elwing, L. Sjöqvist, I. Lundström, L.M. Bjursten, Interaction between hydrogen peroxide and titanium: a possible role in the biocompatibility of titanium, Biomater. 10 (1989) 118-120.

[42] P. Tengvall, I. Lundström, Review Paper: physico-chemical considerations of titanium as a biomaterial, Clin. Mater. 9 (1992) 115-134.

[43] A. Doran, F.C. Law, M.J. Alle, N. Rushton, Neoplastic transformation of cells by soluble but not particulate forms of metals used in orthopaedic implants, Biomater. 19 (1998) 751-759.

[44]   C. Sittig, M. Textor, N.D. Spencer, M. Wieland, P.H. Vallotton, Surface characterization of implant materials c.p. Ti, Ti-6Al-7Nb and Ti-6Al-4V with different pretreatments, J. Mater. Sci. Mater. Med. 10 (1999) 35-46.

[45]   C. Munuera, T.R. Matzelle, N. Kruse, M.F. Lopez, A. Gutiérrez, J.A. Jiménez, C. Ocal, Surface elastic properties of Ti alloys modified for medical implants: A force spectroscopy study, Acta Biomater. 3 (2007) 113-119.

[46]   E.J. Kelly, Electrochemical behavior of titanium, Mod. Aspects Electrochem. 14 (1982) 319-424.

[47]   V. Wadewitz, J. Breme, TiTa-Legierungen für dentale implantate-Korrosionsverhalten, einschließlich kontaktkorrosion, Z. Zahnärztl. Implant 5(2) (1989) 116-120.

[48]   D.F. Williams, Toxicology of implanted metals, In CRC, Fundamental aspects of biocompatibility, vol 2, CRC Press, FL, Boca Raton, 1981, p. 46-61.

[49]   J. Mühlebach, K. Müller, G. Schwarzenbach, The peroxo complexes of titanium, Inorg. Chem. 9(11) (1970) 2381-90.

[50]   D. Schwarzenbach, The structure of a chelated dinuclear peroxytitanium(IV), Inorg. Chem. 9(11) (1970) 2391-2397.

[51]   T. Hanawa, M. Ota, Calcium phosphate naturally formed on titanium in electrolyte solution. Biomater. 12 (1991) 767-774.

[52]   A.R. Dujovne, J.D. Bobyn, J.J. Krygier, J.E. Miller, C.E. Brooks, Mechanical compatibility of nanocemented hip prostheses with the human femur, J. Arthroplasty, 8(1) (1993) 7-22.

[53]   C.A. Engh, J.D. Bobyn, The influence of stem size and extent of porous coating on femoral bone resorption after primary cementless his arthroplasty, Clin. Orthop. Relat. Res. 231 (1988) 7-28.

[54]   L.J. Gibson, Mechanical behavior of metallic foams, Annu. Rev. Mater. Sci. 30 (2000) 191-227.

[55]   H. Nakajima, T. Ikeda, K. Hyun, Fabrication of lotus-type porous metals and their physical properties, Adv. Eng. Mater. 6(6) (2004) 377-384.

[56]   M.F. Ashby, A. Evans, N.A. Fleck, L.J. Gibson, J.W. Hutchinson, H.N.G. Wadley (Eds.), Metal foams- A design guide, Butterworth-Heinemann, Woburn, 2000.

[57]   H.N.G. Wadley, Cellular metals manufacturing, Adv. Eng. Mater. 4(10) (2002) 726-733.

[58]   S. J. Cox, G. Bradley, D. Weaire, Metallic foam processing from liquid state, EJP Appl. Phys. 14 (2001) 87-96.

[59] C. Körner, M. Arnold, M. Thies, R. F. Singer, in: H.P. Degischer, B. Kriszt (Eds.), Handbook of cellular metals, Wiley-VCH, Weinheim, 2002, p. 33-43.

[60] D. Weaire, Foam Physics, Adv. Eng. Mater. 4(10) (2002) 723-725.

[61] C. Körner, M. Hirschmann, V. Bräutigam, R.F. Singer, Endogenous particle stabilization during magnesium integral foam production, Adv. Eng. Mater. 6(6), (2004) 385-390.

[62] N. Babcsan, D. Leitlmeier, H.P. Degischer, J. Banhart, The role of oxidation in blowing particle-stabilised aluminium foams, Adv. Eng. Mater. 6(6) (2004) 421-428.

[63] C. Leyens, M. Peters, Titanium and titanium alloys-fundamentals and applications, Wiley-VCH GmbH and Co. KGaA, Weinheim, 2003, p. 1-57.

[64] W. G. Burgers, On the process of transition of the cubic-body-centered modification into the hexagonal-close-packed modification of zirconium, Physica. 1 (1934) 561-686.

[65] G. Lütjering, J.C. Williams, Titanium- engineering materials and processing, Springer-Verlag, Berlin, Heidelberg, New York, 2003, p. 1-175.

[66] J.C. Williams, Titanium science and technology, Plenum press, New York, 1973, p. 1433.

[67] M. Peters, G. Lütjering, G. Ziegler, Z. Metallke, 74 (1983) 274.

[68] J. Black, Biological performance of materials- fundamentals of biocompatibility, 2nd ed, New York, Marcel Dekker Inc, 1992.

[69] D.-G. Lee, S. Lee, C. Soo, S. Hur, Effects of microstructural factors on quasi-state and dynamic deformation behaviors of Ti-6Al-4V alloys with Widmanstätten structures, Met. Mater. Trans. A34 (2003) 2541-2548.

[70] D. Kuroda, M. Niinomi, M. Morinaga, Y. Kato, T. Yashiro, Design and mechanical properties of new β type titanium alloys for implant materials, Mater. Sci. Eng. A243 (1998) 244-9.

[71] K.H.W. Seah, R. Thampuran, S.H. Teoh, The influence of pore morphology on corrosion, Corros. Sci. 40 (1998) 547-56.

[72] Y. Okazaki, E. Nishimura, H. Nakada, K. Kobayashi, Surface analysis of Ti-15Zr-4Nb-4Ta alloy after implantation in rat tibia, Biomater. 22 (2001) 599-607.

[73] G. Parr, Titanium: the mystery metal of implant dentistry, J. Prosthet. Dent. 54 (1985) 410-3.

[74] D. Velten, V. Biehl, F. Aubertin, B. Valeske, W. Possart, J. Breme. Preparation of TiO$_2$ layers on cp-Ti and Ti6Al4V by thermal and anodic oxidation and by sol-gel coating techniques and their characterization, J. Biomed. Mater. Res. 59(1) (2002) 18 –28.

[75]   D. Scharnweber, R. Beutner, S. Rössler, H. Worch, Electrochemical behaviour of titanium-based materials-are there relations to biocompatibility? J. Mater. Sci. Mater. Med. 13 (2002) 1215-1220.

[76]   C.C. Yang, H. Nakae, The effects of viscosity and cooling conditions on the foamability of aluminum alloy, J. Mater. Proc. Technol. 141 (2003) 202-206.

[77]   C. Park, S.R. Nutt, PM synthesis and properties of steel foams, Mater. Sci. Eng. A288 (2000) 111-118.

[78]   F. Von Zeppelin, M. Hirscher, H. Stanzick, J. Banhart, Desoprtion of hydrogen from blowing agents used for foaming metals, Composites Sci. Tech. 63 (2003) 2213-2300.

[79]   Y. P. Kathuria, Laser assisted aluminum foaming, Surface Coatings Tech. 142-144, (2001) 56-60.

[80]   C.L. Chu, C.Y. Chung, P.H. Lin, S.D. Wang, Fabrication of porous NiTi shape memory alloy for hard tissue implants by combustion synthesis, Mater. Sci. Eng. A366 (2004) 114-119.

[81]   M. Thieme, K.-P. Wieters, F. Bergner, D. Scharnweber, H. Worch, J. Ndop, T.J. Kim, W. Grill, Titanium powder sintering for preparation of a porous functionally graded material destined for orthopaedic implants, J. Mater. Sci. Mater. Med. 12 (2001) 225-231.

[82]   A.E. Markaki, T.W. Clyne, Magneto-mechanical stimulation of bone growth in a bonded array of ferromagnetic fibres, Biomater. 25 (2004) 4805-4815.

[83]   C. Park, S.R. Nutt, Effect of process parameters on steel foam synthesis, Mater. Sci. Eng. A297 (2001) 62-68.

[84]   F. Baumgärtner, I. Duarte, J. Banhart, Industrialization of powder compact foaming process, Adv. Eng. Mater. 2(4) (2000) 168-174.

[85]   W. Deqing, S. Ziyuan, Effect of ceramic particles on cell size and wall thickness of aluminum foam, Mater. Sci. Eng. A361 (2003) 45-49.

[86]   V.C. Srivastava, K.L. Sahoo, Processing, stabilization and applications of metallic foams. Art of science, Mater. Sci-Pol. 25(3) (2007) 733-753.

[87]   M. A. Fortes, The average rate of growth of individual cells in a cellular structure: effect of the number of topological elements, J. Mater. Sci. 21 (1986) 2509-2513.

[88]   H. Nakagawa, M. Asano, K. Kubo, Mass spectrometric investigation of the vaporization of $Li_2TiO_{3(s)}$, J. Nucl. Mater. 110 (1982) 158-163.

[89]   G. Izquierdo, A.R. West, Phase equilibria in the system Li_2O-TiO_2, Mater. Res. Bull. 15 (1980) 1655-1660.

[90]   D.J. Suiter, Lithium based ceramic oxides for titanium breeding applications, McDonnell Douglas Astronautics Co., Report MDC E2677, 1983.

[91]   A.Z. Simoes, A.H.M. Gonzalez, A.A. Cavalheiro, M.A. Zaghete, B.D. Stojanovic, J.A. Varela, Effect of magnesium on structure and properties of $LiNbO_3$ prepared from polymeric precursors, Cer. Inter. 28 (2002) 265-270.

[92]   Ch.D.E. Lakeman, D.A. Payne, Sol-gel processing of electrical and magnetic ceramics, Mater. Chem. Phys. 38 (1994) 305-324.

[93]   K. Nakajima, S. Shimada, M. Ingaki, Electrochemical synthesis and thermal decomposition of zirconia gels containing various metal ions, J. Mater. Chem. 6 (1996) 1795-1797.

[94]   C.H. Phillippi, K.S. Mazdiyasni, Infrared and Raman spectra of zirconia polymorphs, J Am. Cer. Soc. 54 (1971) 254-258

[95]   F.J. Berry, M.H. Loretto, M.R. Smith, Iron-zirconium oxides: an investigation of structural transformations by X-ray diffraction, electron diffraction, and iron-57 Mössbauer spectroscopy, J. Solid State Chem. 83 (1989) 91-99.

[96]   J.Z. Jiang, F.W. Poulsen, S. Mørup, Structure and thermal stability of nanostructured iron-doped zirconia prepared by high-energy ball milling, J. Mater. Res. 14 (1999) 1343-1352.

[97]   W. Cao, O.K. Tan, W. Zhu, B. Jiang, Mechanical alloying and thermal decomposition of $(ZrO_2)_{0.8}$-$(\alpha$-$Fe_2O_3)_{0.2}$ powder for gas sensing applications, J. Solid State Chem. 155 (2000) 320-325.

[98]   M.V. Swain, Structure and properties of ceramics, vol 11, VCH publishers Inc., Weinheim, 1994, p. 103.

[99]   X. Liu, C. Ren, B. Jiang, H. Zhu, Electron emission suppression characteristics of molybdenum grids coated with carbon film by ion beam assisted deposition, J. Vac. Sci. Tecnol. A20 (2002) 1846-1849.

[100] Y. Lu, X. Wu, L. Zhuge, X. Liu, Initial study on the compositional and phase change of BaO/C/Mo under high temperature, Nucl. Instr. Methods Phys. Res. B225 (2004) 555-560.

[101] Y.H. Lu, X.M. Wu, L.J. Zhuge, Interaction between barium oxide and carbon film in BaO/C/Mo system under high temperature, J. Korean Phys. Soc. 46 (2005) S96-S99.

[102] L. Huang, P.K. Liaw, C.T. Liu, Microstructural control of Ti-Al-Nb-W-B alloys, Metal. Mater. Trans. A38 (2007) 2290-2297.

[103] Y.L. Hao, M. Niinomi, D. Kurodo, K. Fukonaga, Y.L. Zhou, R. Yang, A. Suzuki, Aging response of the Young's modulus and mechanical properties of Ti-29Nb-13Ta-4.6Zr for biomedical applications, Metal. Mater. Trans. A34 (2003) 1007-1012.

[104] S.K. Kim, J.K. Park, In-situ measurement of continuous cooling β→ α transformation behavior of CP-Ti, Meter. Mater. Trans. A33 (2002) 1051-1056.

[105] M. J. Donachie Jr, Titanium- a technical guide, 2nd ed, Materials Park, Ohio, ASM International, 2000.